NCAT Report 23-03

July 2023

National Center for Asphalt Technology
NCAT
at AUBURN UNIVERSITY

MnROAD Cracking Group Experiment: Validation of Low-Temperature Cracking Tests for Balanced Mix Design

Michael Vrtis, Carolina Rodezno, Randy West, Joseph Podolsky, Jacob Calvert and Dave Van Deusen

MnROAD Cracking Group Experiment: Validation of Low-Temperature Cracking Tests for Balanced Mix Design

By

Michael Vrtis, PhD, PE
Research Project Engineer
Minnesota Department of Transportation

Carolina Rodezno, PhD
Associate Research Professor
National Center for Asphalt Technology
Auburn University, Auburn, Alabama

Randy West, PhD, PE
Director and Research Professor
National Center for Asphalt Technology
Auburn University, Auburn, Alabama

Joseph Podolsky, PhD
Research Implementation Engineer
Minnesota Department of Transportation

Jacob Calvert, PE
Pavement Engineer
Minnesota Department of Transportation

David Van Deusen, PE
Pavement Engineer
Minnesota Department of Transportation

July 2023

DISCLAIMER

The contents of this report reflect the views of the authors who are responsible for the facts and accuracy of the data presented herein. The contents do not necessarily reflect the official views or policies of the Alabama DOT, National Center for Asphalt Technology, or Auburn University. This report does not constitute a standard, specification or regulation. Comments contained in this paper related to specific testing equipment and materials should not be considered an endorsement of any commercial product or service; no such endorsement is intended or implied.

ACKNOWLEDGEMENTS

This work was sponsored by the Illinois Department of Transportation, the Michigan Department of Transportation, the Minnesota Department of Transportation, the New York Department of Transportation, and the Wisconsin Department of Transportation.

TABLE OF CONTENTS

LIST OF FIGURES

LIST OF TABLES

1. INTRODUCTION

1.1 Background and Research Plan

In 2014-2015, the Minnesota Road Research Facility (MnROAD) and the National Center for Asphalt Technology (NCAT) developed an experimental plan to validate laboratory asphalt mixture cracking tests. Two complimentary experiments were planned: an experiment to validate tests for top-down cracking and an experiment to validate tests for low-temperature thermal cracking (LTC) of asphalt mixtures. The experiment for validating top-down cracking tests would be based on new test sections built on the NCAT Test Track in 2015, and the experiment for LTC would be based on new test sections built at MnROAD in 2016.

The MnROAD Cracking Group (CG) experiment was a pooled-fund project with sponsorship from Illinois, Michigan, Minnesota, New York, and Wisconsin. The CG experiment at MnROAD focused on LTC. The objective of the CG experiment was to validate laboratory cracking tests by establishing correlations between the test results and measured cracking performance in real pavements (test sections) within a very short timeframe. This report provides results on the MnROAD LTC experiment, including a summary of the field performance and pavement response data after five years of trafficking and environmental exposure. Also provided are the comparisons of field cracking performance with results from nine laboratory cracking tests evaluating samples of the plant-produced mixtures collected at the time of construction. The low temperature cracking tests investigated were the disk-shaped compact tension test (DCT), the low-temperature semi-circular bend test (SCB), the uniaxial thermal stress and strain test (UTSST), indirect tensile creep compliance and strength test (IDT-CC&S), asphalt concrete cracking device test (ACCD), and mixture bending beam rheometer (BBR_m). Three intermediate temperature cracking tests were also conducted on the mixtures in the MnROAD CG experiment: Indirect Tensile Asphalt Cracking Test (IDEAL-CT), the Illinois Flexibility Index Test (I-FIT), the NCAT modified version of the Overlay Test.

1.2 Pavement Structure and HMA Mix Details

The MnROAD test cells were located on the westbound lanes of Interstate 94 in Albertville, MN, 40 miles northwest of St. Paul, MN. MnROAD can divert I-94 westbound traffic on or off the MnROAD Mainline test cells. Westbound I-94 traffic is on the MnROAD Mainline cells about 80% of the time; traffic is switched off the Mainline test cells to allow for testing, monitoring, repairs, and section reconstruction. After accounting for the traffic switches, the average annual daily traffic volume at MnROAD is approximately 30,000 vehicles with 13% heavy vehicles resulting in approximately 800,000 equivalent single axle loads (ESALs) per year.

Eight hot mix asphalt (HMA) test cells were constructed in 2016 as MnROAD Cells 16-23. Each cell comprised two 12-foot travel lanes (westbound I-94) with a 10-foot shoulder on the driving lane and a 4-foot shoulder on the passing lane. As shown in Figure 1(a), the shoulders were constructed with the same structure as the travel lanes. The pavement structure is illustrated in Figure 1(b). Each cell was designed with five inches of HMA over 12 inches of MnDOT Class 5

granular base over 12 inches of MnDOT Class 3 over the native clay loam, loam (USDA) subgrade (AASHTO A-6; USCS Lean Clay). Due to condensed timeframe of this experiment the overall thickness was carefully considered. Pavement sections with five inches of HMA have performed very well for periods in excess of 7 years at MnROAD. Using the design inputs listed below and MnPAVE design software, the expected pavement life of the test sections was around 10 years.

- AADT= 30,000 vehicles
- Heavy Vehicle = 13.2%
- Flexible ESALs ~800k per year (design lane)
- MnDOT Traffic level 5
- Clay Loam, Loam Soils (A-6)

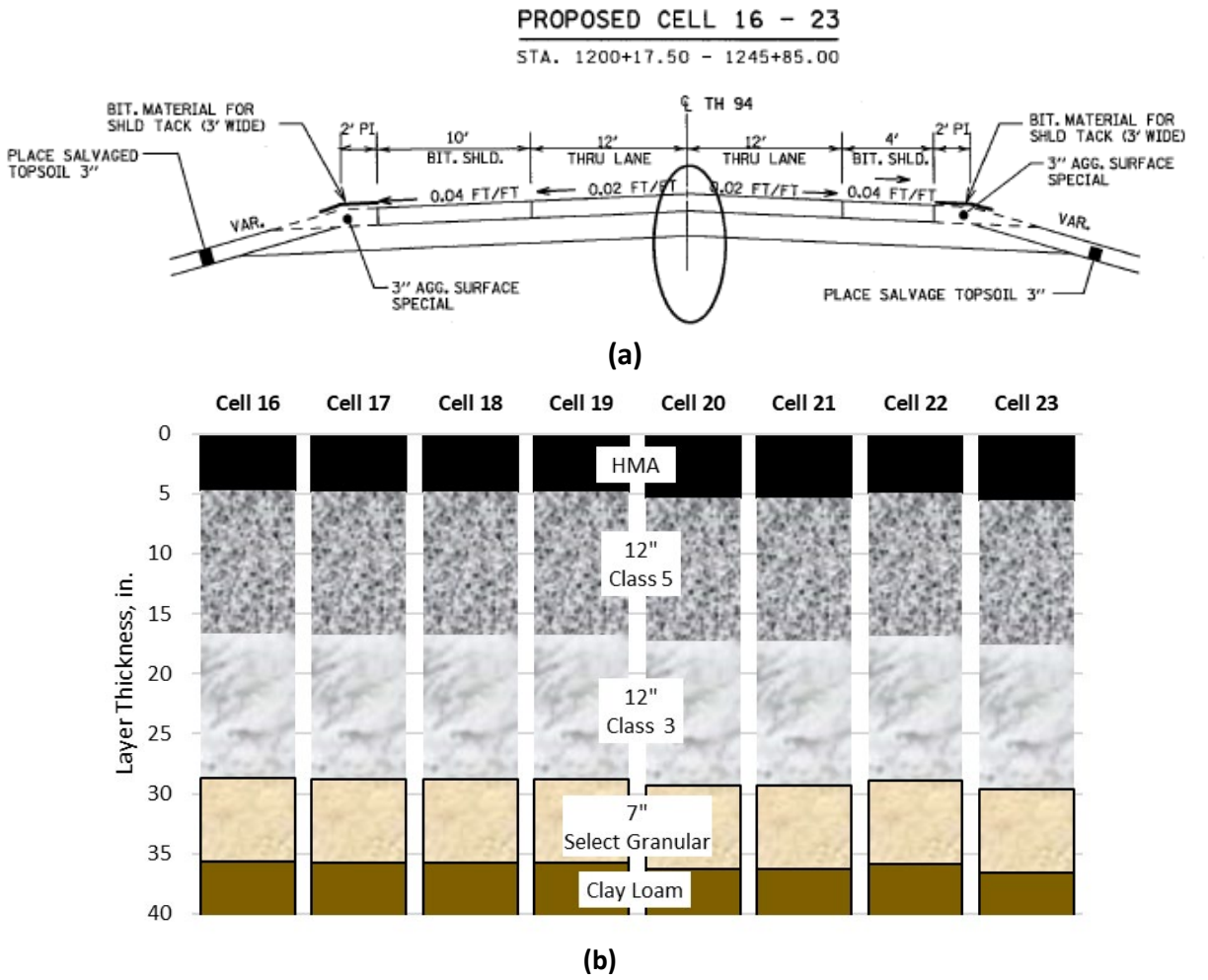

Figure 1 (a) Cross-section of Cracking Group Test Sections MnROAD (b) As-Built Pavement

Eight HMA mixtures were designed with a range of recycled materials contents, binder types, and binder grades. The goal in selecting these mixtures was to have a range of low-temperature cracking performance in a field experiment where the effects of other variables (e.g., traffic, environment, pavement structure) would be minimized. Table 1 provides a summary of general

mix descriptions, compositions, and anticipated cracking resistance based on the expectations of the research team.

The mixes were developed based on a typical MnDOT mix design that would be utilized for new HMA construction with the specific combination of interstate traffic and location. The baseline mix design used a PG 58H-34 binder and contained 20% RAP was constructed in Cell 21. Cells 16-19 used an unmodified PG 64S-22 binder to increase the low-temperature cracking potential. Cell 18 used a similar mix design to Cell 21 except for the binder. Cells 16 and 17 were like Cell 18 but incorporated recycled asphalt shingles (RAS) into the mix to increase the anticipated cracking potential. The RAS used in this project was from manufacturer waste. Cell 19 regressed the air voids to 3.0% by adding additional virgin binder from the 4.0% design used for all other mixes. The regressed air void concept is utilized frequently in Wisconsin and was included in the study to investigate the impact of a higher asphalt content on cracking resistance. Cell 20 contained 30% RAP and a softer unmodified PG 52H-34 binder. Cell 22 used a limestone aggregate instead of the granite aggregates used in all other mixes; limestone aggregates have been shown to decrease resistance to LTC. Cell 22 used a nominal maximum aggregate size (NMAS) of 9.5 mm whereas all other cells used a NMAS of 12.5 mm. Cell 23 used a highly modified binder and had the lowest anticipated cracking potential.

Table 1 Summary of Surface Mixtures Used in the MnROAD Thermal Cracking Experiment

Cell	RAP (%)	RAS	Binder	MnDOT Mix ID	Anticipated Cracking Potential
16	20	5	PG 64S-22	SPWEB540L	High
17	10	5	PG 64S-22	SPWEB540L	High
18	20	0	PG 64S-22	SPWEB540L	Med/High
19	20	0	PG 64S-22	SPWEB530L	Med/High
20	30	0	PG 52S-34	SPWEB540A	Med
21	20	0	PG 58H-34	SPWEB540C	Low
22	20	0	PG 58H-34	SPWEB540C	Low/Med
23	15	0	PG 70E-34	SPWEB540I	Low

1.3 Construction

Construction of CG cells at MnROAD began in mid-July 2016 and was completed on October 14th. Westbound I-94 traffic was switched onto the cells on November 2, 2016. Construction was closely monitored by MnROAD and NCAT. Construction dates are provided in Table 2. Due to the contractor's scheduling, test section construction was performed in 2 phases: Phase 1 for Cell 16-19 and Phase 2 for Cell 20-23. Pavement surface temperatures during the paving were monitored using a paver mounted infrared camera and the data were analyzed using Veta (a map-based tool for viewing and analyzing geospatial data Ver. 4.1). Appendix A contains thermal profile from the paver for each section.

Table 2 Construction Dates per Cell (2016)

Cell	Milling / Base Removal	Base Course Placement	Sensor Installation	Paving
16	Jul. 19 – 21	Aug. 10 - 13	N/A	Aug. 24 - 29
17	Jul. 19 – 21	Aug. 10 - 13	Aug.18 - 22	Aug. 24 - 29
18	Jul. 19 – 21	Aug. 10 - 13	N/A	Aug. 24 - 29
19	Jul. 19 - 21	Aug. 10 - 13	Aug.18 - 22	Aug. 24 - 29
20	Aug. 30	Sep. 16 - 17	N/A	Oct. 7 - 11
21	Aug. 30	Sep. 16 - 17	Oct. 4 -5	Oct. 7 - 11
22	Aug. 30	Sep. 16 - 17	N/A	Oct. 7 - 11
23	Aug. 30	Sep. 16 - 17	Oct. 4 -5	Oct. 7 - 11

A uniform base and subbase material were used throughout each cell as shown in Figure 1 (b). The in-place material in cells 16-23 were part of a 2008 study that had a consistent sub-base and subgrade throughout the cells. The existing base and HMA were removed and replaced with a uniform 12 inches base of Class 6 aggregate followed by five inches of varying HMA mix designs. The HMA was constructed in two lifts; the lower lift was 3 inches, and the top lift was 2 inches. Both lifts used the same mix.

Prior to paving the MnROAD cells, a trial placement of each mix was conducted in other areas of the MnROAD property. The access road behind the MnROAD pole barn was selected for Cell 16-19 trial HMA mixtures and they were placed on Aug. 23, 2016. For each trial mix, volumetric properties were measured and slight modifications were made. The access road to the stockpile area of MnROAD was selected for Cell 20-23 trial asphalt mixture paving. Trial mix paving occurred October 3, 2016.

The final lift thicknesses and HMA densities were recorded after construction. Cores were taken in the transition areas for verification of thickness measurements and nuclear density calibration. The average density values for each lane and lift are shown in Table 3. Density within each section was monitored with nuclear density testing. The values presented in Table 3 are averages from twelve locations within each lane (i.e., 4 offsets from centerline at 3 different stations). Density was measured at nine locations within the driving lane shoulder (i.e., 3 offsets from centerline at 3 different stations).

Table 3 In-place Nuclear Density for each Cell, Lift, and Lane

CELL	PASSING LANE		DRIVING LANE		DRIVING SHOULDER	
	Lift 1	Lift 2	Lift 1	Lift 2	Lift 1	Lift 2
16	91.7	93.2	92.3	93.2	NA	92.0
17	95.6	91.8	NA	91.7	95.7	91.4
18	93.9	93.0	92.0	92.2	91.5	92.5
19	94.5	93.6	94.4	93.7	94.0	93.6
20	93.4	94.4	91.3	94.9	92.8	94.8
21	94.0	94.8	93.9	93.8	93.6	94.0
22	91.2	92.4	91.5	92.2	91.4	NA
23	92.3	92.2	92.4	92.1	92.9	92.2

Loose-mix HMA was collected from each cell to provide sufficient material for the numerous laboratory cracking tests that were conducted. In total, over 1900 buckets of loose production asphalt mix were collected. Over 40 3.5-gallon containers of mix from each section were collected and retained at MnROAD for future material requests. This additional material has proved valuable as new tests were added to the study, which will be discussed further in Chapter 2.

1.3.1 Mix Design and As-Placed Mixture Properties

A summary of mix design and production properties of asphalt mixtures placed in Cells 16-23 is presented in Table 4. The mix design for each cell was conducted by NCAT, with Minnesota materials procured by the contractor and sent to NCAT for design. Testing of mix properties was done once during trial mix production and at least twice each day during paving of each section. This summary of volumetric and mix properties represents average values from MnDOT's Test Summary Sheet data, which details all results obtained during production testing by the contractor.

Table 4 Mix Designs and Production Properties

Cell No.	16		17		18		19		20		21		22		23	
Mix Parameters	MD	AP	MD	AP	MD	AP	MD	AP	MD	AP	MD	AP	MD	AP	MD	AP
% AC	5.3	4.9	5.4	5.3	5.4	5.1	5.7	5.7	5.3	5.1	5.4	5.1	5.7	5.4	5.2	5.1
G_{mm}	2.518	2.523	2.517	2.516	2.511	2.526	2.494	2.496	2.508	2.519	2.514	2.518	2.498	2.496	2.519	2.514
G_{mb}	2.418	2.412	2.416	2.413	2.411	2.413	2.419	2.413	2.408	2.397	2.413	2.415	2.398	2.387	2.418	2.425
% Air Voids	4.0	4.4	4.0	4.2	4.0	4.5	3.0	3.3	4.0	4.9	4.0	4.1	4.0	4.4	4.0	3.6
% VMA	14.5	14.5	14.9	14.9	14.6	14.5	14.8	15.1	14.6	14.8	14.6	14.5	14.4	14.5	14.4	14.2
P_{be}	4.6	4.4	4.7	4.7	4.7	4.3	5.1	5.1	4.6	4.3	4.6	4.4	4.5	4.4	4.5	4.5
P-200/ P_{be}	1.2	1.1	1.1	1.0	1.1	1.2	0.8	0.8	1.0	1.0	1.1	1.0	1.2	1.1	1.1	1.0
Adj. AFT	N/A	8.3	N/A	9.4	N/A	8.2	N/A	10.1	N/A	8.9	N/A	8.8	N/A	9.0	N/A	9.3
% Add AC/Total AC	60	67	73	73	77	74	78	77	65	76	77	77	78	86	82	80
CAA-1 Face	100	99	100	100	100	99	100	99	100	98	100	99	100	99	100	100
CAA-2 Face	100	98	100	99	100	99	100	98	100	98	100	99	100	99	100	99
FAA	47	46	47	47	46	46	47	46	46	46	46	46	45	45	47	46
Ignition Oven Cf	0.09	0.09	0.03	0.03	0.14	0.09	NA	NA	-0.03	0.00	0.08	0.08	0.53	0.53	0.08	0.08
RAP (%)	20	20	10	10	20	20	20	20	30	30	20	20	20	20	15	15
RAS (%)	5	5	5	5	0	0	0	0	0	0	0	0	0	0	0	0
Aggregate Type	Granite		Granite		Granite		Granite		Granite		Granite		Limestone		Granite	
Binder Grade	PG 64S-22		PG 64S-22		PG 64S-22		PG 64S-22		PG52S-34		PG 58H-34		PG 58H-34 + antistrip		PG 64E-34	

Notes:
AC is Asphalt Cement
AP is as-placed
CAA is Coarse Aggregate Angularity
Cf is Correction Factor
FAA is Fine Aggregate Angularity
AFT is Asphalt film thickness
Gmb is the Bulk Relative Density
MD is Mix Design
RAP is Reclaimed Asphalt Pavement
RAS is Recycled Asphalt Shingles

Table 5 summarizes the properties of the virgin binders used in the experiment as well as the extracted and recovered binders from mixes obtained at the time of construction. It can be seen from Table 4 and Table 5 that the mix production successfully met the properties sought during design. For example, cells 18 and 21 were intended to be the same mix but have different virgin binders; cells 18 and 21 had equivalent binder contents and voids in the mineral aggregate. Cell 19 was successfully designed and constructed to investigate regressed 3.0% design air-voids. Cell 16 used 5.0% RAS to increase the asphalt binder ratio (ABR) and cell 17 used the same RAS content but lower RAP content to achieve an ABR like that of cell 18. Cell 22 required a liquid anti-stripping (LAS) agent to be used to successfully use the limestone aggregate. The inclusion of the LAS agent was reviewed with section sponsors and it was decided that including the LAS better represented the handling of limestone aggregate on other agency projects.

Table 5 Properties of Virgin and Recovered Binders (°C)

Cell	Design RAP%	Design RAS %	Production ABR	Extracted RAP Cont. PG	Extracted RAS Cont. PG	Virgin Binder		Extracted Binder Blend	
						Spec. PG	Cont. PG	Cont. PG	ΔTC
16	20	5	42%	86.5-19.8	120.7-23.0	64S-22	64.5-27.0	71.5-26.7	-1.9
17	10	5	28%					73.2-26.2	-2.1
18	20	0	24%		NA			71.1-26.5	-1.4
19	20	0	22%					70.8-25.8	-0.2
20	30	0	37%			52S-34	56.3-35.8	63.3-32.2	-0.9
21	20	0	24%			58H-34	63.2-35.6	70.2-30.3	-2.1
22	20	0	23%			58H-34	63.1-36.5	72.0-30.0	-3.5
23	15	0	18%			64H-34	73.4-37.8	72.0-31.7	-3.6

The constituent material properties did not create as wide of a range of cracking potential as expected during the experimental design stage. A difference of 12° C was intended during the design by selecting low temperature PG of -22 and -34 but the range of extracted low temperature PG was only 6.4° C (-25.8 for cell 19, -32.2 for cell 20). Excluding cell 20, the high temperature PG had an even narrower range of 3° C (70.2 for cell 21, 73.2 for cell 17. This is a result from relatively "soft" RAP and RAS (especially when compared to national values) and the continuous grading of the virgin binders. The continuous PG of the extracted virgin binder had very similar high temperature grades, except cells 20 and 23, because the continuous high PG was 64.5 and 63.2 for the PG 64-22 and PG 58H-34, respectively. On the low temperature side, the PG 64-22 had a continuous grade of -27 and the xx-34 binders were near -36. It is believed that the constituent material properties and the resulting lack of desired spread in the continuous PG contributed to the field performance that was observed, and is discussed, in the following section.

2. FIELD PERFORMANCE RESULTS

This section will discuss the traffic and environment that the cells were subjected to, the in-situ pavement responses measured, and the HMA surface performance throughout the study. The field performance of the MnROAD CG cells was routinely monitored with nondestructive testing and instrumentation embedded within the pavement structure.

2.1 Traffic and Environment

The CG cells were open to I-94 westbound traffic on November 2, 2016. The data in Table 6 shows the total number of vehicles, trucks, and resulting ESALs, that were measured by a weigh-in-motion immediately east of (before) Cell 23.

Table 6 Traffic Data Measured by a Weigh-in Motion

Start date	11/2/2016		
End date	4/1/2022		
Total days	1,976		
Full traffic days on CG	1,102		
Lane	Passing	Driving	Total
Total vehicles	15,697,553	15,275,189	30,972,742
Trucks	1,393,851	3,493,801	4,887,652
ADT	14,245	13,861	28,106
HCADT	1,265	3,170	4,435
%Trucks	9	23	16
ESALs*	839,114	3,225,682	4,064,796

Environmental monitoring of the test cells included embedded thermocouples throughout the pavement structure, moisture content sensors in the base and subgrade, and an onsite weather station to measure air temperature, wind-speed, and precipitation. The annual maximum and minimum pavement temperatures from the CG cells is shown in Figure 2. The HMA temperatures shown are from thermocouples located a half inch under the surface. The lowest air temperature of -30°F (-34.4°C) occurred in January of 2019 and resulted in a HMA temperature of -20°F (-28.9°C).

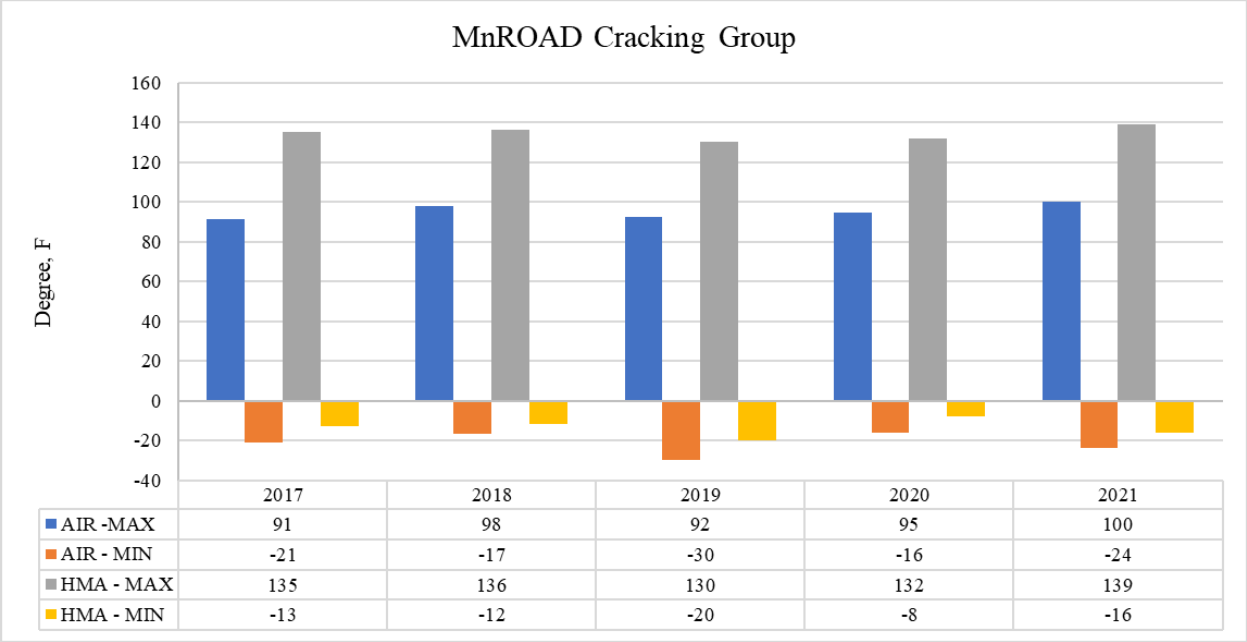

	2017	2018	2019	2020	2021
AIR -MAX	91	98	92	95	100
AIR - MIN	-21	-17	-30	-16	-24
HMA - MAX	135	136	130	132	139
HMA - MIN	-13	-12	-20	-8	-16

Figure 2 Temperature Extremes during CG Experiment

2.2 Structural Response

2.2.1 FWD Collection and Layered Elastic Back-calculation

Falling Weight Deflectometer (FWD) testing was performed in the outer wheel-path (offset 9.5 ft from the centerline) of the driving and passing lanes at ten permanent FWD testing stations located approximately every 50 ft. within each section to monitor structural health at the same location over time. Standard FWD sensor spacing for Long Term Pavement Performance (LTPP) testing was used with one drop at each target load levels of 6, 9, and 12 kips (Schmalzer, 2006). A 6-inch (150 mm) plate was used during pavement testing and a 8.9 inch plate was used for testing directly on the unbound layers. Testing was performed monthly from March through November. Data collected when the pavement structure was completely or partially frozen (as indicated by thermocouple readings at various depths recorded at the same time as FWD collection) were excluded from the analysis discussed in this section. Testing was always conducted in the direction of traffic. Additionally, a set of tests were taken on the unbound material prior to HMA paving and again shortly thereafter. Load-deflection tests on the unbound material were performed using two drops at each target load level of 6 and 9 kips. Test spacing for the unbound material was reduced to 25 ft.

In-situ elastic moduli for the pavement, base, and subgrade were back-calculated using the Odemark-Boussinesq equivalent layer program, Elmod 6 from Dynatest (Schmalzer, 2007). The pre-paved base, subbase, and subgrade were first modeled as a three-layer system (Class 6, Class 3, and Subgrade) with ASTM D5858 suggested seed moduli (ASTM, 2015). Design values were used for aggregate thickness with the subgrade assumed to be semi-infinite. The resulting values were then used to model the pavement system as a three-layer system comprising of an HMA surface layer, a Class 6 aggregate base layer and a combined Class 3/Select Granular/Subgrade

layer assumed to be semi-infinite. The surveyed thickness values for each cell were used for the HMA thickness input. The ASTM D5858 suggested seed modulus was used for the AC layer. Since previous reporting by Stubstad (2002) has shown that FWD results track from layer to layer reasonably well, the previously back-calculated results were used for seed moduli for the base and subgrade layers. Back-calculations were performed using the 9 kip drop on each of the stations.

2.2.2 FWD Results and Analysis

As expected, the deflection data collected showed a strong correlation to temperature. Figure 3 shows the maximum deflections for cell 19 plotted along with the maximum mid-HMA temperature versus the testing date for the duration of the experiment. Deflections vary with the seasonal trends, having the lowest deflections in the early spring and late fall and the highest deflections during the warmer summer months. Similar trends in deflection with respect to temperature were observed in all other cells in the study.

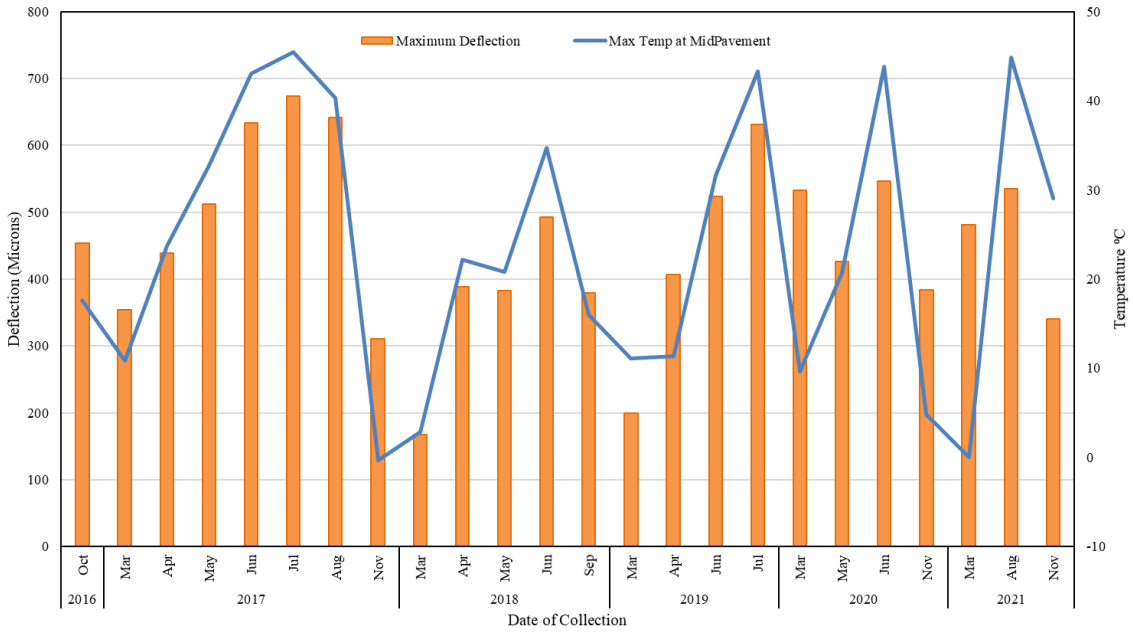

Figure 3 Maximum Deflection against Maximum Temperature for Cell 19 over Time

The back-calculated results of the unbound layers (Figure 4) reflected the construction difficulties in preparing the base for cells 20 through 23. Specifically, it was noticed that the unbound layer values for cell 23 were significantly lower than other cells. Slight variances were noted in cells 20 and 22, but due to the reduced spacing of the unbound testing these appeared mostly in between the future stations. However, cell 23 appeared to have lower unbound moduli throughout its entirety as was therefore noted as an outlier and removed from the average seed moduli values. As shown previously in Table 2, the CG cells were constructed in two phases. Cells 20-23 were constructed relatively late in the Minnesota paving season (September and October 2016) also show more variability in unbound material properties.

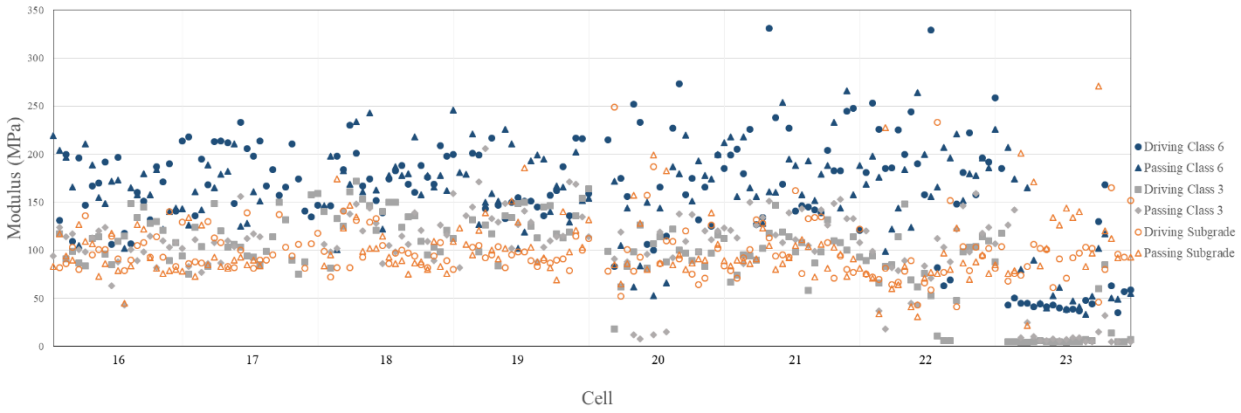

Figure 4 Back-calculated Layer Moduli at 9 kip for Unpaved Cells

Back-calculations were performed using a three-layered system with seed moduli of 508 ksi, 25.4 ksi, 16.0 ksi for the asphalt, class 6, and subgrade layers, respectively. The asphalt moduli (E1) were then adjusted to 68°F by establishing an individual logarithmic asphalt temperature adjustment factor for each cell, per LTPP guidelines (Miller and Dellinger, 2003). The shift in moduli (E1') is shown for Cell 19 in Figure 5.

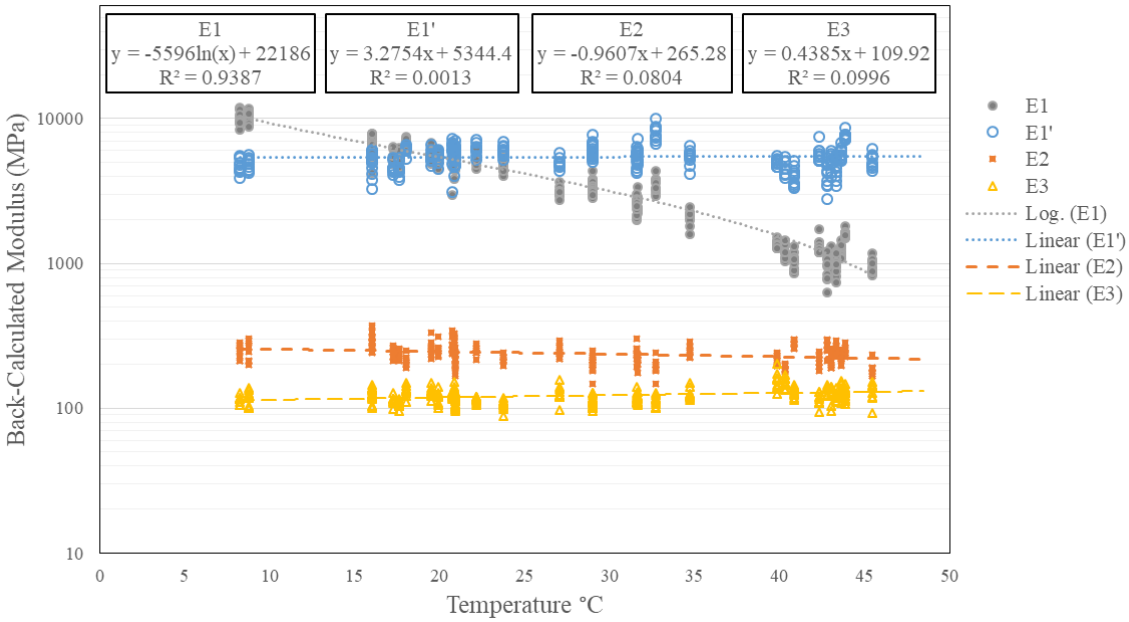

Figure 5 Moduli for Cell 19 With Temperature Adjustment Made to Asphalt Modulus

Moduli were then averaged at each station for each year of testing and plotted for comparison. A scatterplot of the HMA moduli at a reference temperature of 68°F (Figure 6) shows two distinguishable groupings that correspond to the lower temperature binder grade, PG XX-22 and PG XX-34. Each data point represents the yearly average for stations 1 through 10 within each

cell. Moduli appear to have some spatial dependency, which may be caused by the variations in pavement thickness and subgrade conditions at those points. Cells showed a varying dependency on lane, but no overall trend was evident. Moduli showed some seasonal dependency, likely because of subgrade conditions, but did not otherwise show a dependency on time indicating a lack of widespread degradation of the pavement structures.

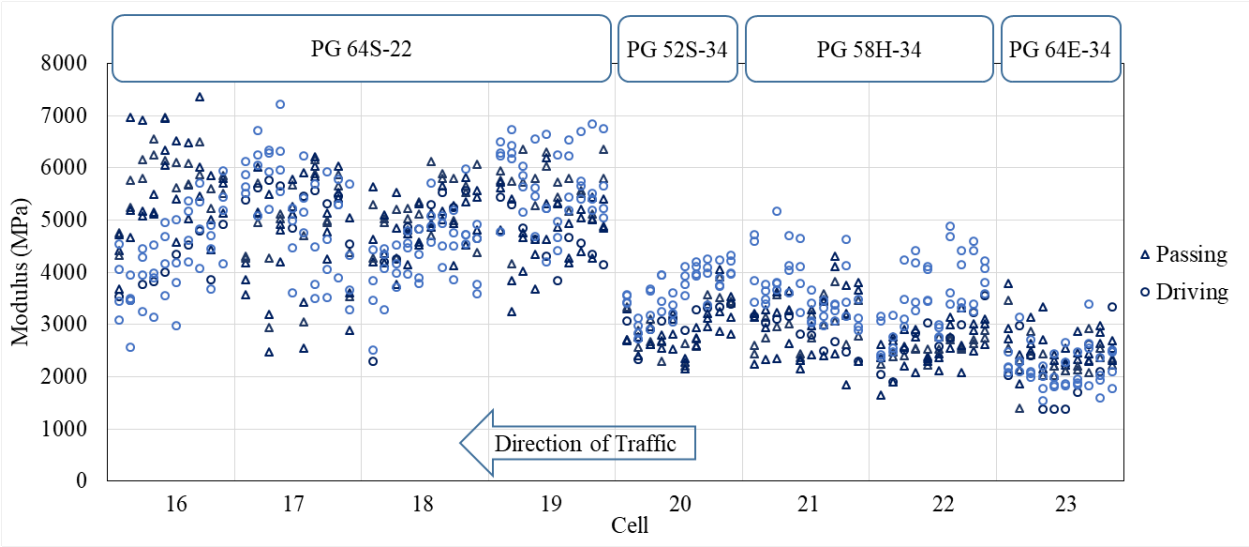

Figure 6 40 kN (9 kip) Back-calculated Asphalt Layer Moduli for Test Cells

Upon closer inspection, individual stations did show some loss of HMA modulus consistent with cracking surveys. Moduli for the passing lane of Cell 17, shown in Figure 7 displayed both tendencies of spatial dependence on station and loss of moduli corresponding with pavement distress. At stations where little cracking was observed, as in Cell 20 shown in Figure 8**,** moduli tended to have less variation.

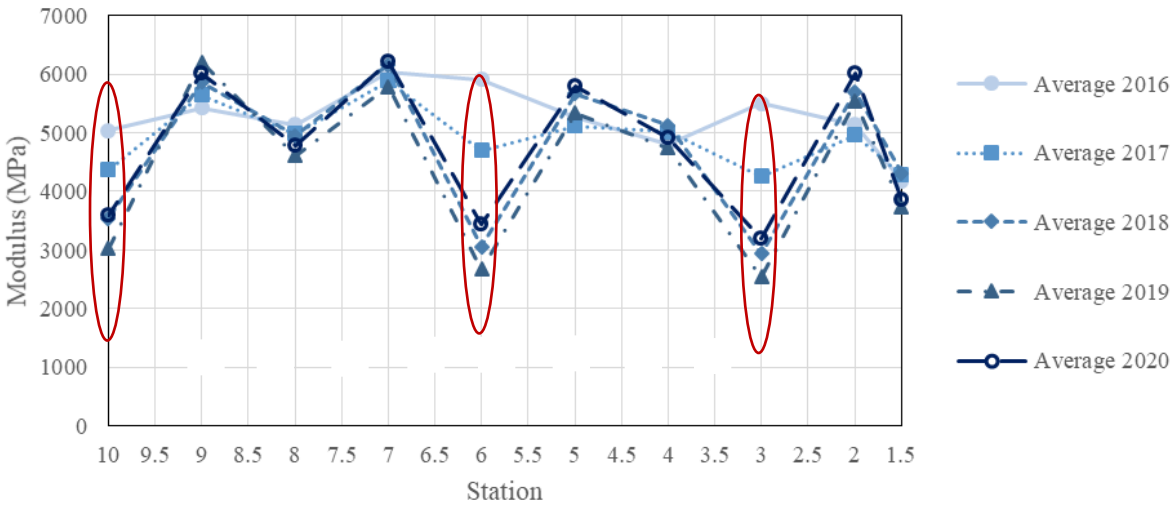

Figure 7 Temp Adjusted Asphalt Moduli for Cell 17 Passing Lane (Highlighted around Cracking)

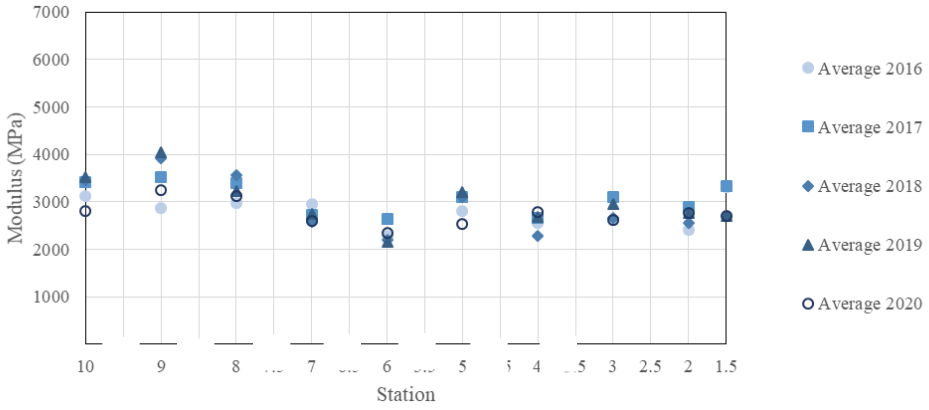

Figure 8 Temp Adjusted Asphalt Moduli for Test Cell 20 Passing Lane

2.3 Rutting, Ride, And Cracking

2.3.1 Rutting

Rutting was measured in both wheel-paths in the driving and passing lane biannually, in the late spring and fall, during the experiment. The rutting results presented for each cell were measured using MnROAD's automated laser profile system (ALPS) (Worel et al., 2004). The ALPS was used to measure the transverse profile at fixed monitoring points spaced every 50 ft (15.2 m). The results are presented in Figure 9. All sections had maximum rutting values classified by FHWA MAP-21 (FHWA, 2017) as "Good", rut depth less than 5 mm, except for the outside wheel path of the driving lane of cell 18. It is an important finding that all sections had equivalent rutting performance considering that different binders were used, especially with respect to the PG 52S –34 used in cell 20 which had a substantially lower high temperature PG than the other cells. The results presented are from November 2019 after three full years; rutting was collected through the end of the study however localized cracking and potholing began to impact rutting results.

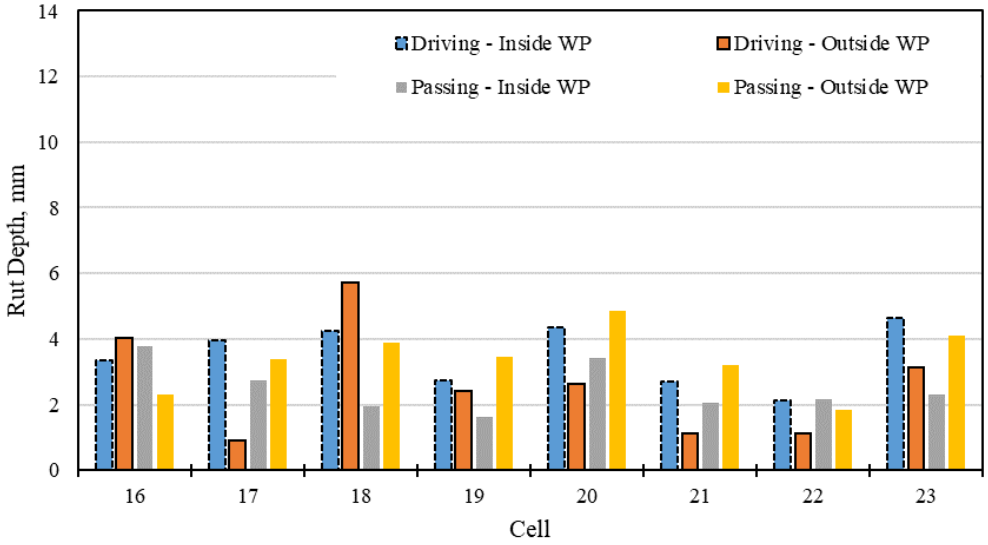

Figure 9 Rut Depth Measured November 2019

2.3.2 Ride

The longitudinal profile was measured using MnROAD's lightweight inertial profiling system (LISA) (Izevbekhai et al., 2017) and was used to calculate the International Roughness Index (IRI) as presented in Figure 10. Similar IRI results were evident amongst the cells except for cell 23. Cell 23 initially had higher IRI values, and it stayed rougher throughout the experiment. The data were scrutinized to ensure that a "bump" in front of cell 23 was not artificially influencing the IRI for cell 23. This was further supported when the "bump" was repaired in summer 2018 and the IRI of cell 23 did not change. Seasonal spikes can also be seen in the data in March 2018, 2019, and 2020 that is attributed to winter/spring thaw. All sections except cell 23 and the driving lane of cell 18 in 2021 stayed under the FHWA MAP-21 (Miller and Dellinger, 2003) threshold between "good" and "fair" of 105 in/ mile, even while surface distress developed. Roughness data are also presented in tabular format in Table 7 and Table 8 to better show the results for each individual section.

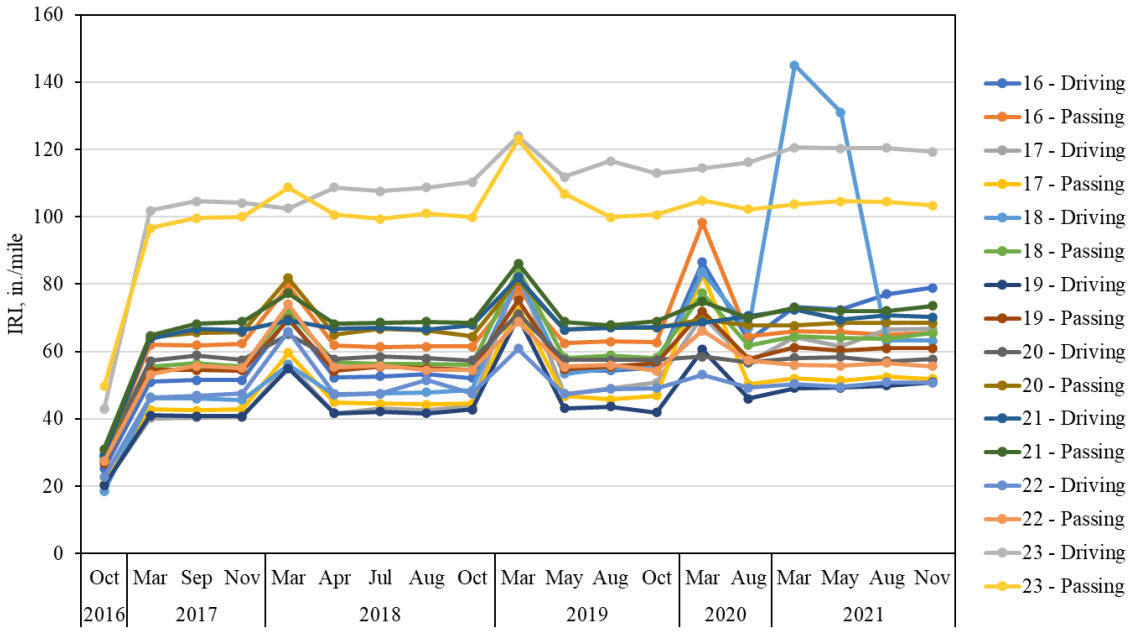

Figure 10 Roughness from October 2016 through November 2021

Table 7 Roughness for Cells 16-19

	Average of IRI (in / mile)							
Year - Month	16 - Driving	16 - Passing	17 - Driving	17 - Passing	18 - Driving	18 - Passing	19 - Driving	19 - Passing
2016 - Oct	25.2	29.3	20.4	20.6	18.4	30.7	20.1	26.6
2017 - Mar	51.0	62.0	40.1	42.8	46.1	55.6	41.1	54.5
2017 - Sep	51.5	61.8	40.4	42.5	46.0	56.4	40.7	54.5
2017 - Nov	51.5	62.3	40.6	43.0	45.6	55.6	40.7	54.4
2018 - Mar	70.2	79.4	56.3	59.6	56.1	72.0	55.0	69.6
2018 - Apr	52.3	61.8	41.7	44.9	47.1	56.7	41.7	54.2
2018 - Jul	52.6	61.3	43.1	44.5	47.5	56.3	42.2	55.5
2018 - Aug	53.3	61.5	42.6	44.2	47.9	56.3	41.7	55.0
2018 - Oct	52.1	61.5	43.7	44.5	48.5	56.1	42.8	54.5
1019 - Mar	80.8	78.5	83.2	73.4	82.6	84.5	70.4	75.3
2019 - May	54.2	62.4	47.4	46.8	53.4	58.2	43.1	54.7
2019 - Aug	54.4	62.9	49.0	45.8	55.0	58.8	43.6	55.5
2019 - Oct	55.3	62.8	50.7	46.9	55.3	58.2	41.8	56.4
2020 - Mar	86.5	98.3	70.5	83.1	83.5	77.3	60.5	72.0
2020 - Aug	63.4	64.5	56.9	50.2	66.9	61.8	46.0	57.7
2021 - Mar	73.2	66.1	64.2	52.0	145.0	64.5	49.1	61.2
2021 - May	72.4	65.8	61.7	51.4	131.1	64.0	49.3	60.4
2021 - Aug	77.0	65.1	66.4	52.5	63.2	63.9	49.9	61.0
2021 - Nov	78.9	65.6	66.7	51.8	63.2	65.5	50.9	61.0

Table 8 Roughness for Cells 20-23

	Average of IRI (in / mile)							
Year - Month	20 - Driving	20 - Passing	21 - Driving	21 - Passing	22 - Driving	22 - Passing	23 - Driving	23 - Passing
2016 - Oct	28.5	27.4	29.3	31.1	22.7	27.4	43.0	49.6
2017 - Mar	57.2	64.3	63.9	64.7	46.4	53.3	101.9	96.7
2017 - Sep	58.8	65.6	66.7	68.2	46.9	55.8	104.6	99.7
2017 - Nov	57.5	65.8	66.3	68.8	47.5	55.2	104.1	100.0
2018 - Mar	65.1	81.8	69.3	77.3	65.9	74.0	102.5	108.7
2018 - Apr	57.7	65.0	66.9	68.2	47.4	55.3	108.7	100.6
2018 - Jul	58.5	66.7	67.0	68.6	47.5	55.8	107.6	99.4
2018 - Aug	58.0	66.3	66.6	68.8	51.5	54.5	108.7	101.0
2018 - Oct	57.4	64.5	67.8	68.6	47.5	54.5	110.3	99.9
1019 - Mar	71.2	81.1	82.1	86.2	60.9	68.8	123.9	123.0
2019 - May	57.5	66.4	66.4	68.8	47.4	55.5	111.9	106.8
2019 - Aug	57.5	67.2	67.0	67.8	48.8	55.9	116.7	99.9
2019 - Oct	57.5	67.0	67.2	68.9	49.1	54.2	113.0	100.6
2020 - Mar	58.5	69.4	68.6	74.8	53.1	66.3	114.4	104.9
2020 - Aug	56.7	67.8	70.5	69.9	49.3	57.4	116.2	102.2
2021 - Mar	58.2	67.7	72.4	73.1	50.4	55.9	120.6	103.8
2021 - May	58.3	68.5	69.4	72.1	49.5	55.8	120.3	104.6
2021 - Aug	57.1	68.6	70.8	72.1	50.9	56.6	120.5	104.4
2021 - Nov	57.7	68.5	70.2	73.5	50.7	55.6	119.3	103.3

2.3.3 Cracking

Cracking in each cell was monitored and quantified by conducting visual distress surveys following LTPP Pavement Distress classifications. It should be kept in mind that the cracking values reported at MnROAD are conducted under ideal conditions and, as a result, is greater than the amount that would be detected at typical travel speeds. The percentage of total lane area with cracking is shown over time for each cell in Figure 11. It can be observed that prior to the winter of 2018/2019, very little cracking was evident in any of the cells. In early 2019, the amount of cracking began to dramatically increase for many of the cells.

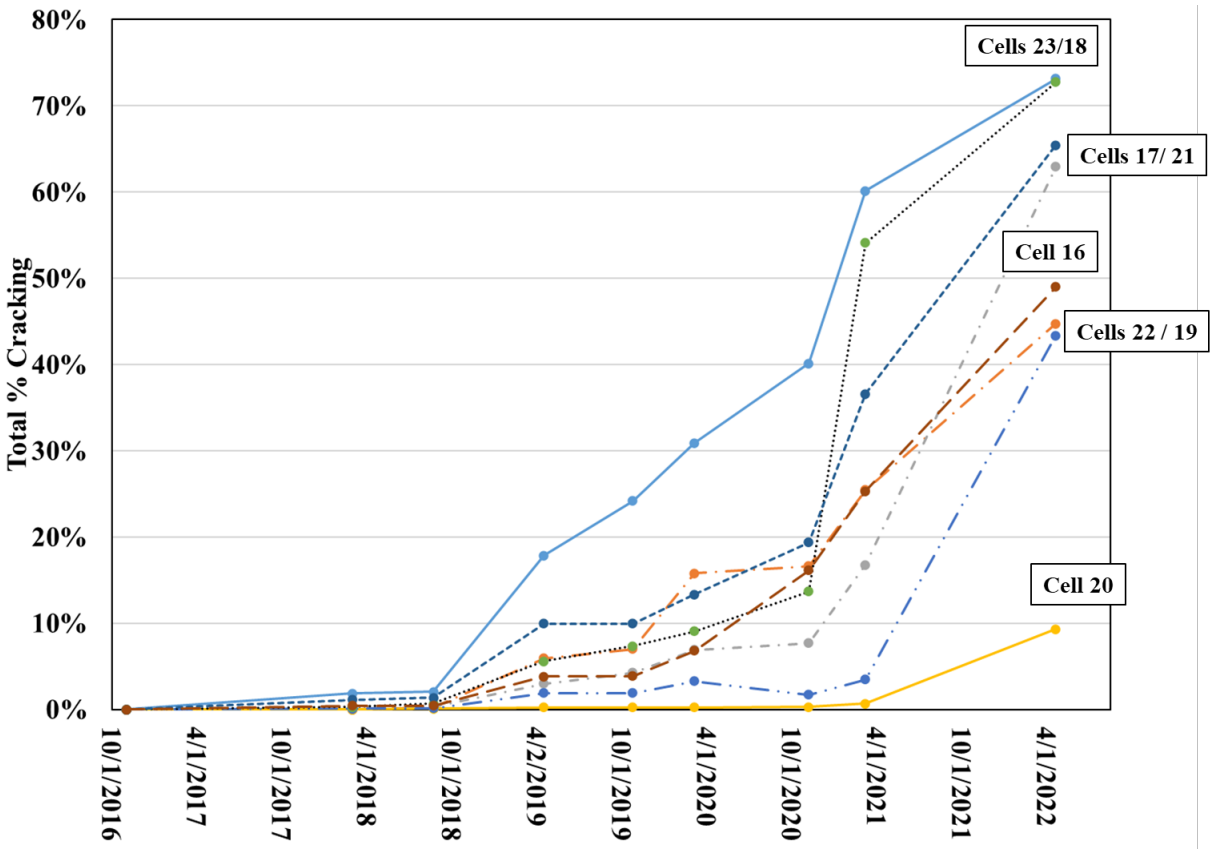

Figure 11 Total Cracking of Each Cell over Time

Although low temperature (i.e., transverse) cracking was the intended and expected mode of cracking for the experiment, the majority of the cracking observed was in the wheelpaths, which suggests that the cracking was load related. Forensic investigations conducted from 2019 to 2021 sought to identify the causes of the observed cracking and to possibly identify areas within the cells to exclude from the laboratory to field correlations due to other cracking mechanisms.

In 2019, cores were taken in each section with distress to help identify the source and extent of the observed cracking. Several notable conclusions were drawn:

- Very little traditional transverse low-temperature thermal cracks were observed. Most transverse cracks observed were less than 4 ft and located in the wheel-paths.
- Cores taken on transverse cracks showed cracks extended full depth through the total 5-inch HMA thickness (Figure 122(a)- (b)).
- Cores taken in fatigue cracking areas were removed in two pieces with the surface and lower HMA layers separating at the interface. The lower lift of HMA did not have any observable cracks or deterioration (Figure 12(c)- (d)).
- Cracking that was most likely caused by traffic or a construction related issue was separated from the transverse cracking investigation. Cracking within the wheelpaths was identified as traffic related. Cracking along the longitudinal construction joints and

non-wheelpath cracking were the primary construction related cracking observed.

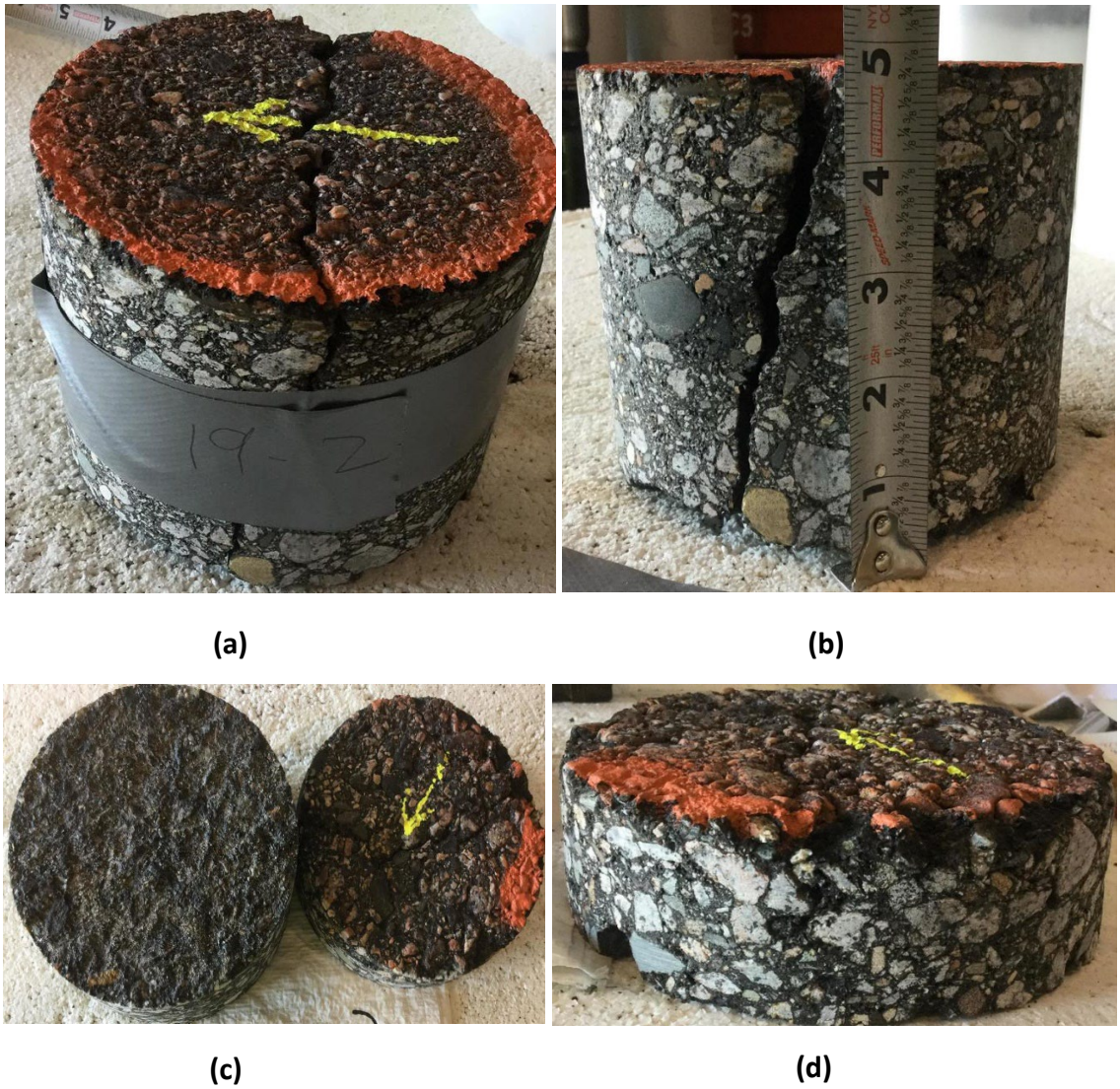

Figure 12 Cores taken in April 2019. (a)-(b) Cell 19 Cores Showing Transverse Crack Extending Full Depth of Core. (C)-(D) Cell 23 Cores Showing Fatigue Cracking on Surface Does Not Extend Into Lower Lift

In early 2020, the observed cracking from the distress surveys identified more cracking had occurred over the winter months, especially the amount of wheel-path cracking. Based on the 2019 coring efforts, it was known that areas with surface fatigue also had weak interface bonding, but the extent of the weak bonding condition was not known. A testing plan was developed to obtain and test the bond strength of cores taken in non-distressed areas between the wheelpaths every 50 feet within a section. All bond strength values of these cores passed the recommended minimum threshold of 100 psi (West et al., 2005) indicating that the sections had originally been constructed with an adequate bond and that the delamination and surface distress were developing simultaneously. Also in early 2020, potholes were observed in the driving lane of cell

18 along the outside wheel-path and lane/shoulder edge stripe, as shown in Figure 13. The potholes were 2 inches deep, which was the thickness of the surface layer.

Figure 13 Cell 18 Potholes along Longitudinal Construction Joint in 2020

In spring 2021, the number of potholes continued to increase. As the potholes were being cleaned and prepared for patching material, it was noticed that the surface 2-inch lift was debonded over the whole driving lane area (Figure 14a). In May 2021, the entire driving lane of cell 18 and 300 feet of the driving lane in cell 23 were milled (Figure 14b). Prior to repaving with 2 inches of HMA, the milled surface was inspected, and no fatigue cracking or major structural distress was observed on the lower 3 inches of HMA pavement structure. Subsequently, no cracking has been observed in the milled and repaved areas (Figure 14c).

(a)

(b)

(c)

Figure 14 Cell 18 (a) Potholes Along Longitudinal Construction Joint in March 2021; (c) Milling of Surface Lift; (c) Repaved Driving Lane

From the documented cracking distress and forensic investigations, it was apparent that moisture induced HMA layer delamination occurred in these test sections and confounded the low-temperature cracking performance that was the intended focus of the experiment. The research team's hypothesis is that moisture initially entered the pavement structure through the longitudinal construction joints. With the cumulative degenerative effects of traffic and freeze/thaw cycles, the HMA interface was weakened to the extent that the surface HMA no longer behaved monolithically with the remainder of the pavement structure. Thus, the cracking that developed and was observed at the surface was confined within the upper lift of HMA.

To evaluate the HMA performance without the confounding influences of delamination and traffic loading, the shoulders of each test sections were evaluated for low temperature cracking since they were constructed with the same mixtures and cross-section as the travel lanes, but were not subjected to traffic. Table 9 presents the cracking results for each cell from visual distress surveys at three survey dates. Cracking is reported as total cracking and cracking in meters per 500 m considering the area of the shoulder in each section is 4.27 m x 152.4 m (14 ft x 500 ft). Based on distress survey results from shoulders, cell 20 was found to have the least amount of transverse cracking while cell 22 had the most transverse cracking. This field cracking data (specifically thermal cracking/transverse cracking) was used for assessing correlations between laboratory test results and field performance in section 3. The appropriateness of using the shoulder cracking data for lab test correlations was confirmed by matching trends in the cracking data from the shoulders and travel lanes (e.g., cell 20 had very little cracking in shoulders and travel lanes).

Table 9 Transverse Cracking in the Shoulder of Test Sections

Cell #	Survey Time					
	Spring 2020		Spring 2021		Spring 2022	
	Age = 3 ½ years		Age = 4 ½ years		Age = 5 ½ years	
	Total Transverse Cracking (ft)	Transverse Cracking (m/500m)	Total Transverse Cracking (ft)	Transverse Cracking (m/500m)	Total Transverse Cracking (ft)	Transverse Cracking (m/500m)
16	94	22.0	216	50.6	269	63.0
17	68	15.9	211	49.4	273	64.0
18	52	12.2	263	61.6	294	68.9
19	66	15.5	150	35.2	180	42.2
20	0	0.0	0	0.0	5	1.2
21	34	8.0	105	24.6	212	49.7
22	557	130.5	682	159.8	1037	243.0
23	122	28.6	256	60.0	335	78.5

2.4 Conclusions from Field Performance

Based on the field performance summarized in this section, the following conclusions were made:

- The Cracking Group cells generally matched expected trends (except for cell 23) with respect to deflection and stiffness; however, the range was tighter than expected due to material properties of the HMA components.
- Field monitoring and forensic investigation identified delamination as a major contributor to the observed cracking performance for all test cells. It is believed that water entered the HMA structure through longitudinal construction joints (both centerline joint and driving lane/ shoulder joint). The combination of water, traffic, and environment deteriorated the bond between HMA layers resulting in severe distress in the surface two inches of HMA. This progression occurred in all sections.
- Cell 23 (HiMA) did not have the expected field performance. Oversaturation of the base and subgrade during construction and a high initial roughness led to non-LTC distress throughout the section. This section does not match expected behavior and trends for

HiMA. The performance of Cell 23 further emphasizes the importance of the base and subgrade in the overall performance of the pavement structure. This section was expected to be the most crack resistant, but it had the most cracking due to poor base and subgrade support.

- Cell 20 (PG 52-34) had the least amount of cracking and the best overall field performance. It is an important finding that this section had equivalent rutting performance under Interstate traffic despite having a significantly lower high temperature virgin binder grade than the other cells. Cell 20 used a PG 52S-34 binder with 30% RAP and had less than 3 mm of rutting.
- Transverse cracking in the shoulders was quantified to capture the LTC performance of each mix without the influence of traffic and delamination. Using the shoulder data for laboratory to field correlations was reaffirmed by similar trends in test section performance from traveled lanes to the shoulders (i.e., cell 20 had very little cracking in traveled lanes and very little in shoulders.)

3. LABORATORY RESULTS AND FIELD PERFORMANCE CORRELATIONS

This section discusses the results of the cracking tests conducted in this experiment, and their correlations with the low temperature cracking performance of the test cells. The discussion covers tests that are used to assess low temperature cracking performance of asphalt mixtures, as well as intermediate temperature cracking tests that have gained popularity for evaluating load-related cracking to determine if meaningful correlations exist with the field performance of the cells. The low temperature cracking tests included the disk-shaped compact tension test (DCT), the low-temperature semi-circular bend test (SCB), the uniaxial thermal stress and strain test (UTSST), the Indirect Tensile Creep Compliance and Strength Test (IDT-CC&S), the asphalt concrete cracking device test (ACCD), and the mixture bending beam rheometer test (BBR_m). The intermediate temperature cracking tests include the Indirect Tensile Asphalt Cracking Test (IDEAL-CT), the Illinois Flexibility Index Test (I-FIT), and the NCAT Overlay Test (NCAT-OT). Table 10 summarizes the cracking tests conducted in the study, the test procedures followed, the research parameters evaluated, and the labs that conducted the tests.

Table 10 Cracking Tests Evaluated in the Study

Test	Test Method	Research Parameter	Lab Conducting Test
DCT	ASTM D7313	Fracture Energy	MnDOT
Low Temperature SCB	AASHTO TP 105[1]	Fracture Energy, toughness	University of Minnesota
UTSST	ASTM WK60626	CRI_{Env}	University of Nevada Reno
IDT&CCS	AASHTO T 322	Critical Temperature	NCAT
ACCD	N/A	Cracking Temperature	Ohio University
BBR_m	AASHTO TP 125-16	Creep Modulus and m-value	University of Minnesota
I-FIT	AASHTO TP 124[2]	FI	NCAT
IDEAL-CT	ASTM D8225-19	CT Index	NCAT
NCAT-OT	TEX-248-F[3]	β	NCAT

[1]Test has been standardized as AASHTO T 394.

[2] Conducted with modified frequency, gap and failure definition.

[3]Test has been standardized as AASHTO T 393

The cracking tests were conducted on plant mixes sampled during construction. For each mix, two sets of plant mixed, laboratory compacted (PMLC) specimens were prepared. The first set was compacted after samples were reheated to the compaction temperature (referred to as PMLC-RH). The second set of specimens were prepared using reheated mix then critically aged for six hours at 135°C prior to compaction (referred to as PMLC-CA). For the UTSST, the second set of PMLC specimens were prepared with reheated mix then the compacted samples were long-term oven aged at 85°C for 5 days per AASHTO R30. Low-temperature SCB tests were only conducted on PMLC-RH specimens.

The field cracking data used to assess the correlations with the different test parameters corresponds to transverse cracking in the shoulders of each section (driving and passing lane shoulders). As discussed in Section 2, the shoulders were used to assess the low temperature cracking performance because the shoulder performance was not confounded by delamination and traffic. Correlations were made using distress survey results from 2020, 2021, and 2022 to see how pavement age compared to laboratory results of tested specimens produced under different aging conditions; RH and CA. Correlation plots using SPR 2022 distress surveyed transverse cracking results from the shoulders against laboratory results from the test methods used in this work are presented in sections 3.1 through 3.9. All summarized correlation results are presented in section 3.10.

3.1 Disk-shaped Compact Tension Test (DCT)

The DCT test (ASTM D7313-20) is a monotonic test with specimens fabricated from larger Superpave gyratory compactor (SGC) samples or from cores that are then cut to 50 mm in thickness. A flat edge is cut on one side of the specimen for mounting gage points, a 62.5 ± 5.0 mm notch is cut toward the center of the specimen from the flat edge, and two 1-inch diameter holes are drilled on each side of the notch. The test is performed by pulling the specimen apart at a specified rate measured with a crack mouth opening displacement (CMOD) gage. The recommended test temperature is the low PG grade of the binder plus 10°C. Fracture energy is calculated by determining the area under the Load-CMOD curve normalized by the initial ligament length and thickness. After conditioning to the test temperature, the specimens are tested at a constant rate of 0.017 mm/sec until the load drops below 0.1 kN.

The DCT test has been reported to have a coefficient of variation (COV) ranging between 10 and 15% depending on variables such mixture composition and test temperature (Braham et al., 2007). Marasteanu et al. (2012) conducted research as part of a national fund pool study and reported that typical COV associated with the test was around 10%. However, higher COVs were reported for some mixes evaluated. A preliminary fracture energy threshold of 400 J/m^2 was recommended for short-term aged, lab-compacted specimens. Higher thresholds were recommended for more critical projects and higher traffic level as presented in Table 11.

Table 11 Recommended DCT Fracture Energy (G_f) Criteria (Marasteanu et al., 2012)

Criteria	Project Criticality/Traffic Level		
	High, >30M ESALs	Moderate, 10-30M ESALs	Low, <10M ESALs
Fracture Energy, minimum (J/m^2), Low PG +10°C	690	460	400

A statistical summary of the DCT results for PMLC-RH and PMLC-CA specimens is shown in Table 12. The number of replicates per mix ranges from 10 to 12. The effect of aging is consistently reflected in these results with lower values for the PMLC-CA samples compared to the PMLC-RH samples. These results generally yielded good repeatability with COVs between 10 to 16%. For PMLC-RH results, all the mixes except mix from cell 22 had results above the 400 J/m^2 threshold. Mix from Cell 22 is the only mix with limestone aggregate. Previous studies have shown that there is a significant effect of aggregate type on the DCT fracture energy, with limestone aggregate yielding lower values (Braham et al., 2007, Mandal et al., 2017).

Table 12 Fracture Energy DCT Test Results

Cell #	Mixture Description	PMLC-RH			PMLC-CA		
		G_f (Avg.)	Std. Dev.	COV (%)	G_f (Avg.)	Std. Dev.	COV (%)
16	Moderate RAP + RAS	455	48	11	407	66	16
17	Low RAP + RAS	425	59	14	381	40	11
18	Moderate RAP	419	43	10	395	55	14
19	Moderate RAP, extra AC	445	65	15	413	47	11
20	High RAP, softer binder	508	72	14	474	70	15
21	Moderate RAP, softer binder	573	64	11	445	64	14
22	Limestone, 9.5 mm NMAS, PMA	341	43	13	301	31	10
23	Moderate RAP, HiMA	668	95	14	509	72	14

Figure 15 presents the correlations between PMLC-RH and PMLC-CA DCT results and transverse cracking. As presented in this figure, the DCT results show very good correlations to the field performance of the sections with R^2 value of 0.76 and 0.85 for the results of PMLC-RH and PMLC-CA samples, respectively. In addition, DCT results on PMLC-CA and PMLC-RH samples were able to identify the mixes with the worst performance (Cell 22).

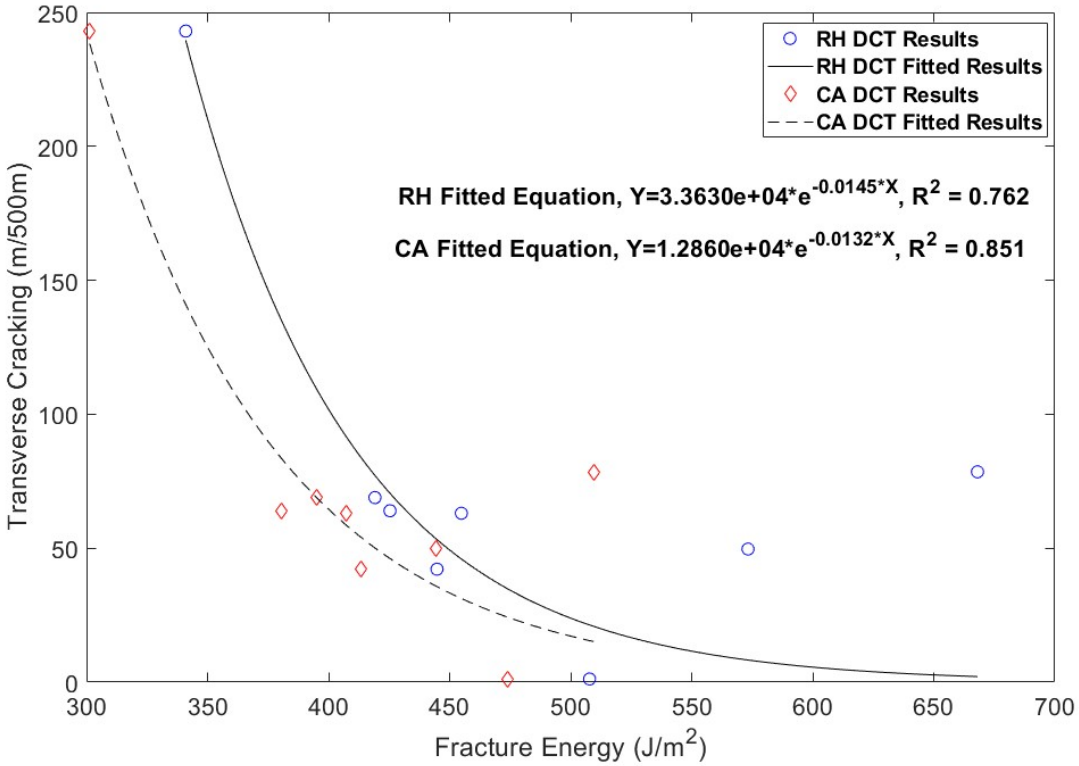

Figure 15. Correlation of DCT Fracture Energy Results and Transverse Cracking Performance

Figure 16 shows the DCT results from best to worst for the PMLC-CA samples. The whiskers represent plus and minus one standard deviation of the fracture energy results. The chart also includes the cracking performance of the test sections. As indicated in this plot, the DCT test does a good job capturing the overall expected trend for most mixes (higher DCT values equal better cracking performance) except for mixes from Cell 23 and Cell 19. An ANOVA (α=0.05) with Tukey statistical grouping method was used to statistically rank the DCT results for the PMLC-CA samples. The results of these groupings are also shown in Figure 16 with the letters on top of the bars (A, B, C and D) indicating four groups. In this analysis, statistical means that do not share a letter are significantly different. From this analysis, mix from cell 22 did not share a letter with any of the other mixes. All the other mix groupings showed some overlap.

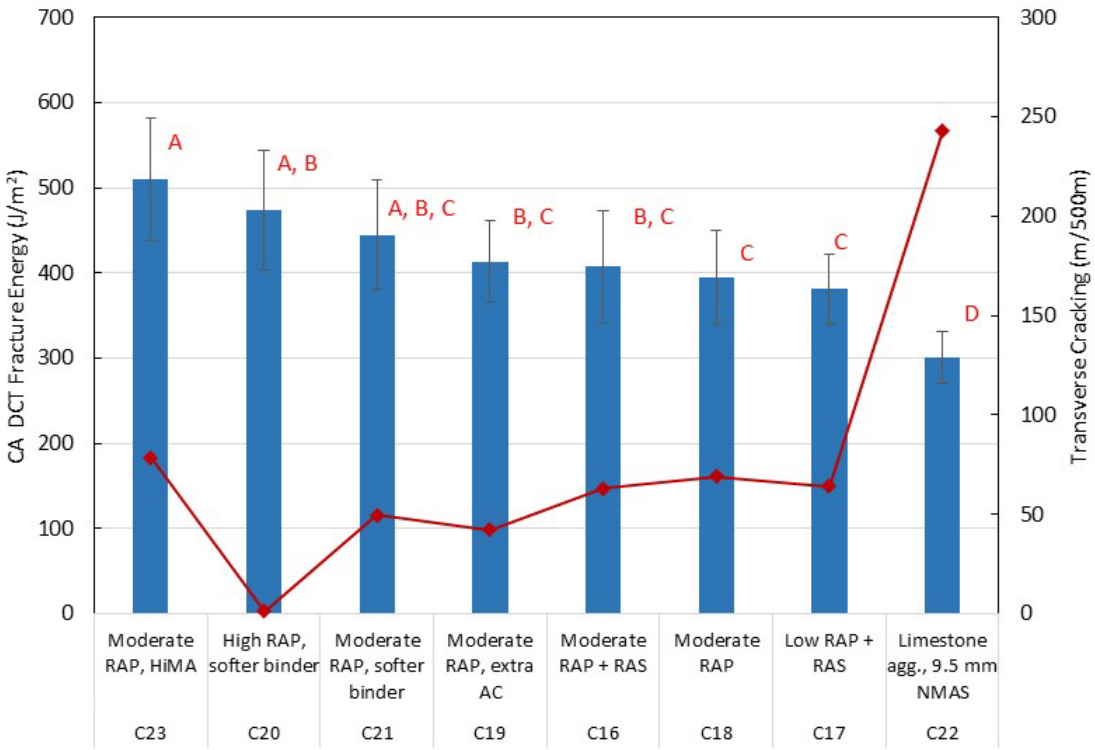

Figure 16 Statistical Comparison of CA DCT Fracture Energy Results for Mixtures and Low Temperature Cracking Field Performance

3.2 Low Temperature Semi-Circular Bend Test (SCB)

The low temperature SCB test (AASHTO T 394-21) is the "Standard Method of Test for Determining the Fracture Energy of Asphalt Mixtures Using the Semicircular Bend Geometry". For this test, specimens are semicircular with a thickness of 25 mm cut from SGC cylinders or field cores. A notch is cut at the bottom of specimen with a depth of 15 mm. The procedure recommends testing at two temperatures, the low PG grade plus 10°C and the low PG grade minus 2°C. The specimens are simply supported by two bars on the flat surface and the load is applied to the curved surface above the notch. The load is applied such that the notch opens at a rate of 0.0005mm/s. Fracture energy and fracture toughness are calculated from the load and displacement data. The COV for within lab results has been reported to be around 20% (Zhou et al., 2016). Marasteanu (2012) proposed limits for the SCB test results using a correlation with field cracking performance and results obtained from cores (tests conducted at 10°C warmer than the low temperature grade). Based on this relationship, a minimum fracture energy of 350 J/m^2 was proposed. It was recommended to adjust this limit to 400 J/m^2 to account for the aging effect. In addition, the researchers suggested a fracture toughness value of 800 kPa×m$^{0.5}$ as a possible limit.

The average fracture energy and toughness results at -12°C and -24°C for PMLC-RH are presented in Table 13 and Table 14. Three replicates per mix were tested. SCB tests were only conducted on PMLC-RH specimens. The fracture energy results yielded COVs between 7 to 35%, and 9 to 37%

for tests cunducted at -12°C and -24°C, respectively The fracture toughness results had COVs between 5 to 15%, and 6 to 17% for tests conducted at -12°C and -24°C, respectively. Most of the mixes showed the expected trends with respect to temperature, with fracture energy decreasing at the lower temperature due to the embrittlement of the mix. Fracture toughness increased as temperature decreased as this parameter is related to the peak stress the specimen experiences during testing. Mix from Cell 22 (limestone mix) showed the worst performance in terms of fracture energy and toughness at both test temperatures. Previous research indicates the sensitivity of the test to aggregate type with granite mixtures has higher fracture energy than mixtures with limestone (Lie et al. 2008).

Figure 17 through Figure 21 show the correlations between transverse cracking for the cells and the results of the reheated SCB fracture energy and toughness at -12°C, and -24°C, respectively. From these correlations, the two parameters at both temperatures were able to identify the mix with the worst performance. In addition, the fracture energy results at -12°C were able to identify the mix with the best performance (Cell 20). Finally, fracture energy and toughness at -24°C showed the best correlations to field performance in terms of R^2, with values of 0.79 and 0.89, respectively.

Table 13 Semi-Circular Bend (SCB) Fracture Energy Results

Cell #	Parameter	Fracture Energy (kJ/m^2)					
	Test Temperature	-12°C			-24°C		
	Mixture Description	Avg.	Std. Dev.	COV	Avg.	Std. Dev.	COV
16	Moderate RAP + RAS	0.34	0.07	21.0	0.25*	N/A	N/A
17	Low RAP + RAS	0.49	0.10	20.3	0.24	0.05	20.8
18	Moderate RAP	0.39	0.10	25.1	0.28	0.10	37.0
19	Moderate RAP, extra AC	0.34	0.05	15.5	0.26	0.06	22.6
20	High RAP, softer binder	0.61	0.11	18.5	0.30	0.03	8.5
21	Moderate RAP, softer binder	0.56	0.04	7.4	0.30	0.06	20.8
22	Limestone, 9.5 mm NMAS, PMA	0.31	0.11	34.8	0.20	0.04	22.7
23	Moderate RAP, HiMA	0.42	0.03	8.1	0.32	0.06	18.5

Note: * Cell 16 tested at -24°C only had two replicates.

Table 14 Semi-Circular Bend (SCB) Fracture Toughness Results

Cell #	Parameter	Avg. Fracture Toughness (MPa*m$^{0.5}$)					
	Test Temperature	-12°C			-24°C		
	Mixture Description	Avg.	Std. Dev.	COV	Avg.	Std. Dev.	COV
16	Moderate RAP + RAS	0.58	0.05	8.1	0.67*	N/A	N/A
17	Low RAP + RAS	0.60	0.03	4.6	0.65	0.11	17.0
18	Moderate RAP	0.60	0.09	15.1	0.64	0.08	12.1
19	Moderate RAP, extra AC	0.60	0.05	7.7	0.66	0.11	16.6
20	High RAP, softer binder	0.60	0.04	5.9	0.71	0.09	12.8
21	Moderate RAP, softer binder	0.70	0.01	1.3	0.72	0.07	10
22	Limestone, 9.5 mm NMAS, PMA	0.57	0.04	6.3	0.54	0.03	5.5
23	Moderate RAP, HiMA	0.63	0.02	2.6	0.71	0.10	13.8

Note: * Cell 16 tested at -24°C only had two replicates.

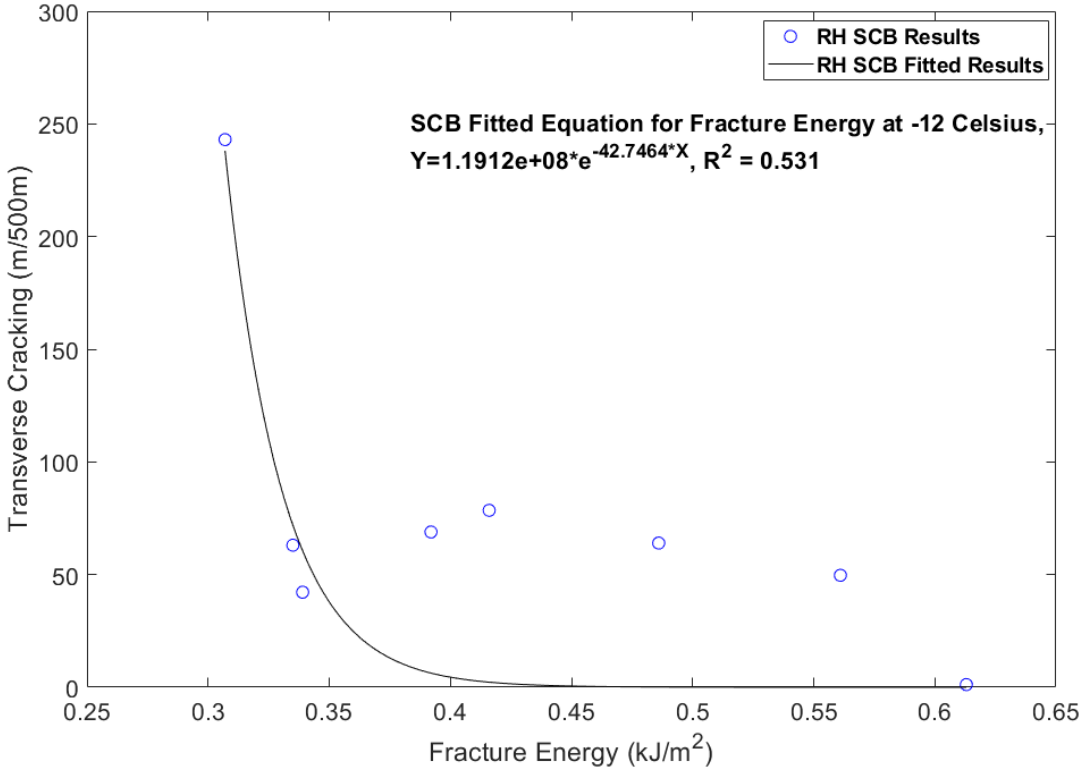

Figure 17 Correlation of Reheated SCB Fracture Energy Results at -12°C and Transverse Cracking Performance

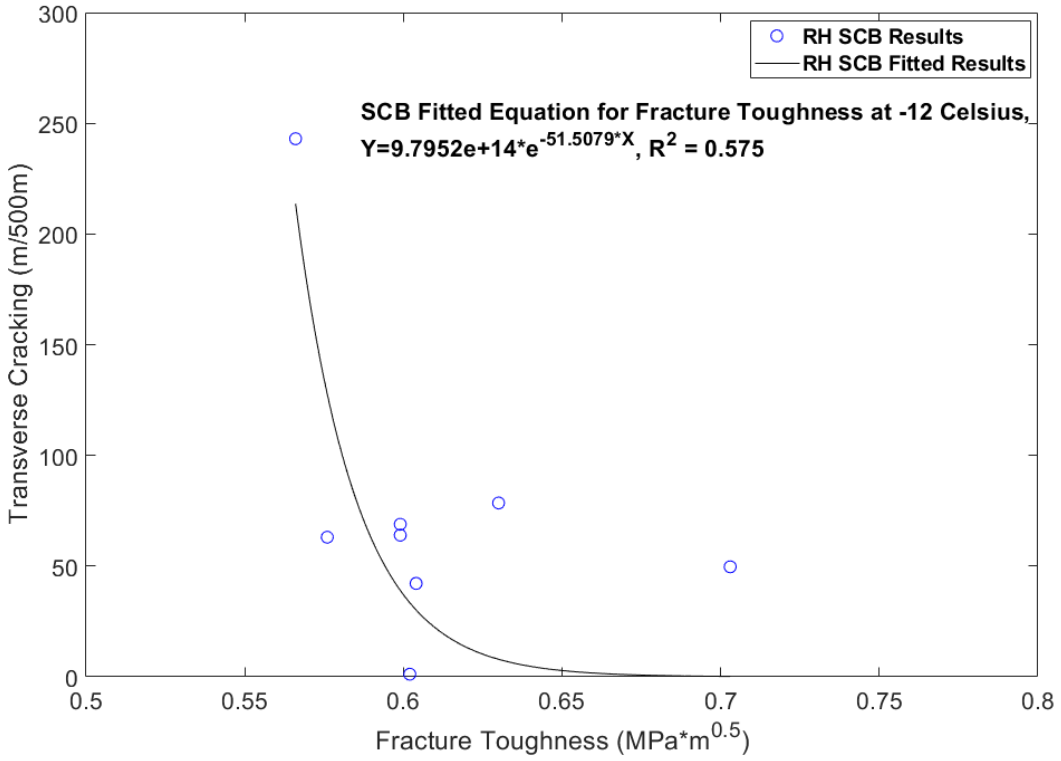

Figure 18. Correlation of Reheated SCB Toughness Results at -12°C and Transverse Cracking Performance

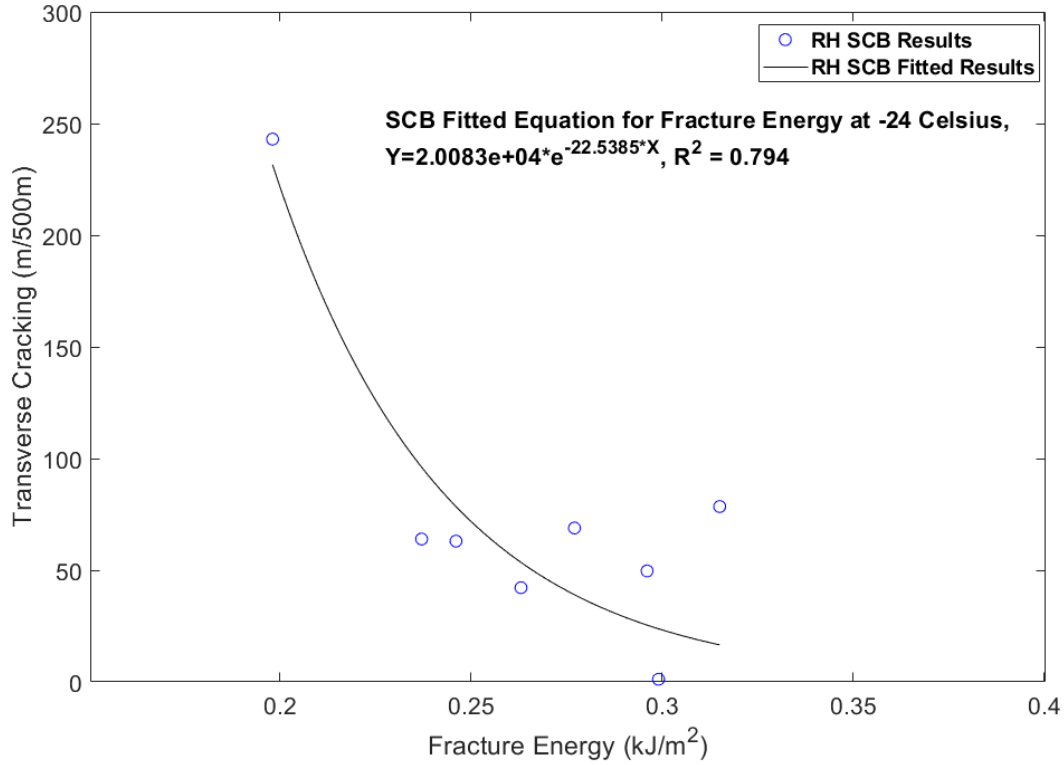

Figure 19 Correlation of Reheated SCB Fracture Energy Results at -24°C and Transverse Cracking Performance

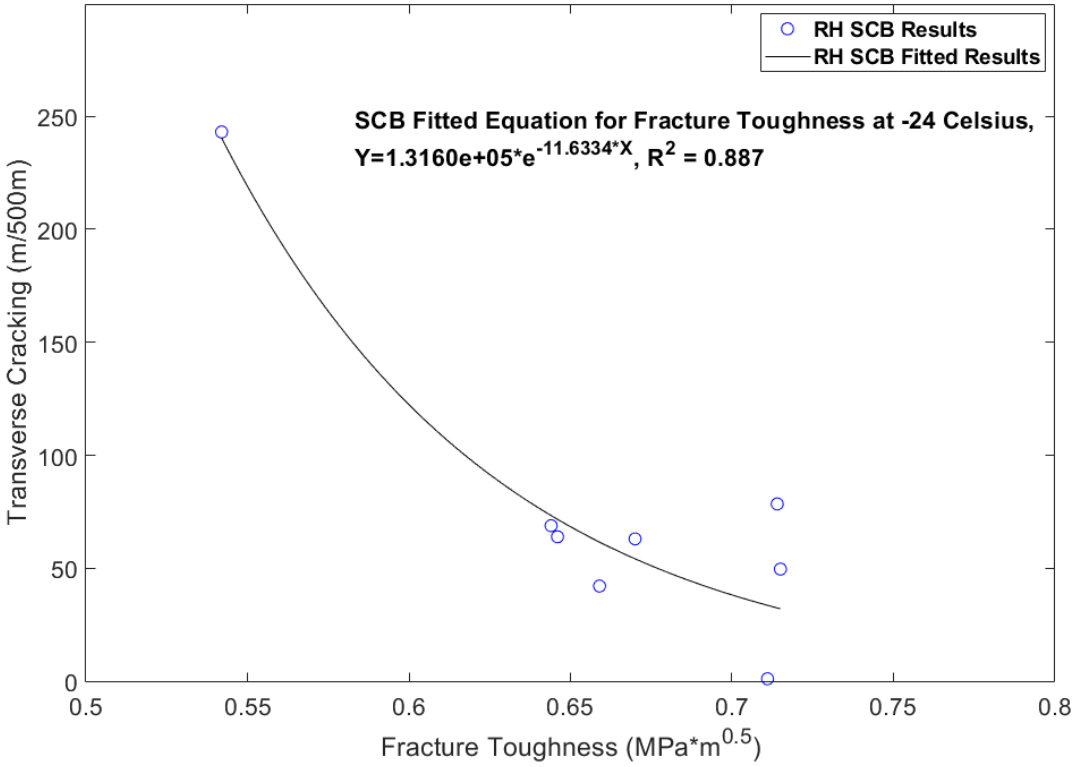

Figure 20 Correlation of Reheated SCB Toughness Results at -24°C and Transverse Cracking Performance

Figure 21 to Figure 24 show the SCB fracture energy and toughness results ranked from best to worst for the PMLC-RH samples. The whiskers represent plus and minus one standard deviation of the fracture energy results. The low-temperature cracking performance of the test sections (right y-axis) are also included in these figures. As presented, the SCB test generally captures the expected trend for most mixes (higher fracture energy and toughness values correspond to better cracking performance).

An ANOVA (α=0.05) with Tukey statistical grouping method was used to statistically rank the SCB results for the PMLC-RH samples. The results of these groupings are also shown in Figure 21 (fracture energy for tests conducted at -12°C) and Figure 23 (fracture toughness for tests conducted at -12°C) with the letters on top of the bars (for fracture energy, letters A, B, and C; for fracture toughness letters A and B) indicating that mixtures that do not share a letter are significantly different. For the results at -24°C (fracture energy and toughness), no significant differences in the means were found and thus no groupings are displayed on Figure 22 and Figure 24. For the results at -12°C, all the mixes groupings showed some overlap with no delineation between the mixes despite the differences observed in the mean values.

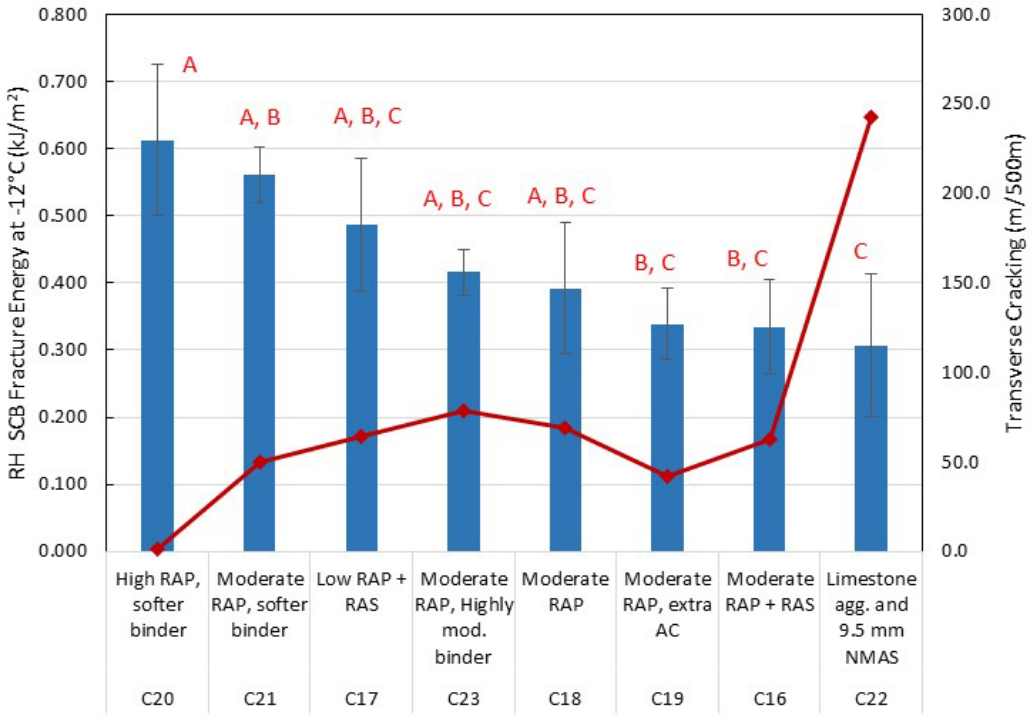

Figure 21 Statistical Comparison of RH SCB Fracture Energy Results at -12°C among Mixtures and Field Performance

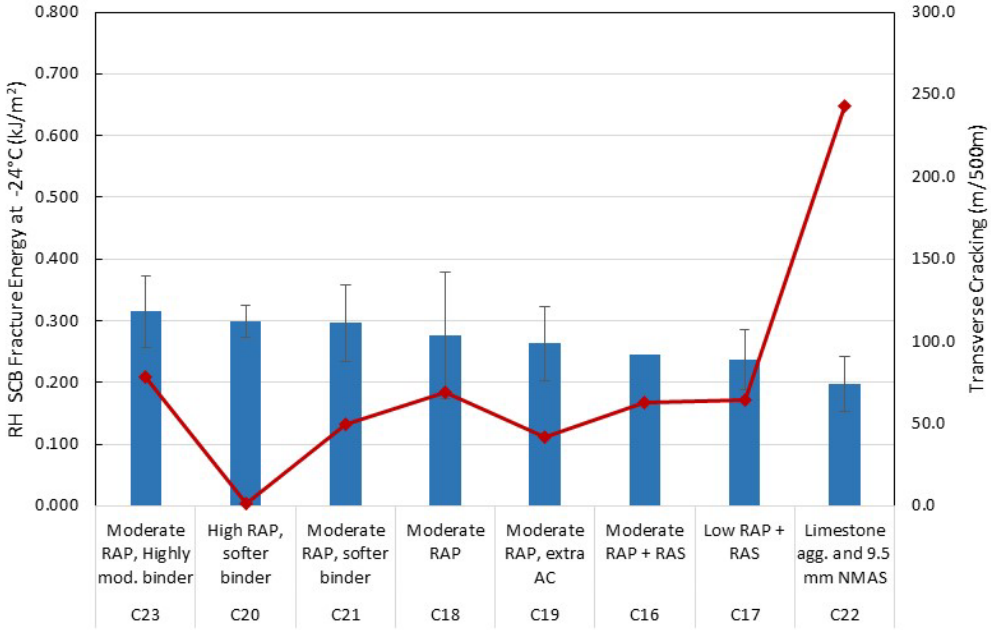

Figure 22 Statistical Comparison of RH SCB Fracture Energy Results at -24°C among Mixtures and Field Performance

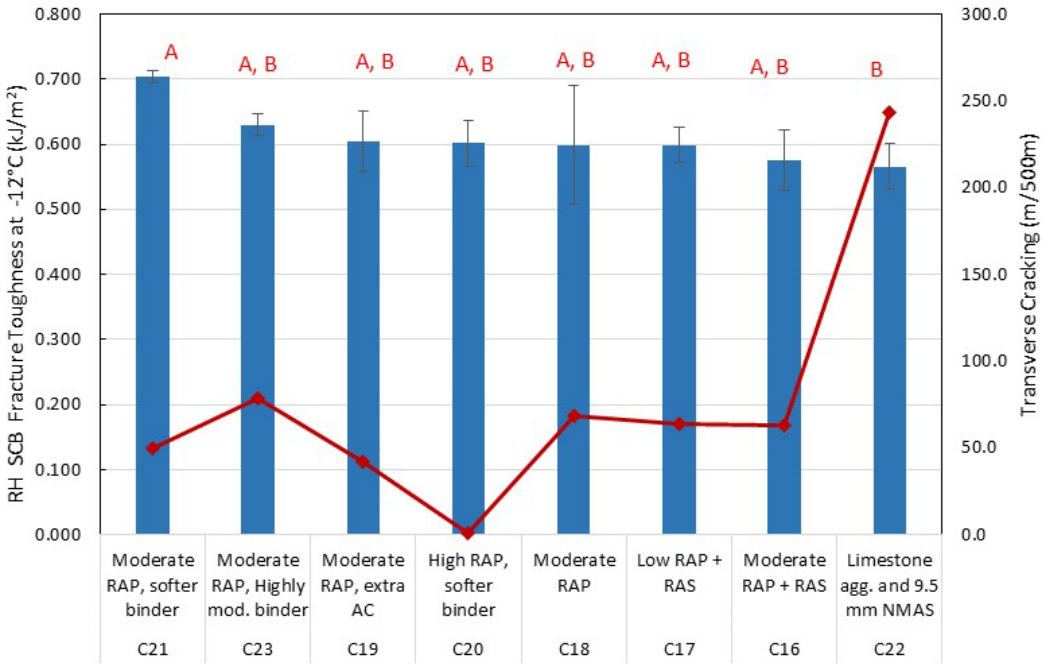

Figure 23 Statistical Comparison of RH SCB Fracture Toughness Results at -12°C among Mixtures and Field Performance

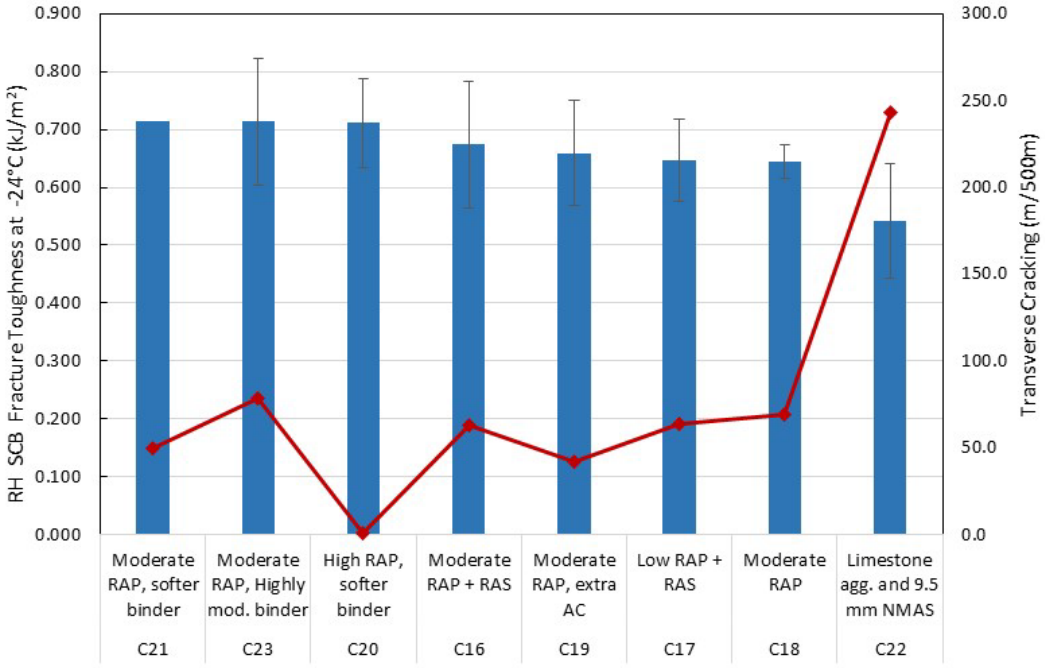

Figure 24 Statistical Comparison of RH SCB Fracture Toughness Results at -24°C among Mixtures and Field Performance

3.3 Uniaxial Thermal Stress and Strain Test (UTSST)

The thermal stress restrained specimen test (TSRST) was developed in the Strategic Highway Research Program (SHRP) to simulate field conditions in which low-temperature cracking might occur (Jung and Vinson, 1994). The test procedure was published as AASHTO Provisional Standard TP 10 "Standard Test Method for Thermal Stress Restrained Specimen Tensile Strength," but later withdrawn from the standards.

Over the past several years, research has been conducted to develop a modified version of the test, known as the Uniaxial Thermal Stress and Strain Test (UTSST). The test is currently an ASTM work item, ASTM WK60626 "New Test Method for Determining Thermal Cracking Properties of Asphalt Mixtures through Measurement of Thermally Induced Stress and Strain". This modified procedure utilizes cylindrical specimens cored from SGC specimens or field cores instead of beam specimens. Additionally, the test measures the thermal strain developed in an unrestrained specimen simultaneously with the stress developed in the strained specimen. (Hajj et al., 2010, Morian, et al., 2014, Morian et al., 2018). During the test the restrained and unrestrained specimens are cooled at a rate of 10°C/hr. starting from an initial temperature of 20°C, while continuously measuring the stress and strain. From the test, a cracking resistance index (CRI) is determined, and when adjusted for the environment it is referred to as CRI_{Env}. (Morian et al. 2018). CRI_{Env} is sensitive to mixtures containing recycled materials and recycling agents (Kasser et al., 2018, Morian et al., 2018). NCHRP Project 9-58 suggested a minimum CRI_{Env} value of 17.0 for LMLC specimen after LTOA as a threshold for low temperature cracking resistance based on correlations to performance of field test sections included in the study (Epps-Martin et al., 2019). A summary of the UTSST CRI_{Env} results for PMLC-RH and PMLC-LTOA specimens is presented in Table 15 The CRI results were adjusted for the MnROAD climate according to LTPP Bind. Four replicates per mix were tested. As observed in this table, the long-term aging caused CRI_{Env} to decrease. Mix from Cell 20 had the highest CRI_{Env} for the reheated samples, but the biggest drop in CRI_{Env} after LTOA. In contrast, the mix from cell 19 had very similar CRI_{Env} results for the reheated and long-term aged specimens. When the test results after LTOA are compared with the preliminary threshold of 17.0, mixes from Cells 16, 17 and 22 failed the requirement.

Table 15 UTSST Results

Cell #	Mixture Description	PMLC- RH	PMLC -LTOA
		Avg. CRI_{Env} (adjusted for -28°C -LTPP)	
16	Moderate RAP + RAS	34	15
17	Low RAP + RAS	36	13
18	Moderate RAP	27	19
19	Moderate RAP, extra AC	34	30
20	High RAP, softer binder	132	33
21	Moderate RAP, softer binder	83	61
22	Limestone, 9.5 mm NMAS, PMA	28	14
23	Moderate RAP, HiMA	45	9

Figure 25 presents the correlations between PMLC-RH and PMLC-LTOA UTSST results and low temperature crack density for each cell. As presented in this figure, the results indicate poor correlations to the field performance of the sections with R^2 values of 0.33 and 0.20 for the results of PMLC-RH and PMLC-LTOA samples, respectively. In addition, UTSST results on PMLC-RH samples were only able to identify the mix with best performance (Cell 20).

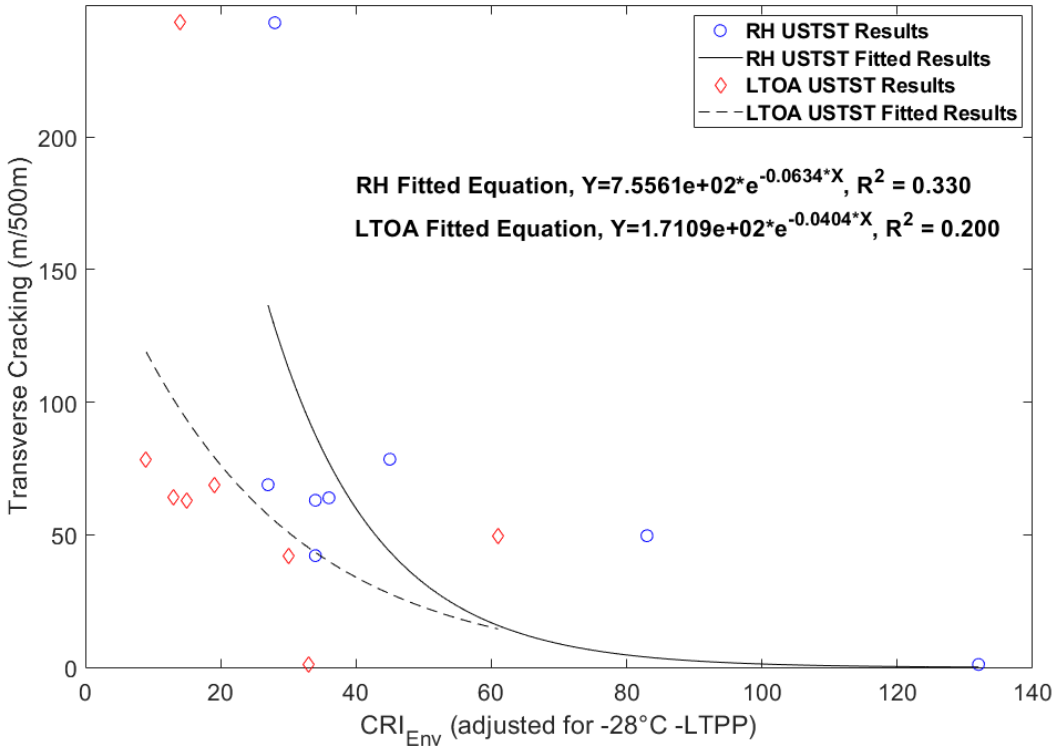

Figure 25 Correlation of UTSST Results and Transverse Cracking Performance

3.4 Indirect Tensile Creep Compliance and Strength Test (IDT-CC&S)

The indirect tension creep compliance and strength test (IDT-CC&S) per AASHTO T 322 is used to assess the low temperature cracking resistance of asphalt mixtures. The test is currently an input in the AASHTOWare Pavement ME program. The IDT-CC&S test is designed to obtain the viscoelastic properties of a mixture needed to predict thermal stress build-up and the fracture properties needed in modeling cracking potential (Hiltunen and Roque, 1994). The test determines the creep compliance as a function of displacement, load, and time and is used to determine a critical temperature where the estimated thermal stress exceeds the indirect tensile strength of a mixture.

In accordance with AASHTO T 322-07, creep compliance at 0°C, -10°C, and -20°C and tensile strength at -10°C are measured. These temperatures are specified as a function of the low-temperature PG grade of the binder in AASHTO T322-07. The creep test applied a constant load to the asphalt specimen for 100 seconds while the horizontal and vertical strains were measured on each face of the specimen using on-specimen instrumentation.

The critical temperature analysis was conducted using the EXCEL® worksheet 'LTSTRESS_JUN_2013' developed by Don Christensen. The program fits a mastercurve to the creep compliance data, using the lowest temperature as the default reference temperature. These data are then used to model the development of thermal stresses in the mixture as a function of temperature. The modeled thermal stresses, along with the tested mixture indirect tensile strength, are then used to estimate the critical cracking temperature of the mixture. This analysis is described in-depth by Christensen (1998) and Hiltunen and Roque (1994).

Table 16 presents the critical low temperature obtained for the PMLC-RH and PMLC-CA specimens. As can be observed for most of the mixes, aging decreases the critical temperature (less negative) as expected. Critical temperature ranged from -30°C to -21°C for the PMLC-RH specimens, and from -26°C to -21°C for the PMLC-CA specimens.

Figure 26 presents the correlations of PMLC-RH and PMLC-LTOA IDT-CC&S critical temperature results and transverse cracking for each cell. As presented in this figure, the results indicated an unexpected trend between PMLC-RH results and cracking performance, while the correlation between PMLC-CA showed the right trend, with a fair correlation (R^2=0.60). The PMLC-RH results were able to identify the mix with the best performance (Cell 20), but the worse performing mixture (Cell 22) also showed the best critical temperature results (-30°C). The PMLC-CA results were able to identify both the worst and the best performing mix.

Table 16 IDT-CC&S Critical Low Temperature

Cell #	Mixture Description	PMLC-RH	PMLC-CA
		Crit. Temp. ˚C	Crit. Temp. ˚C
16	Moderate RAP + RAS	-26	-24
17	Low RAP + RAS	-27	-24
18	Moderate RAP	-25	-21
19	Moderate RAP, extra AC	-21	-21
20	High RAP, softer binder	-30	-26
21	Moderate RAP, softer binder	-29	-21
22	Limestone, 9.5 mm NMAS, PMA	-30	-20
23	Moderate RAP, HiMA	-29	-24

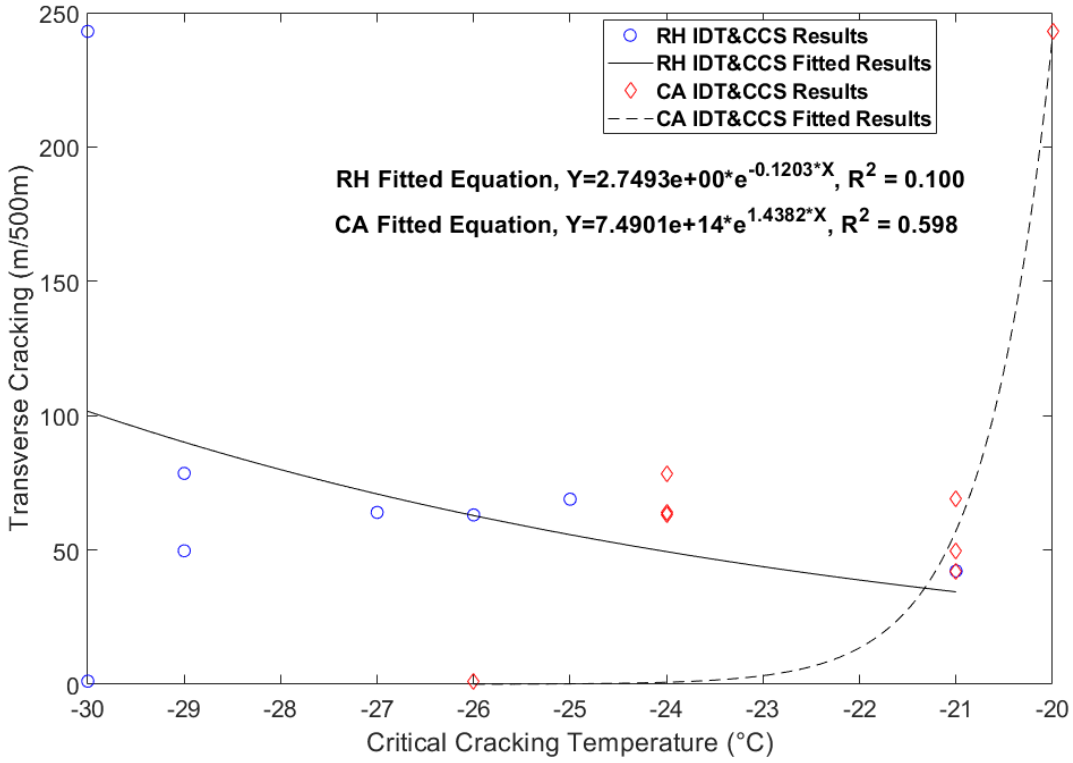

Figure 26 Correlation of IDT Creep Compliance and Strength Results and Transverse Cracking Performance

3.5 Asphalt Concrete Cracking Device (ACCD)

The Asphalt Concrete Cracking Device (ACCD) is a testing method used as an alternative to the TSRST. The ACCD ring is an Invar ring with near zero coefficient of thermal expansion (CTE). The ring dimensions are 61.00 ± 0.05 mm (outer diameter), 60.00 ± 0.05 mm (height), and 19.2 ± 0.05 mm (thickness). This ring is instrumented with a strain gage and a temperature sensor on the inside wall of the ring. Laboratory compacted samples or field cores with a 150 mm diameter are sawn into 52.5 mm thick specimens. The center of each sample is cored out so that the inner diameter is 60.75mm. A notch with a depth of 22.4 mm is cut on the specimen. During the test, as the ACCD sample is cooled, tensile stress develops within the asphalt specimen as it contracts around the Invar ring. When the tensile stress in the asphalt specimen exceeds its tensile strength the sample cracks. The temperature at which this stress is released is defined as the ACCD cracking temperature (Akentuna, et al., 2016; Kim, 2020). A study conducted by Kim et al. (2007) indicated that ACCD results of five mixes correlate well with TSRST.

Table 17 presents the average critical low temperature obtained for the PMLC-RH and PMLC-CA specimens. As can be observed for all of the mixes, aging increased the critical temperature (less negative), with mix from cell 23 having the biggest change in critical temperature. Critical temperatures ranged from -31.4°C to -26.5°C for the PMLC-RH specimens, and from -30.4°C to -22.1°C for the PMLC-CA specimens.

Figure 27 presents the correlations of PMLC-RH and PMLC-LTOA ACCD critical low temperature results and low temperature cracking. As presented in these figures, the results indicate poor correlations to the field performance of the sections with R^2 values of 0.28 and 0.21 for results of PMLC-RH and PMLC-CA samples, respectively. ACCD results for PMLC-RH samples were able to identify the mixes with the best (Cell 20) and worst performance (Cell 22), while results on PMLC-CA samples were only able to identify the mix with best performance (Cell 20). A statistical analysis was not conducted on the test results because of the low correlation found with this test.

Table 17 ACCD Critical Low Temperature

Cell #	Mixture Description	PMLC-RH			PMLC-CA		
		Avg.	Std. Dev.	COV	Avg.	Std. Dev.	COV
16	Moderate RAP + RAS	-28.4	0.50	1.8	-26.7	0.31	1.2
17	Low RAP + RAS	-27.6	0.47	1.7	-26.2	0.49	1.9
18	Moderate RAP	-27.1	0.31	1.1	-24.9	0.61	2.4
19	Moderate RAP, extra AC	-26.5	0.20	0.7	-25.0	0.35	1.4
20	High RAP, softer binder	-32.1	0.38	1.2	-30.4	0.24	0.8
21	Moderate RAP, softer binder	-31.4	0.08	0.2	-30.1	0.88	2.9
22	Limestone, 9.5 mm NMAS, PMA	-26.5	1.14	4.3	-24.2	1.68	6.9
23	Moderate RAP, HiMA	-31.0	0.59	1.9	-22.1	1.21	5.5

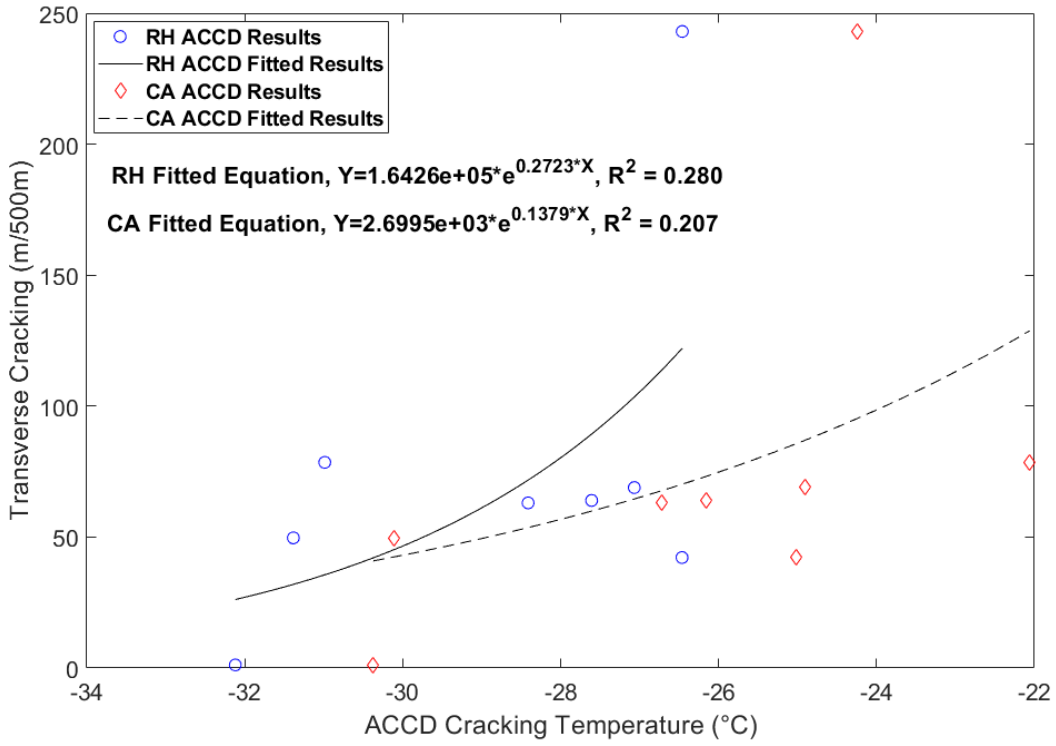

Figure 27 Correlation of ACCD Results and Transverse Cracking Performance

3.6 Bending Beam Rheometer for Asphalt Mixtures (BBR_m)

This test method was developed at the University of Minnesota under an NCHRP IDEA project to determine the creep stiffness of mixture beams utilizing the BBR equipment used for asphalt binders (Marasteanu, Velasquez, and Falchetto 2009). The test has been standardized as AASHTO TP 125. The test utilizes thin beams (12.7 mm wide, 6.35 mm thick, and 127 mm long) cut from SGC specimens or field cores and is conducted at a temperature equal to the continuous low performance grade of the target binder plus 10°C.

Romero (2016) refined the testing procedure originally proposed by Marasteanu, Velasquez, and Falchetto (2009) and assessed the correlation of BBR_m results to field performance. Figure 28 shows the low temperature mixture black space diagram using creep modulus (S) and m-values from the BBR_m and proposed thresholds based on field performance of seven field projects in Utah. Romero (2016) concluded that mixtures with a combination of high creep moduli and low m-values are susceptible to thermal distresses but recommended further refinement of the preliminary thresholds. Figure 29 and Figure 30 show this methodology applied to the CG mixes at -22° C and -34° C, respectively. At -22°C, cell 20 was identified as the best performer and cells 19 and 22 were the closest to the "redesign" range. At -34°C, all Cells are in the "redesign" zone emphasizing the need for further testing and threshold refinement using Minnesota mixes and field performance.

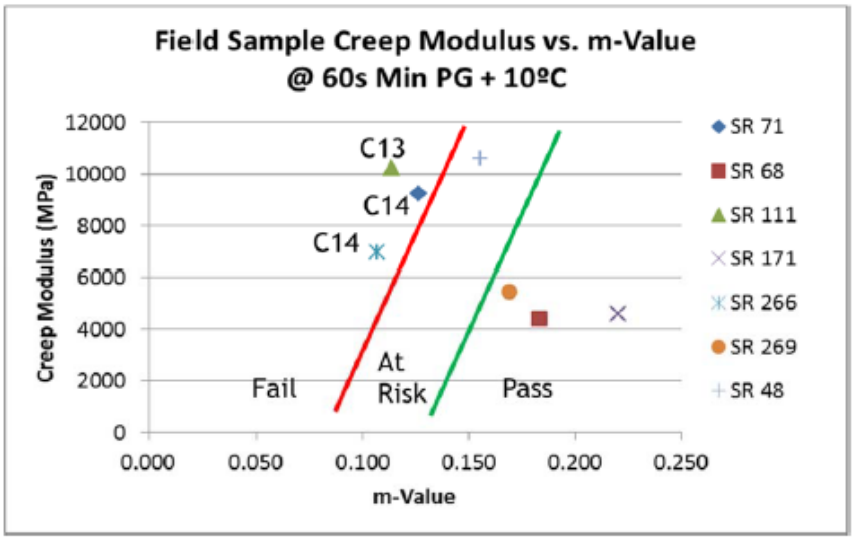

Figure 28 BBR_m Black Space Diagram Proposed Thresholds (Romero, 2016).

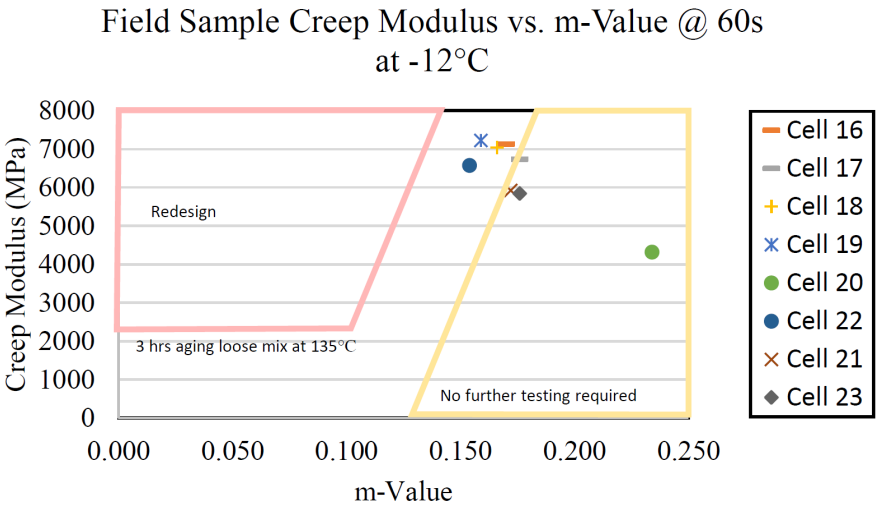

Figure 29 Hypothetical BBR_m Black Space Diagram for Design Temperature of -22°C (Marasteanu, 2016).

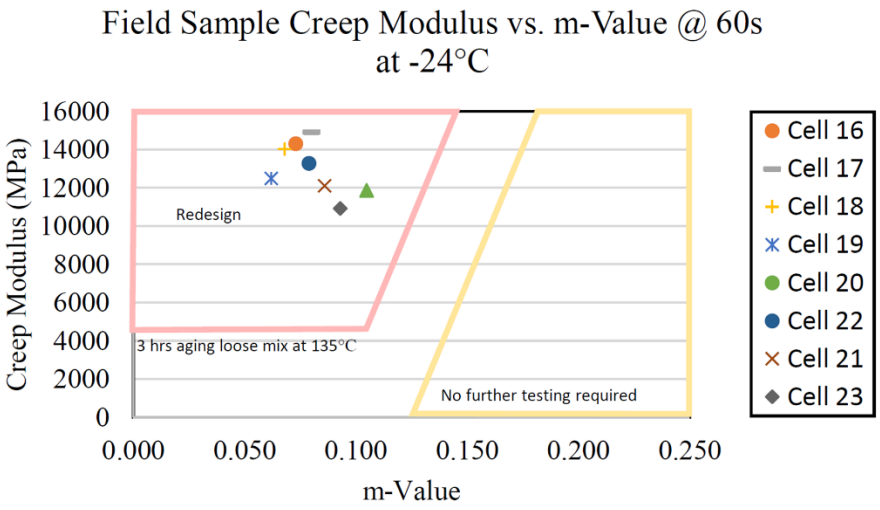

Figure 30 Hypothetical BBR_m Black Space Diagram for Design Temperature of -34°C (Marasteanu, 2016).

3.7 IDEAL-CT

The IDEAL-CT (ASTM D8225-19) uses a monotonic load applied along gyratory specimens at a constant displacement rate of 50 mm/min. The test is commonly performed at 25°C. The load-displacement curve is analyzed to calculate the cracking tolerance index (CT_{index}) determined from the work of fracture, or the total area under the load displacement curve, and the slope of the curve at 25% reduction from the peak load. Higher CT_{index} values are desired for better cracking resistance of asphalt mixtures.

Table 18 summarizes the result of the IDEAL-CT test. Three to six replicates were tested per mix. These results show the effect of aging is consistent for all the mixes with a decrease in CT_{index} results for the PMLC-CA samples compared to the PMLC-RH samples. The COV of the test results ranged from 5 to 26% for the PMLC-RH samples and from 6 to 28% for the PMLC-CA samples.

Figure 31 shows the correlations of CT_{Index} for the PMLC-RH and PMLC-CA specimens with the observed transverse cracking. The results showed a poor correlation (R^2=0.48) between CT_{Index} for the PMLC-RH specimens and the amount of low temperature cracking, but a strong correlation with CT_{Index} for PMLC-CA specimens (R^2=0.84) and cracking performance. In addition, both sets of test results were able to discriminate the worst performing mix; however, the results were not able to identify the best performing mix.

Table 18 IDEAL-CT Test Results

Cell #	Mixture Description	PMLC-RH			PMLC-CA		
		CT_{Index} (Avg.)	Std. Dev.	COV (%)	CT_{Index} (Avg.)	Std. Dev.	COV (%)
16	Moderate RAP + RAS	29.4	4	14.2	19.7	1.3	6.7
17	Low RAP + RAS	53.2	3	5.3	30.3	5.9	19.4
18	Moderate RAP	52.3	8	14.8	30.6	8.6	28.2
19	Moderate RAP, extra AC	106.6	28	26.0	39.6	8.4	21.2
20	High RAP, softer binder	63.8	7	11.2	31.6	8.1	25.5
21	Moderate RAP, softer binder	28.8	5	16.9	20.4	3.8	18.5
22	Limestone agg., 9.5 mm NMAS	22.4	3	13.3	7.6	0.5	6.0
23	Moderate RAP, HiMA	48.3	13.2	27.3	16.3	2.1	12.9

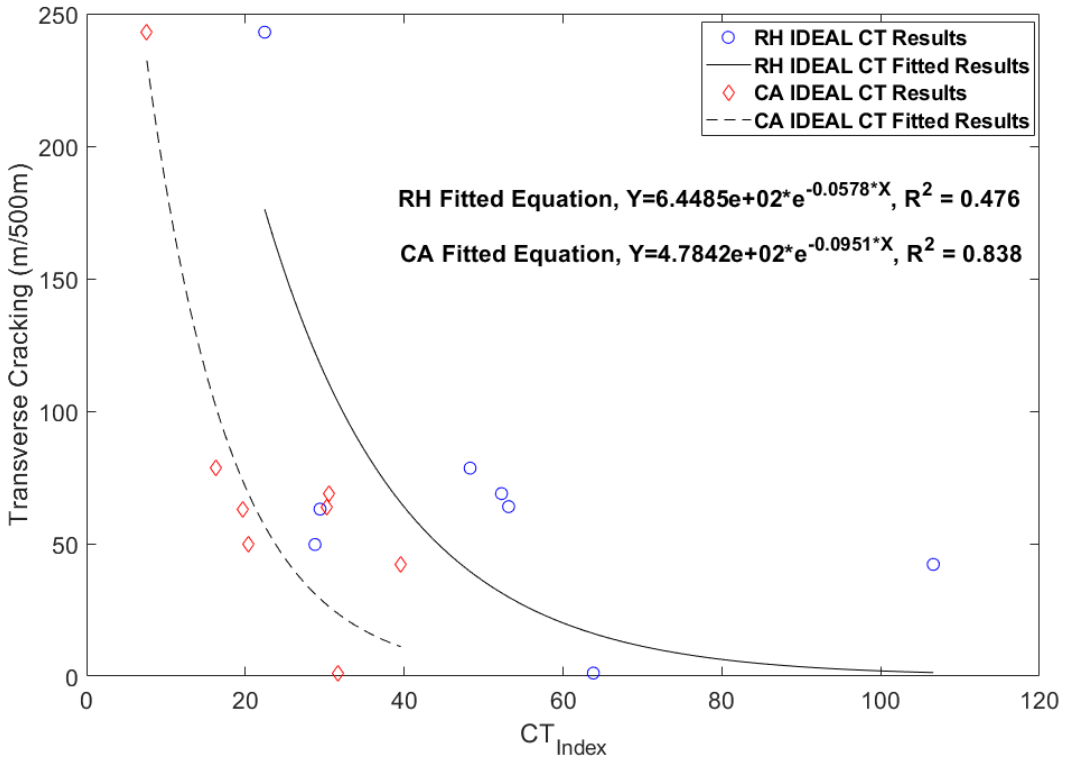

Figure 31 Correlation of IDEAL-CT Results and Transverse Cracking Performance

Figure 32 shows the IDEAL-CT results from best to worst for the PMLC-CA samples. As indicated previously, the whiskers represent plus and minus one standard deviation of the CT_{Index} results. The figure also includes the cracking performance of the test sections (right y-axis). As presented in this figure, the IDEAL-CT can capture the overall expected trend for most mixes (higher CT_{Index} values equal better cracking performance). An ANOVA (α=0.05) with Games-Howell statistical grouping was used to statistically rank the IDEAL-CT results. The results of these groupings are also presented in Figure 32 with letters on top of the bars (A, B, and C). Games-Howell groupings

were used instead of Tukey-Kramer groupings for this dataset because it had unequal variances which violated the Tukey-Kramer requirement for equal variances. All the mixes groupings showed some overlap with no clear delineation between the mixtures. This is partially attributed to the variability of the test results and difference in sample size per mix, as well as the narrower range of mix properties than intended during design (e.g., continuous PG grade of each cell).

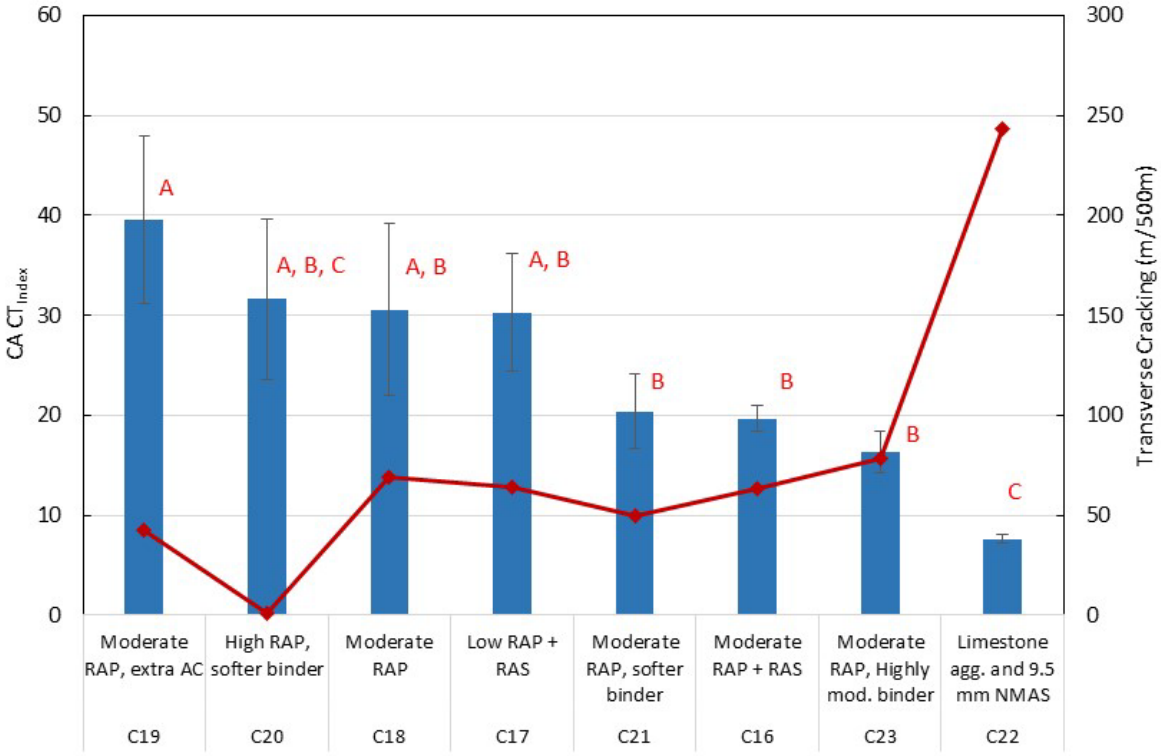

Figure 32 Statistical Comparison of CA IDEAL-CT Results among Mixtures and Field Performance

3.8 I-FIT

The I-FIT was performed in accordance with AASHTO TP 124 (now AASHTO T 393). For this test, semi-circular asphalt specimens are trimmed from a larger 160 mm tall by 150 mm diameter SGC specimen. A notch is then trimmed into each specimen at a target depth of 15 mm and width of 1.5 mm along the center axis of the specimen. The test is conducted at a temperature of 25.0°C. Specimens are tested monotonically at a rate of 50 mm/min until the load drops below 0.1 kN after the peak is recorded. The Flexibility Index (FI) is calculated as the area under the load-displacement curve (fracture energy) divided by the slope at the curve inflection point post-peak. Mixtures with a higher FI are considered more cracking resistant.

Table 19 summarizes the results of the I-FIT test. These results showed that the aging effect was consistent for all the mixes with a decrease in FI results for PMLC-CA samples compared to the PMLC-RH samples. The COV of the test results for some of the mixes were high, ranging from 16 to 39% for the PMLC-RH samples and from 18-63% for the PMLC-CA samples.

Table 19 I-FIT Test Results

Cell #	Mixture Description	PMLC-RH			PMLC-CA		
		FI (Avg.)	Std. Dev.	COV (%)	FI (Avg.)	Std. Dev.	COV (%)
16	Moderate RAP + RAS	3.2	0.5	16	1.9	0.4	22
17	Low RAP + RAS	8.7	2.1	24	3.2	1.2	39
18	Moderate RAP	7.9	1.9	24	3.2	2.0	63
19	Moderate RAP, extra AC	6.2	1.6	26	3.6	0.9	26
20	High RAP, softer binder	12.3	4.8	39	5.7	1.0	18
21	Moderate RAP, softer binder	9.5	2.9	31	1.4	0.4	29
22	Limestone agg., 9.5 mm NMAS	7.1	1.4	20	0.7	0.3	43
23	Moderate RAP, HiMA	14.9	3.6	24	1.5	0.3	20

Figure 33 shows the correlations between the FI for the PMLC-RH and PMLC-CA specimens and the transverse cracking. The results showed no correlation between the FI for the PMLC-RH specimens and the amount of low temperature cracking, but a fair correlation (R^2=0.70) between FI for PMLC-CA specimens and field cracking data. In addition, the PMLC-CA results were able to identify the mixes with the best and worst performance.

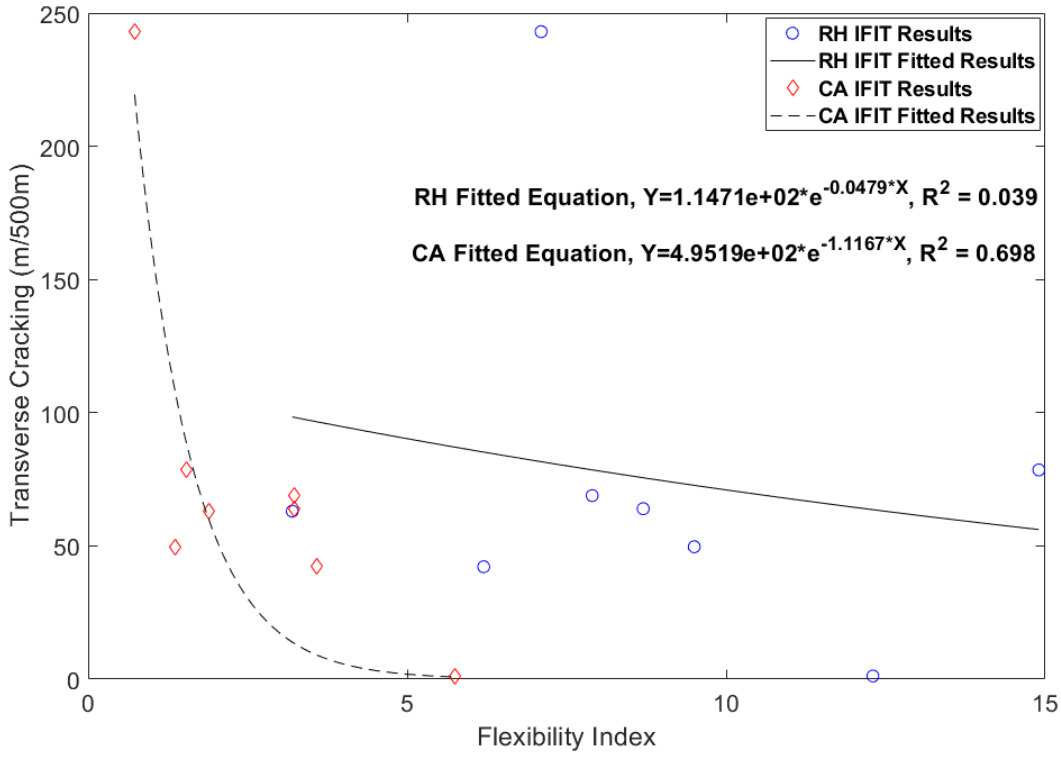

Figure 33 Correlation of I-FIT Results and Transverse Cracking Performance

Figure 34 shows the I-FIT results from best to worst for the PMLC-CA samples. The whiskers represent plus and minus one standard deviation of the FI results. The cracking performance of

the test sections is also presented in this figure (right y-axis). The I-FIT does a good job capturing the overall expected trend for most mixes (higher FI values equal better cracking performance). An ANOVA (α=0.05) with Games-Howell statistical grouping was used to statistically rank the I-FIT results. The results of these groupings are also presented in Figure 34 with letters on top of the bars (A, B, C, D, and E) indicating five groups. All the mix groupings showed some overlap with no delineation between the mixtures. As mentioned previously, this is partially attributed to the high variability of the test results, the difference in sample size per mix, and the tight range of mix properties.

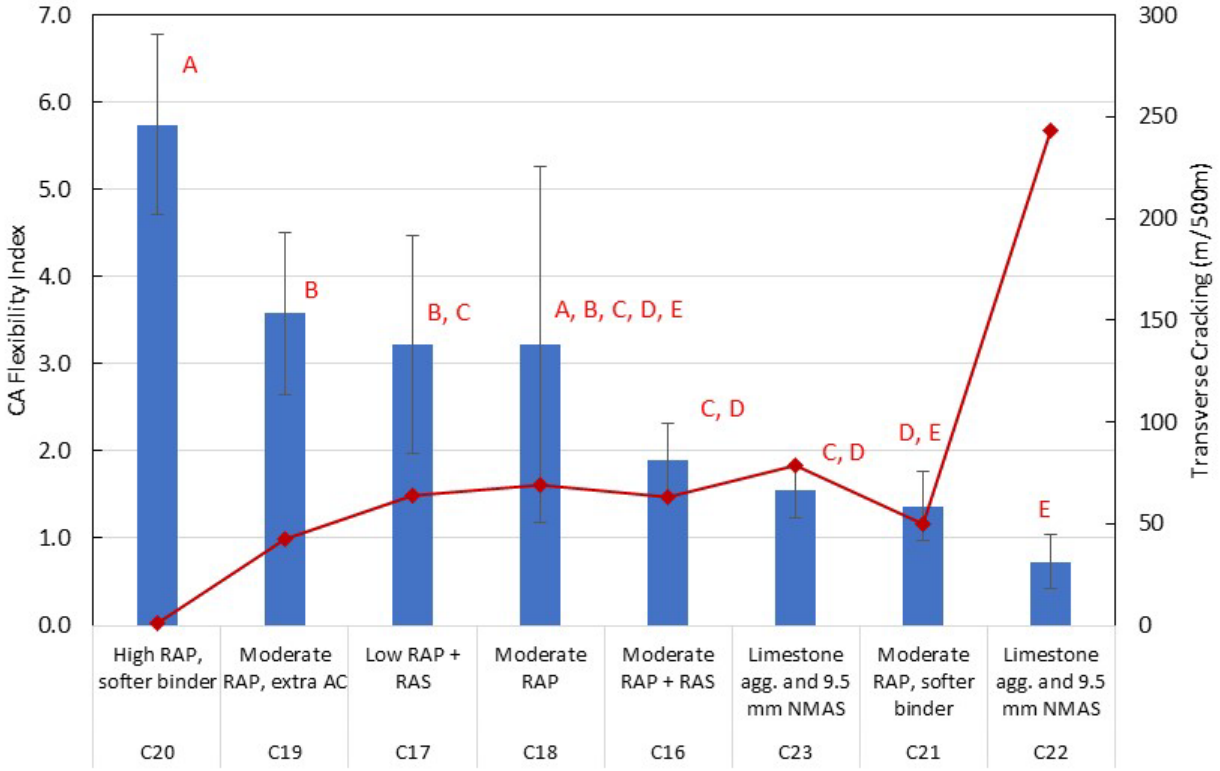

Figure 34 Statistical Comparison of CA I-FIT FI Results among Mixtures and Field Performance

3.9 NCAT Overlay Test (OT)

The OT per Tex-248-F is designed to simulate reflective cracking of asphalt mixtures. It was specifically designed to simulate the reflective cracking of an asphalt overlay atop a jointed Portland cement concrete (PCC) pavement. During the test, one plate remains fixed while the other plate moves in a displacement control mode. Loading occurs at a rate of one cycle every 10 seconds with a sawtooth waveform at a maximum opening displacement of 0.635 mm. The test is conducted at a temperature of 25°C. During the test, the peak load of each cycle is measured, and the test is terminated when a cycle registers a 93 percent reduction of the initial peak load. The number of cycles to failure is recorded to evaluate the cracking resistance of asphalt mixes. NCAT modified this test with a one second cycle, a maximum displacement of 0.381mm, and the peak of the "normalized load x cycle" curve to identify failure (Ma, 2014).

Zhou et al. (2005) used the OT test to evaluate field cores for low temperature cracking resistance of asphalt mixtures from a previous MnROAD study. The low temperature cracking of three test cells from MnROAD were compared to OT results conducted at a temperature of 25°C. The results provided in Table 20 show that the OT results were consistent with observed thermal cracking performance of the three mixes.

Table 20 Comparison of OT Test to Field Performance in MnROAD (*Zhou*, 2007)

Test Cells	Asphalt Grade	Linear Feet of Cracking	OT Test Results (Number of Cycles)
15	PG 64-22	475	91
18	PG 64-22	315	153
20	PG 58-28	100	500

More recently, Texas has started to use two new parameters obtained from the OT, the crack progression rate (β), and the critical fracture energy (CFE). The β parameter is obtained by fitting a power function to the normalized peak load versus number of cycles curve. The peak load versus number of cycles curve is normalized by the peak load of the first loading cycle. The β parameter corresponds to the absolute value of the power coefficient and is indicative of a mixture's resistance to cracking propagation. The second parameter, CFE is defined as the area under the load-displacement curve for the first OT load cycle and it has been used as a measure of mixture toughness (Garcia et al., 2017). In this study, only the β parameter was used to assess the potential correlation with field performance.

Table 21 summarizes the results of the OT-NCAT test using the β parameter. Five to seven replicates were used per mix. As presented in this table, the COVs ranged from 7 to 35% for the PMLC-RH samples and from 31 to 73% for the PMLC-CA samples, which highlights the high variability of the test, particularly for the critically aged specimens.

Figure 35 presents the correlation between the β parameter of the PMLC-RH and PMLC-CA specimens and the low temperature crack density of each cell. The results showed a very good correlation (R^2=0.91) between the β parameter for reheated specimens and the amount of low temperature cracking, and a strong correlation between the β parameter for critically aged specimens (R^2=0.85) and cracking data.

Table 21 NCAT-OT β Parameter Test Results

Cell #	Mixture Description	PMLC-RH			PMLC-CA		
		β (Avg.)	Std. Dev.	COV (%)	β (Avg.)	Std. Dev.	COV (%)
16	Moderate RAP + RAS	0.45	0.08	16.8	0.52	0.19	35.6
17	Low RAP + RAS	0.36	0.03	8.2	0.51	0.18	35.4
18	Moderate RAP	0.54	0.14	26.1	0.48	0.10	21.2
19	Moderate RAP, extra AC	0.39	0.03	7.4	0.63	0.16	25.6
20	High RAP, softer binder	0.34	0.03	9.5	0.60	0.20	32.5
21	Moderate RAP, softer binder	0.37	0.04	10.5	1.07	0.78	72.5
22	Limestone agg., 9.5 mm NMAS	1.57	0.54	34.5	2.11	0.87	41.1
23	Moderate RAP, HiMA	0.45	0.09	20.3	0.61	0.32	51.3

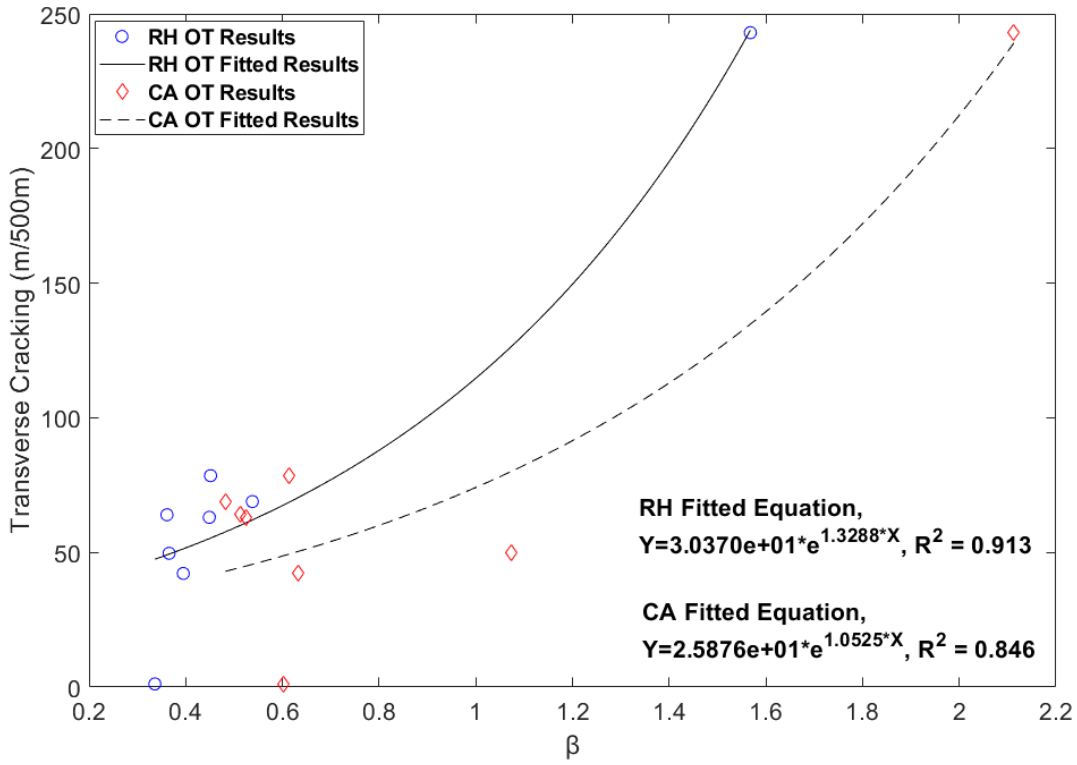

Figure 35 Correlation of NCAT-OT β Parameter Results and Transverse Cracking Performance

Figure 36 shows the NCAT-OT results arranged from best to worst for the PMLC-CA samples. The cracking performance of the test sections is also presented in this figure (right y-axis). An ANOVA (α=0.05) with Games-Howell statistical grouping method was used to statistically rank the β results for the PMLC-RH samples. However, the analysis showed no significant differences in the means values because of the high variability of the test results.

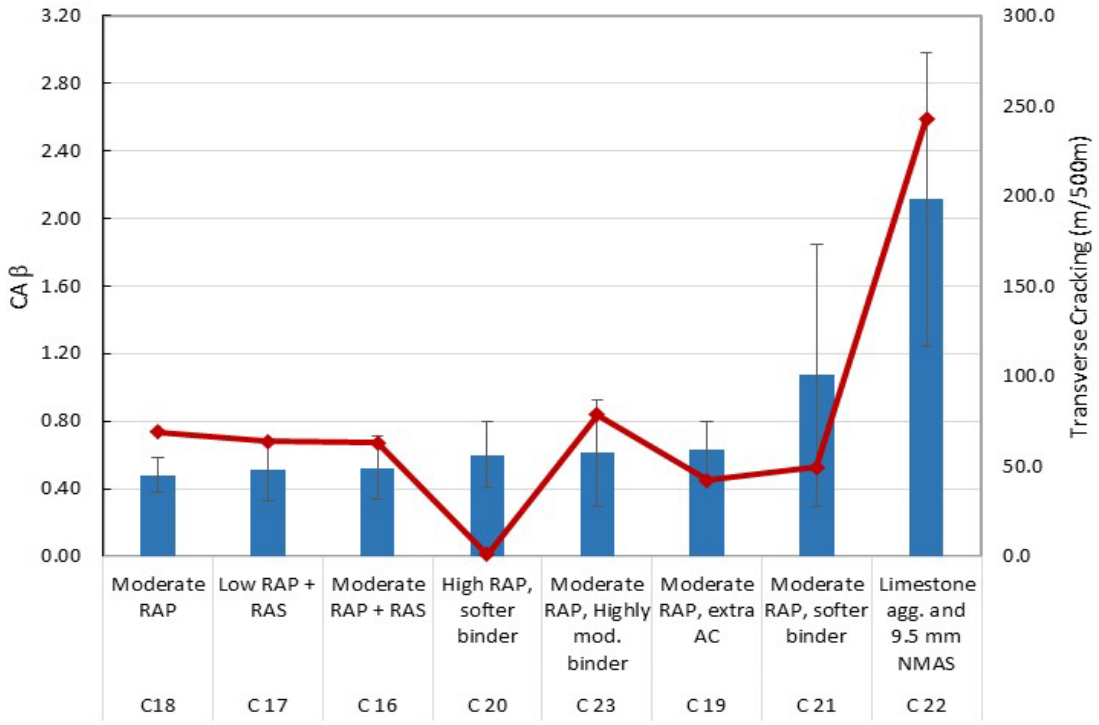

Figure 36 Statistical Comparison of CA OT β Results among Mixtures and Field Performance

3.10 Summary of Correlations Between Laboratory Test Results and Field Performance for Three Survey Dates

Table 22 summarizes all coefficient of determination values (R^2) for relationships between the laboratory results and field performance distress survey results (shoulder transverse cracking) for three survey dates (Spring 2020, 2021, and 2022), and two mix aging conditions (RH and CA). For the low temperature SCB test, since only RH test results were available, and for the UTSST, only LTOA results were available.

For RH produced specimens, the relationships improve with longer term field data (R^2 increases as the field sections age) for the DCT and low temperature SCB test, with some improvement seen for the IDEAL-CT test as well. The I-FIT results for RH specimens did not correlate with field transverse cracking performance for any of the distress surveys. For tests on CA specimens, the DCT, I-FIT and IDEAL-CT tests results correlated better as the age of the field sections increased. Overall, the OT showed good correlation with field performance for both RH and CA specimens. Results from the other three tests (UTSST, IDT-CC&S, and ACCD) did not correlate well with any of the survey dates.

Table 22 Correlation of Laboratory Test Results to Surveyed Transverse Cracking with Age

	Test	R^2 by Survey Date		
		Spring 2020	Spring 2021	Spring 2022
	Age	3 ½ years	4 ½ years	5 ½ years
Reheated (RH)	DCT	0.24	0.27	0.76
	UTSST	0.17	0.39	0.33
	IDT-CC&S	0.11*	0.04*	0.10*
	ACCD	0.20	0.35	0.28
	I-FIT	0.04	0.06	0.04
	IDEAL-CT	0.19	0.21	0.48
	OT	0.96	0.89	0.91
	SCB Parameter	R^2 by Survey Date		
		Spring 2020	Spring 2021	Spring 2022
	G_F -12°C	0.33	0.47	0.53
	G_F -24°C	0.52	0.53	0.79
	k_{IC} -12°C	0.20	0.23	0.58
	k_{IC} -24°C	0.72	0.78	0.89
	Test	R^2 by Survey Date		
		Spring 2020	Spring 2021	Spring 2022
Critically Aged (CA)	DCT	0.50	0.56	0.85
	IDT-CC&S	0.24	0.32	0.60
	ACCD	0.19	0.36	0.21
	I-FIT	0.36	0.44	0.70
	IDEAL-CT	0.52	0.48	0.84
	OT	0.81	0.62	0.85
LTOA	UTSST	0.14	0.25	0.20

Note:* Unexpected trend was observed

4. PROJECT SUMMARY AND CONCLUSIONS

The MnROAD Cracking Group experiment constructed eight test sections on MnROAD's I-94 mainline in 2016. The main objective of this experiment was to assess correlations between laboratory cracking tests and field low temperature cracking performance. The field performance of each section was closely monitored for structural response (FWD) and surface performance (ride, rutting, and cracking). The environmental conditions and traffic loading at MnROAD were monitored from Fall 2016 through the section removal in Spring 2022. Based on the field performance, the following conclusions were made.

- The Cracking Group cells generally matched expected anticipated trends (except for the variability of cell 23) with respect to deflection and stiffness; however, the range was tighter than expected due to material properties of the HMA components. The RAP and

RAS used in the project were relatively soft and the low temperature performance grades were closer than intended in the experimental design.

- Field monitoring and forensic investigation identified delamination as a major contributor to the observed cracking performance for all the test cells. It is believed that water initially entered the pavement structure through longitudinal construction joints. The combination of water, traffic, and environment deteriorated the bond between HMA layers, resulting in severe distresses in the two-inch surface layer of HMA. This progression occurred in all of the test cells.
- Cell 23 (HiMA) did not have the expected field performance. Oversaturation of the base and subgrade during construction and a high initial roughness led to non-LTC distress throughout the section. This section did not match expected behavior and trends for HiMA. The performance of cell 23 further emphasizes the importance of the base and subgrade in the overall performance of pavement structures. This section was expected to be the most cracking resistant and had the most cracking due to poor base and subgrade support.
- Cell 20 (30% RAP with PG 52S-34) had the least amount of cracking and the best overall field performance. It is an important finding that this section had equivalent rutting performance as the other cells under interstate traffic, as the high temperature PG was significantly lower than the other cells. Cell 20 used a soft binder with 30% RAP and had less than 3 mm of rutting.
- Transverse cracking in the shoulders was measured to capture the LTC performance of each mix without the influence of traffic and delamination. The use of shoulder performance data for laboratory to field correlations was supported by similar trends in test section performance from the traveled lanes to the shoulders (i.e., cell 20 had very little cracking in the traveled lanes and very little in the shoulders.)

Plant-mixed HMA was collected during construction and an array of laboratory cracking tests were conducted for comparison between laboratory test results and field performance using the transverse cracking in the shoulders. For each mix, two sets of samples were prepared. The first set was compacted after samples were reheated to the compaction temperature (referred to as PMLC-RH), and the second set of samples were prepared using reheated mix and critically aged prior to compaction (referred to as PMLC-CA).

Based on the laboratory to field performance comparisons, the following conclusions were made.

- Overall, the narrow range of material properties for many of the mixtures caused results for many of those mixtures to be clustered, which diminished the ability of the lab to field relationships to represent a more comprehensive range of results.
- The DCT fracture energy results for reheated and critically aged specimens showed moderate to strong correlations with transverse cracking in the eight cells after 3½ to 5½ years of service. DCT results on critically aged specimens had the strongest correlation (R^2 = 0.85) with thermal cracking measured at six years.

- The low temperature SCB results on reheated mix specimens at -24°C had moderate to strong correlations with transverse cracking over 3½ to 5½ years of service with correlations improving with time. Fracture toughness provided a better correlation with field performance than fracture energy. The low-temperature SCB fracture energy and toughness results for tests conducted at -24°C had better correlations to field performance than the tests conducted at -12°C. This test was not conducted on critically aged mixtures.
- The results from UTSST, IDT-CC&S, and ACCD tests did not correlate well with the field performance of the Cracking Group cells.
- For reheated mix specimens, IDEAL-CT results yielded a poor to moderate correlation with thermal (transverse) cracking. For critically aged mixtures, CT_{Index} provided moderate correlations with thermal cracking at the 3 ½ and 4 ½ year field performance data, but the correlation was much stronger for the 5 ½ year field performance data.
- For reheated mix specimens, I-FIT results yielded a poor correlation with thermal (transverse) cracking. For critically aged mixtures, FI provided weak correlations with thermal cracking at the 3 ½ and 4 ½ year field performance data, but the correlation was stronger for the 5 ½ year field performance data.
- For reheated mix specimens, the β parameter from the NCAT OT had very strong correlations with thermal (transverse) cracking. For critically aged mix specimens, the strength of the correlations between the β parameter and field data was reduced but still moderate to strong.

From the CG study, the following takeaways will be implemented and further evaluated with future MnROAD studies.

- The mix in cell 20 (30% RAP with PG 52S-34 binder) had the best field performance (lowest cracking and very good rutting and ride) and had superior results in many of the laboratory tests. Further usage of PG 52S-34 binder is suggested, especially considering the economic and environmental benefits of high ABR content allowed with this binder (37% ABR).
- To mitigate the influence on longitudinal construction joints and moisture penetration in the pavement structure on future MnROAD studies, a longitudinal joint treatment will be used during construction and cracks will be sealed annually. Additionally, the driving lane will be paved 13 feet wide with a 12-foot painted lane; thus, the longitudinal construction joint between the driving lane and shoulder will be further outside of the driving lane.

5. REFERENCES

1. American Society for Testing and Materials. Standard Guide for Calculating in Situ Equivalent Elastic Moduli of Pavement Materials Using Layered Elastic Theory, In Annual Book of ASTM Standards, Vol. 04.03, 2015.

2. Braham, A.F., W.G. Buttlar, and M.O. Marasteanu. Effect of Binder Type, Aggregate, and Mixture Composition on Fracture Energy of Hot-Mix Asphalt in Cold Climates. Transportation Research Record: Journal of the Transportation Research Board No. 2001, 2007, pp. 102-109.

3. Epps Martin, A., F. Kaseer, E. Arámbula-Mercado, A. Bajaj, L. Garcia Cucalon, F. Yin, A. Chowdhury, J. Epps, C. Glover, E.Y. Hajj, N. Morian, J. Sias Daniel, M. Oshone, R. Rahbar-Rastegar, C. Ogbo, and G. King. Evaluating the Effects of Recycling Agents on Asphalt Mixtures with High RAS and RAP Binder Ratios, NCHRP Research Report 927. Transportation Research Board, Washington, D.C., 2019.

4. Federal Highway Administration. National Performance Management Measures; Assessing Pavement Condition for the National Highway Performance Program and Bridge Condition for the National Highway Performance Program. Federal Register, Vol. 82, No. 11, January 2017.

5. Garcia, V.M., Miramontes, A. Garibay, J. Abdallah, I., Carrasco, G. Lee, R., and Nazarian, S. Alternative Methodology for Assessing Cracking Resistance of Hot Mix Asphalt Mixtures with Overlay Tester, Journal of the Association of Asphalt Paving Technologists, pp. 527-548, 2017

6. Jung, D.H. and T.S. Vinson. Low-Temperature Cracking: Test Selection. Report SHRP-A-400, Washington, D.C., 1994.

7. Hajj, E., Sebaaly, P., Porras, J., and J. Azofeifa. (2010). “Reflection Cracking of Flexible Pavements Phase III: Field Verification,” Research Report No. 13KJ-1, Nevada Department of Transportation, Research Division, University of Nevada, Reno.

8. Izevbekhai, Bernard Igbafen, and Hung Jun Ahn. Line Laser and Triple Laser Quantification of the Difference in International Roughness Index Between Textured and Non-Textured Strips. No. 2017-28. Minnesota. Dept. of Transportation. Research Services & Library, 2017.

9. Kaseer, F., F. Yin, E. Arámbula-Mercado, A. Epps Martin, J. Daniel and S. Salari. Development of an Index to Evaluate the Cracking Potential of Asphalt Mixtures using the Semi-circular Bending Test. Construction and Building Materials 167, 286-298, 2018.

10. Li, Xinjun, M. O. Marasteanu, R. C. Williams, and T. R. Clyne. Effect of Reclaimed Asphalt Pavement (Proportion and Type) and Binder Grade on Asphalt Mixtures, Journal of Transportation Research Record, No. 2051, 2008, pp. 90–97.

11. Lukanen, E. O., Stubstad, R. And R. Briggs. Temperature Predictions and Adjustment Factors for Asphalt Pavement. Publication Fhwa-Rd-98-085. FHWA, U.S. Department of Transportation, 2000.

12. Ma, W. Proposed Improvements to Overlay Test for Determining Cracking Resistance of Asphalt Mixtures. MS thesis. Auburn University, Auburn, Ala., 2014.

13. Marasteanu, M., W. Buttlar, H. Bahia, and C. Williams. Investigation of Low Temperature Cracking in Asphalt Pavements. National Pooled Fund Study – Phase II, Report No. MN/RC 2012-23, Minnesota Department of Transportation, 2012.

14. Miller, J.S., Dellinger, W.Y. Distress Identification Manual for The LTPP (Fourth Revised Edition) Publication FHWA-RD-03-031, FHWA, U.S. Department of Transportation, 2003.

15. Morian, N. E., E. Hajj, S. Pournoman, S. Habbouche, and D. D. Batioja-Alvarez. Low Temperature Behavior of Asphalt Binders, Mortars, and Mixtures with High Recycled Materials Content. Journal of the Association of Asphalt Paving Technologists, Vol. 87, 2018.

16. Morian, N.E., M.Z. Alavi, E.Y. Hajj, and P.E. Sebaaly. Evolution of Thermo-viscoelastic Properties of Asphalt Mixtures with Oxidative Aging. Transportation Research Record No. 2447, Transportation Research Board, National Research Council, Washington, DC, pp. 1-12, 2014.

17. Schmalzer, P. N. Long-Term Pavement Performance Program Manual For Falling Weight Deflectometer Measurements, Version 4.1. Publication FHWA-HRT-06-132. FHWA, U.S. Department of Transportation, 2006.

18. Schmalzer, P. N., Rada, G.R. And J. S. Miller. Falling Weight Deflectometer (FWD)Testing and Analysis Guidelines Volume II: Supporting Documentation. Publication FHWA-FLH-07-001. FHWA, U.S. Department of Transportation, 2007.Stubstad, R. N., NCHRP Web Document 52: LTPP Data Analysis: Feasibility of Using FWD Deflection Data to Characterize Pavement Construction Quality. Transportation Research Board, Washington, D.C., 2002.

19. Tirupan Mandal, Andrew J. Hanz & Hussain U. Bahia. Challenges in using the Disc-Shaped Compact Tension (DCT) test to determine role of asphalt mix design variables in cracking resistance at low temperatures, International Journal of Pavement Engineering, 20:11, 1275-1284, 2019.

20. West, Randy C., Jingna Zhang, and Jason Moore. Evaluation of bond strength between pavement layers. No. NCAT Report 05-08. Auburn University. National Center for Asphalt Technology, 2005.

21. Worel, B., B. Chadbourn, and R. Strommen. "MnROAD Automated Laser Profile System (ALPS)." 2nd International Conference on Accelerated Pavement Testing, Minneapolis, MN. 2004.

22. Zhou, F., Newcomb, D., Gurganus, C., Banihashemrad, S., Park, E., Sakhaeifar, M., and Lytton, R. Experimental Design for Field Validation of Laboratory Tests to Assess Cracking Resistance of Asphalt Mixtures. NCHRP Project No. 9-57, Project Final Report, 2016.

23. Zhou, F. and T. Scullion, Overlay Tester: A Rapid Performance Related Crack Test, FHWA/TX-05/0- 4467-2, Final Report, Texas Transportation Institute, College Station, Texas, 2005.

Appendix A – Paver Mounted Thermal Profile

Cell 16 Lift 1 Driving Lane

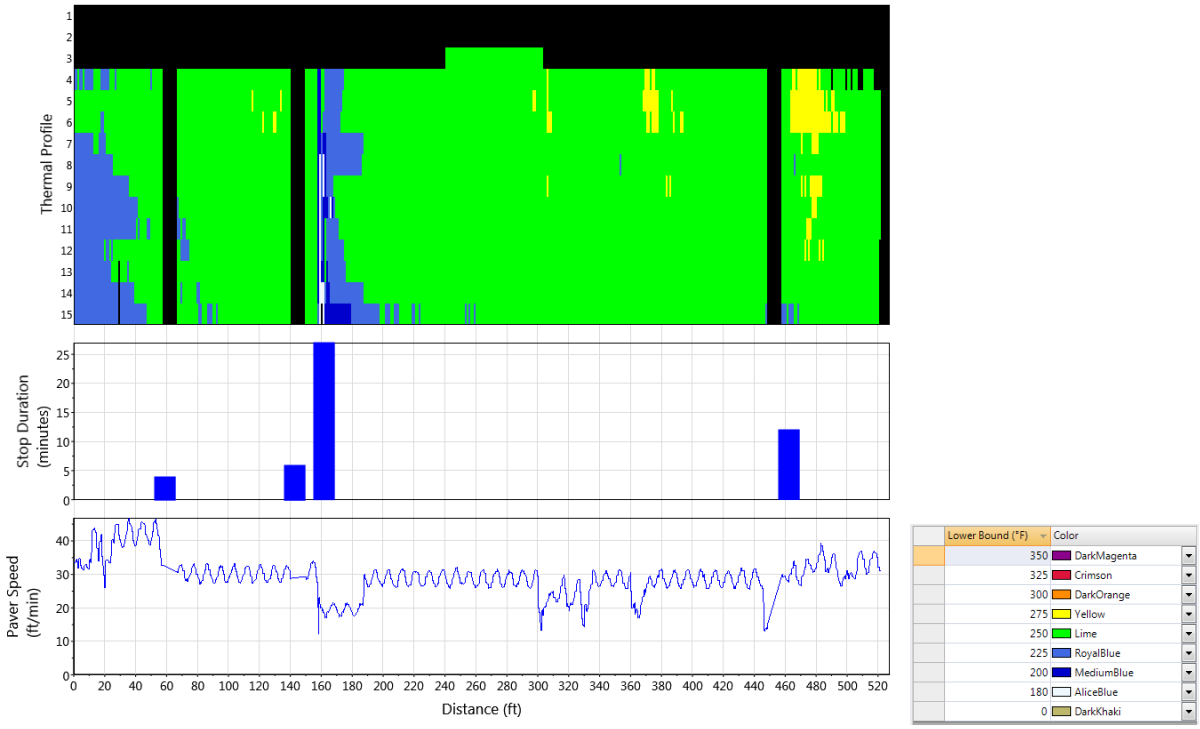

Cell 16 Lift 1 Passing Lane

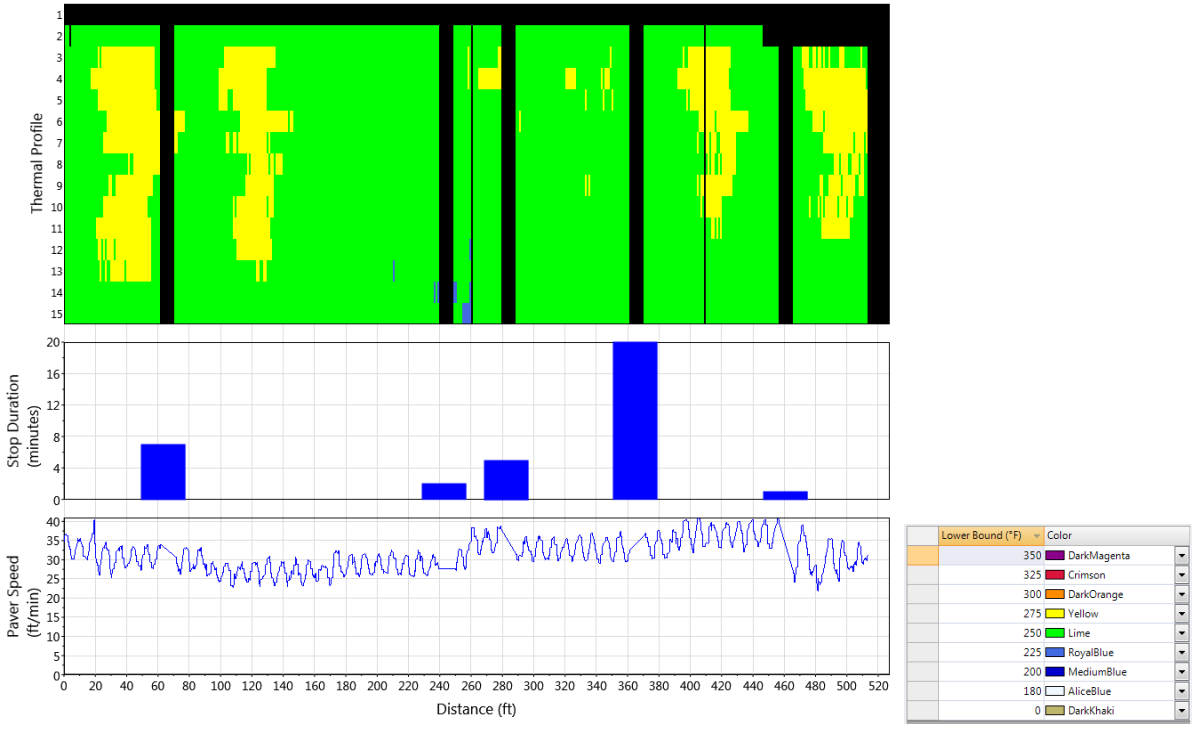

Cell 16 Lift 2 Driving Lane

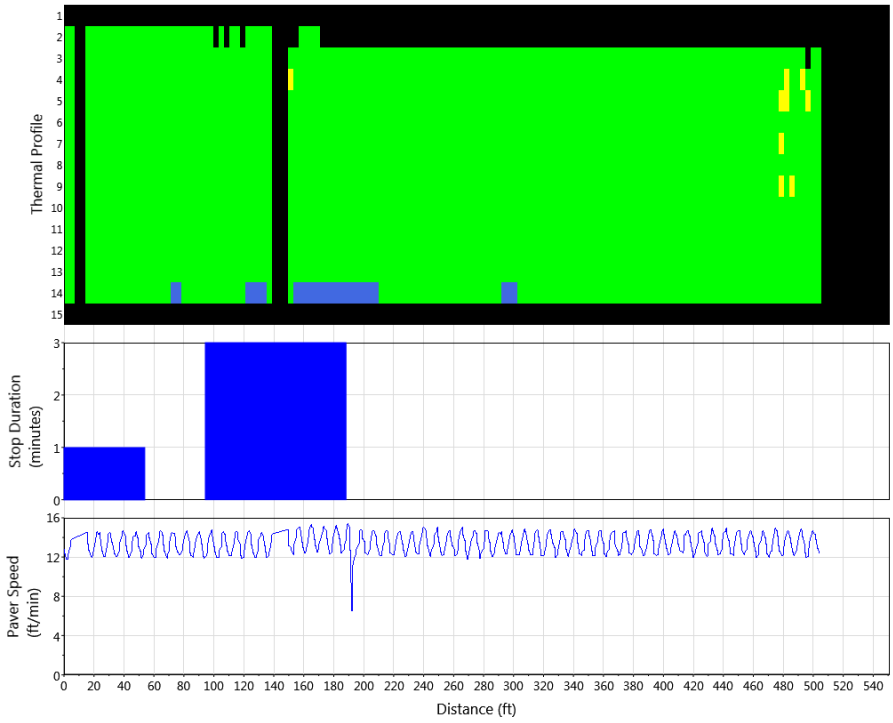

Lower Bound (°F)	Color
350	DarkMagenta
325	Crimson
300	DarkOrange
275	Yellow
250	Lime
225	RoyalBlue
200	MediumBlue
180	AliceBlue
0	DarkKhaki

Cell 16 Lift 2 Passing Lane

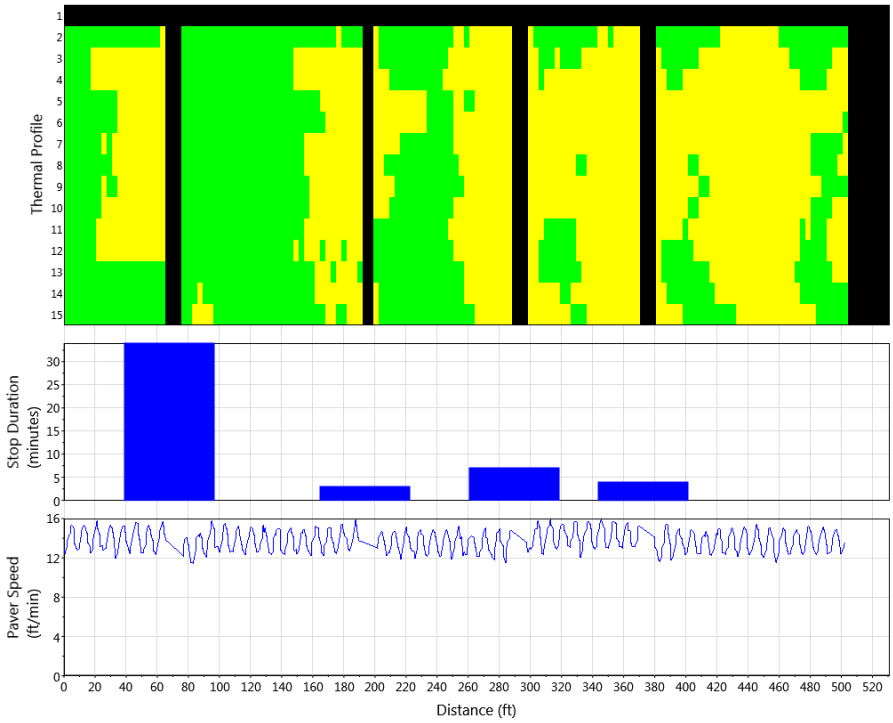

Lower Bound (°F)	Color
350	DarkMagenta
325	Crimson
300	DarkOrange
275	Yellow
250	Lime
225	RoyalBlue
200	MediumBlue
180	AliceBlue
0	DarkKhaki

Cell 17 Lift 1 Driving Lane

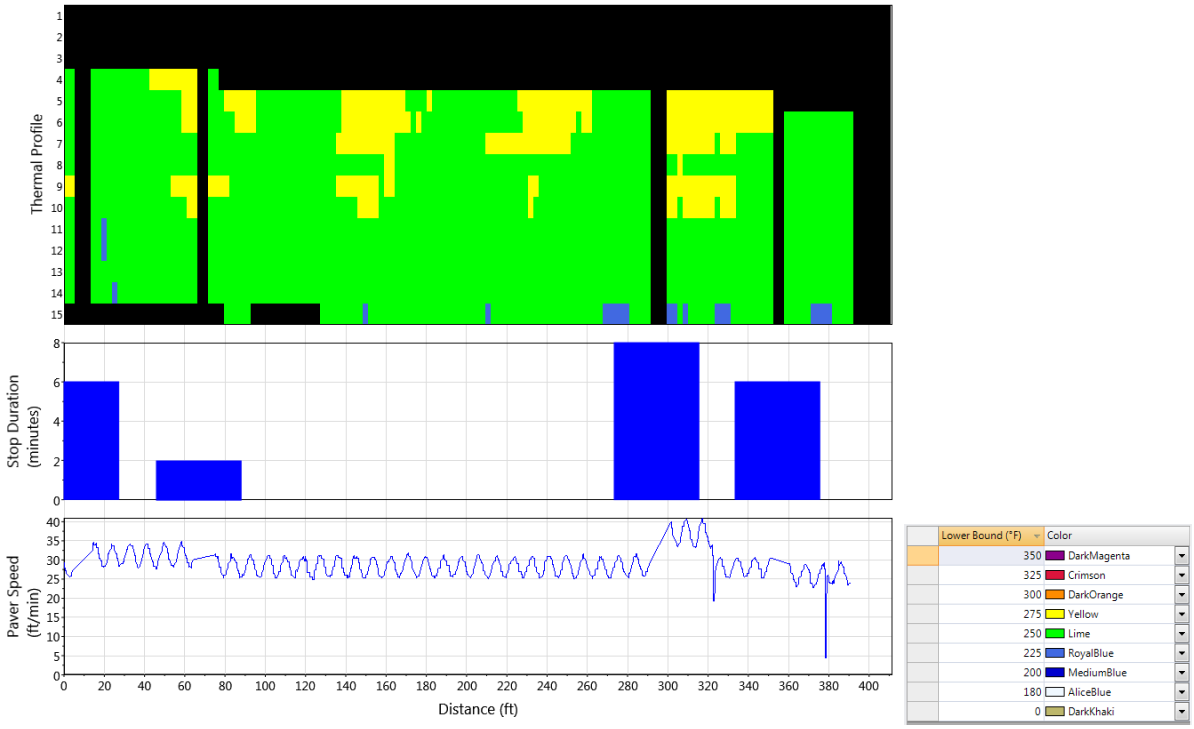

Cell 17 Lift 1 Passing Lane

NA due to data collection error.

Cell 17 Lift 2 Driving Lane

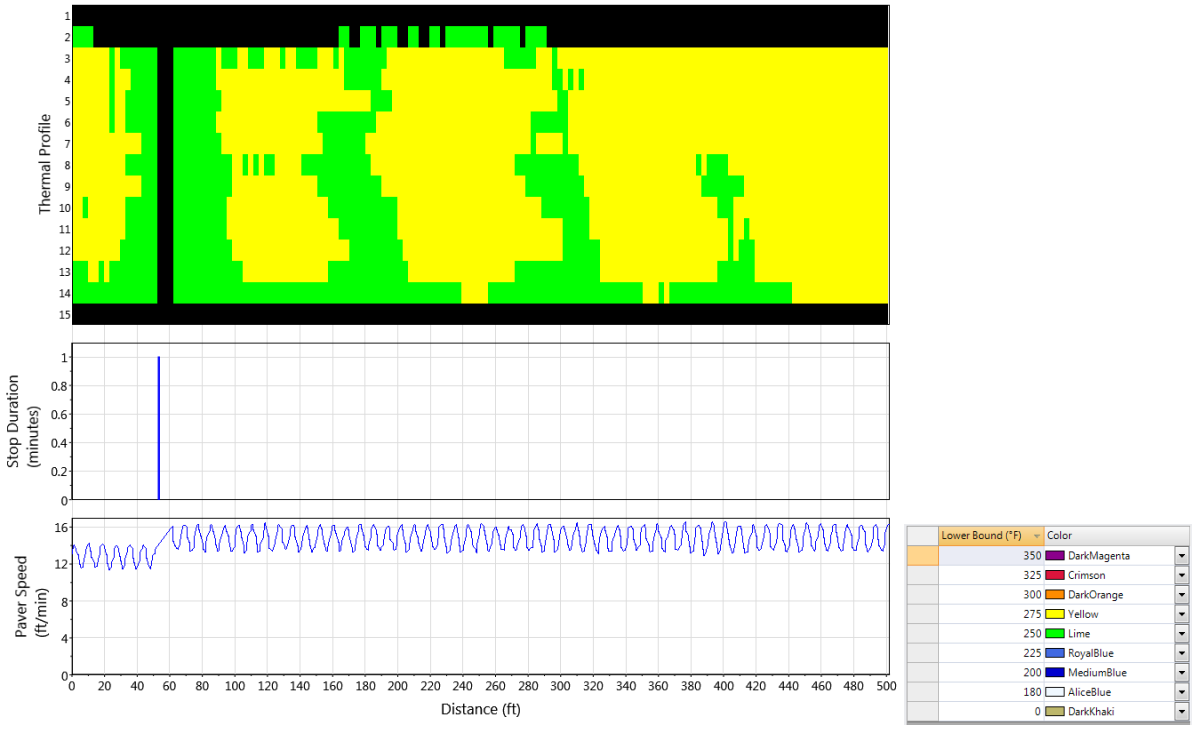

Cell 17 Lift 2 Passing Lane

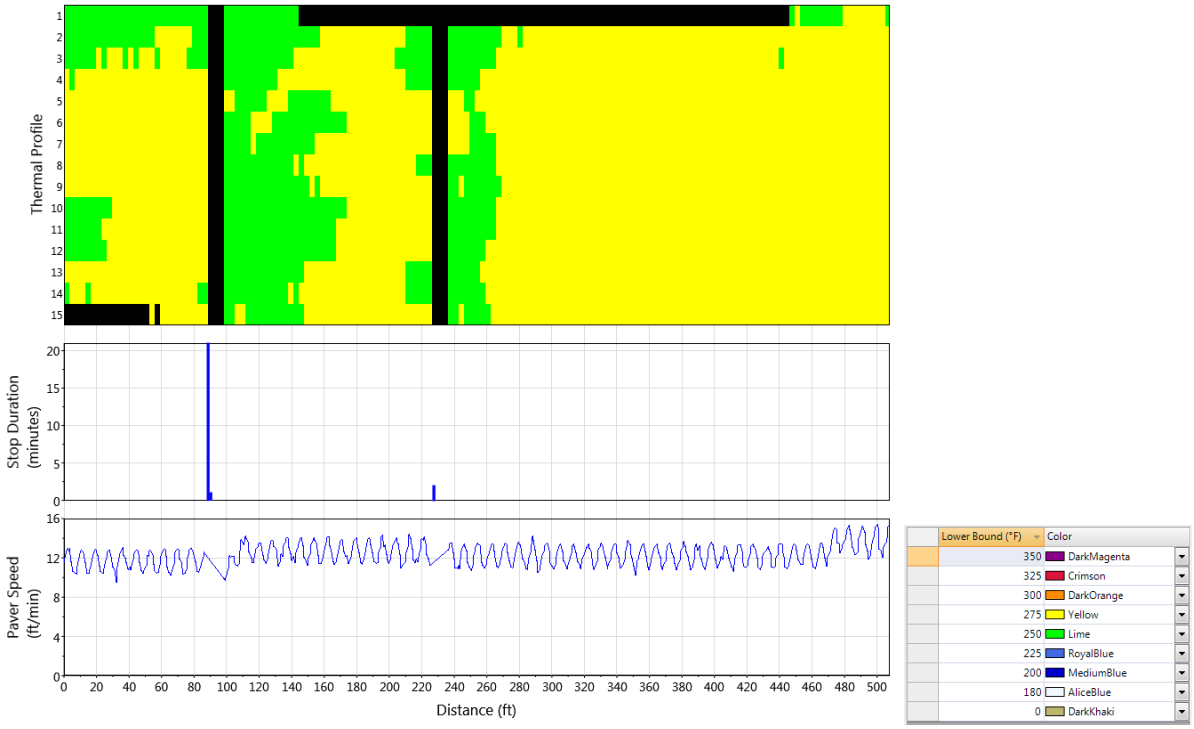

Cell 18 Lift 1 Driving Lane

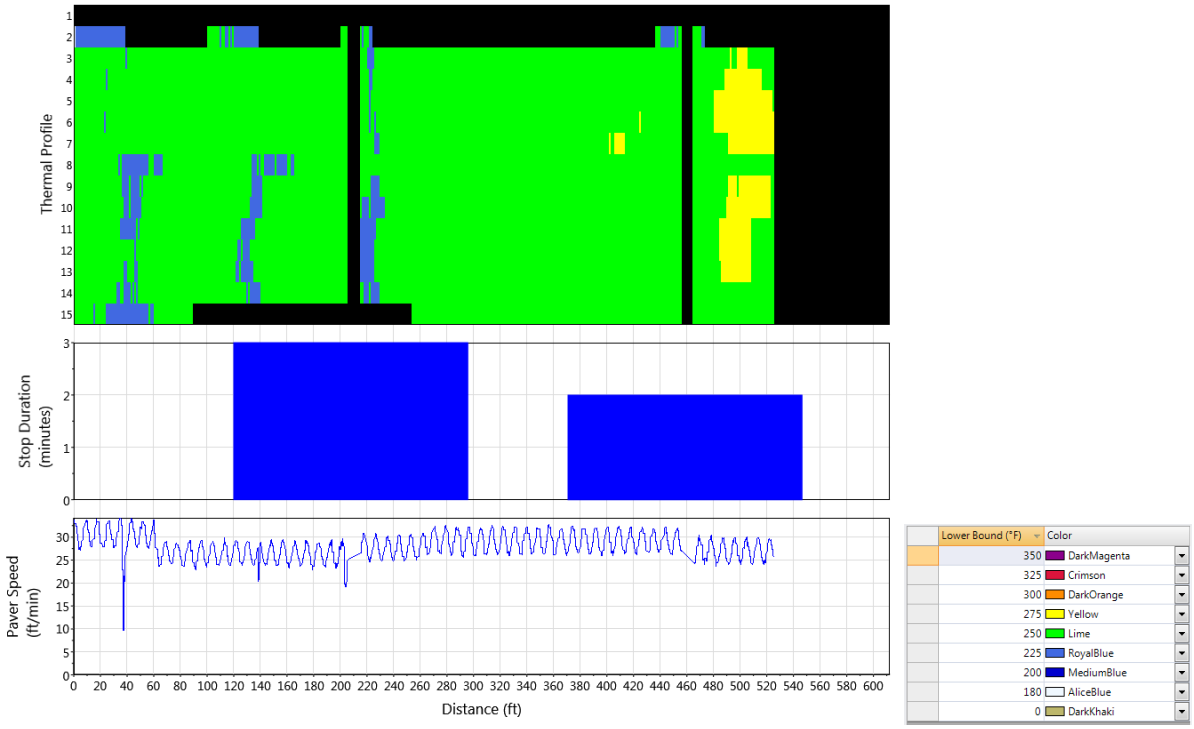

Cell 18 Lift 1 Passing Lane

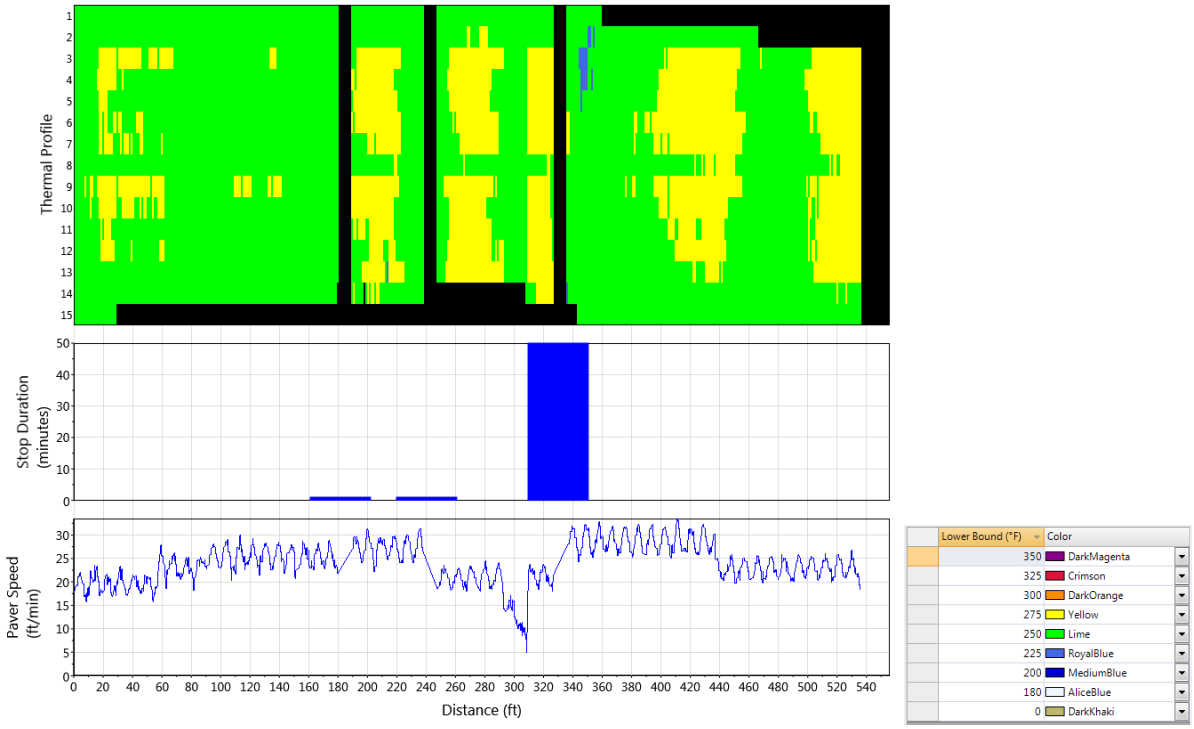

Cell 18 Lift 2 Driving Lane

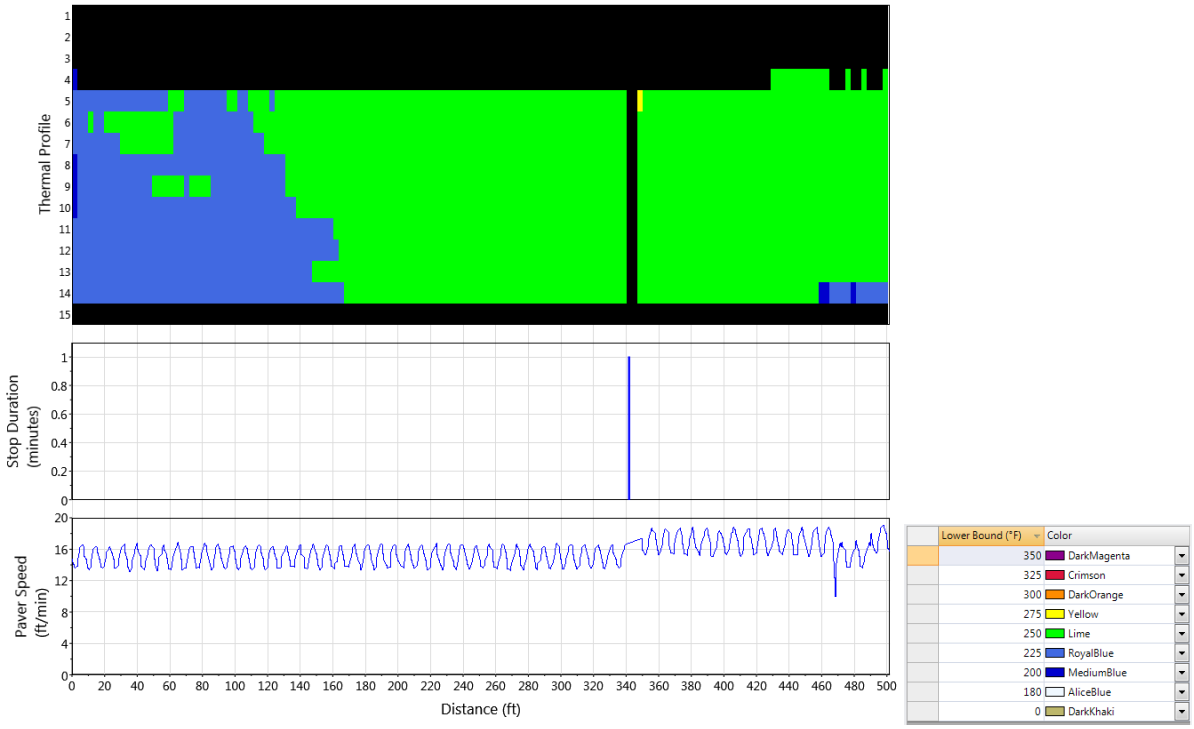

Cell 18 Lift 2 Passing Lane

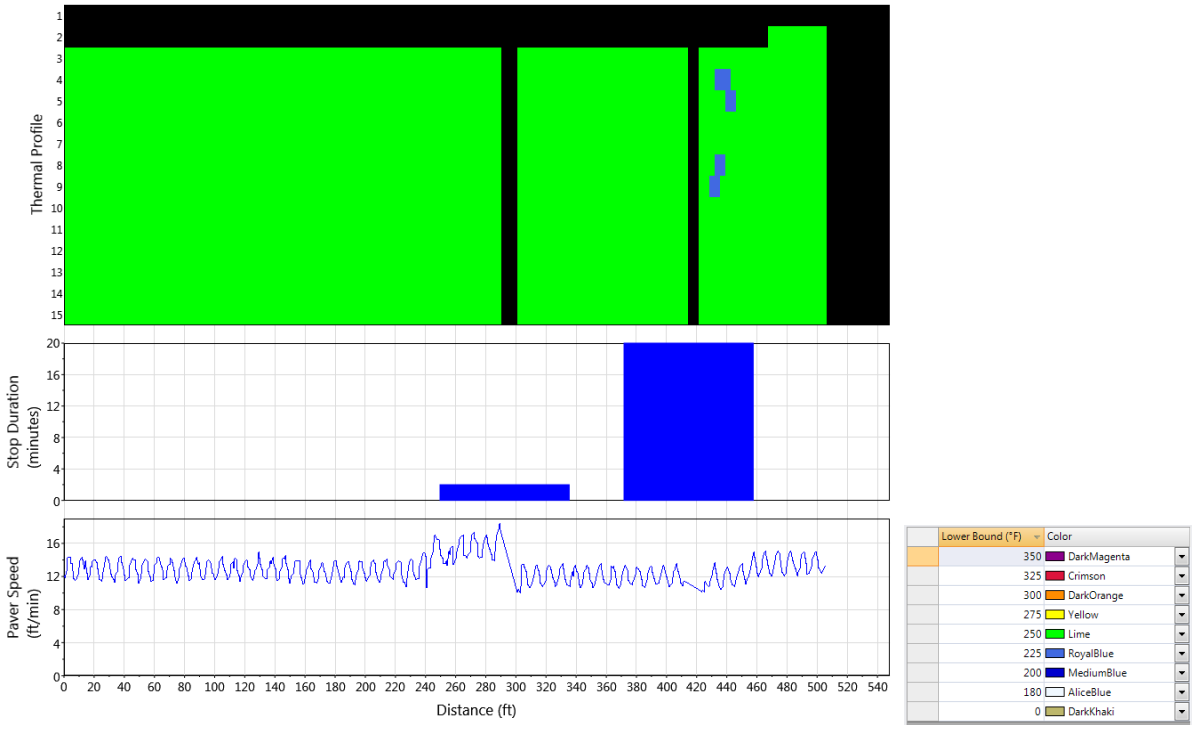

Cell 19 Lift 1 Driving Lane

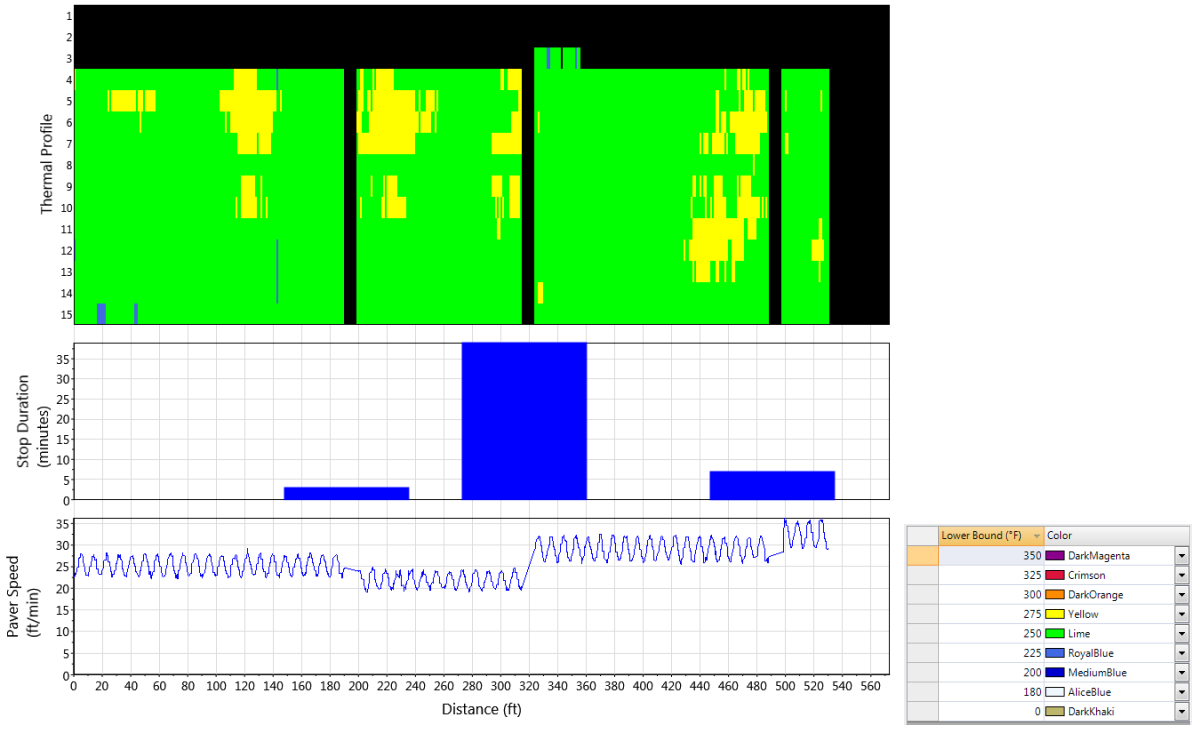

Cell 19 Lift 1 Passing Lane

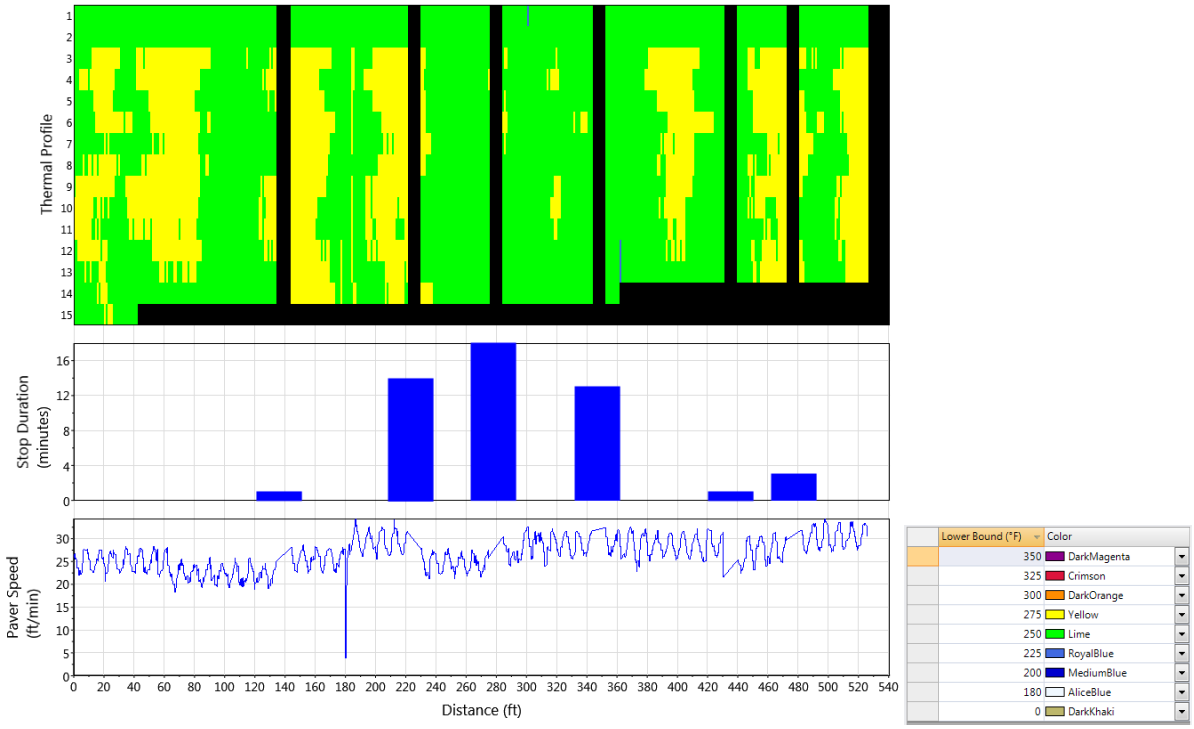

Cell 19 Lift 2 Driving Lane

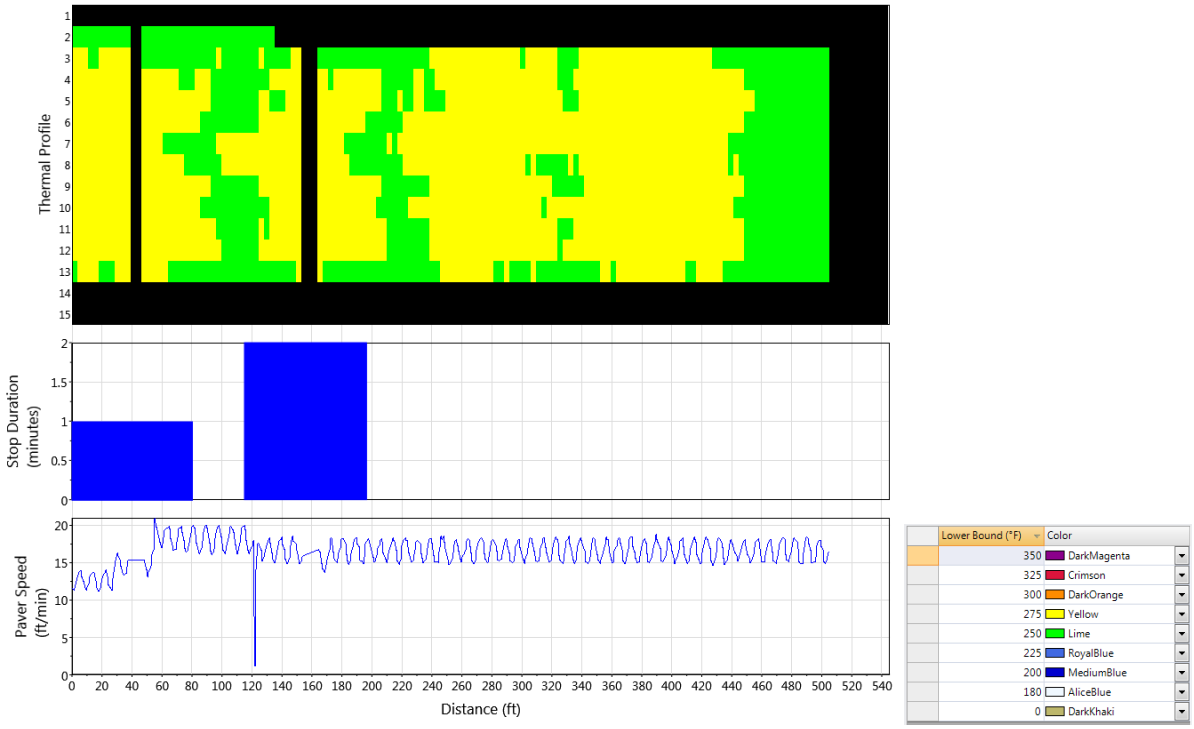

Cell 19 Lift 2 Passing Lane

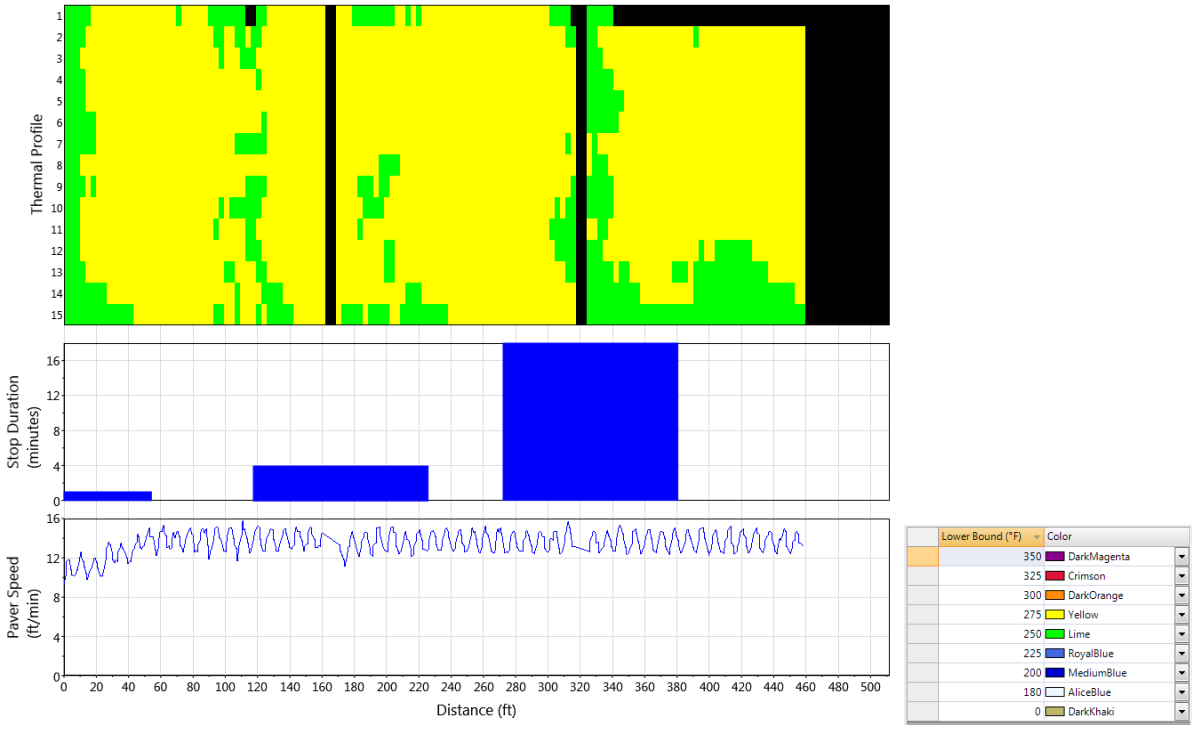

Cell 20 Lift 1 Driving Lane

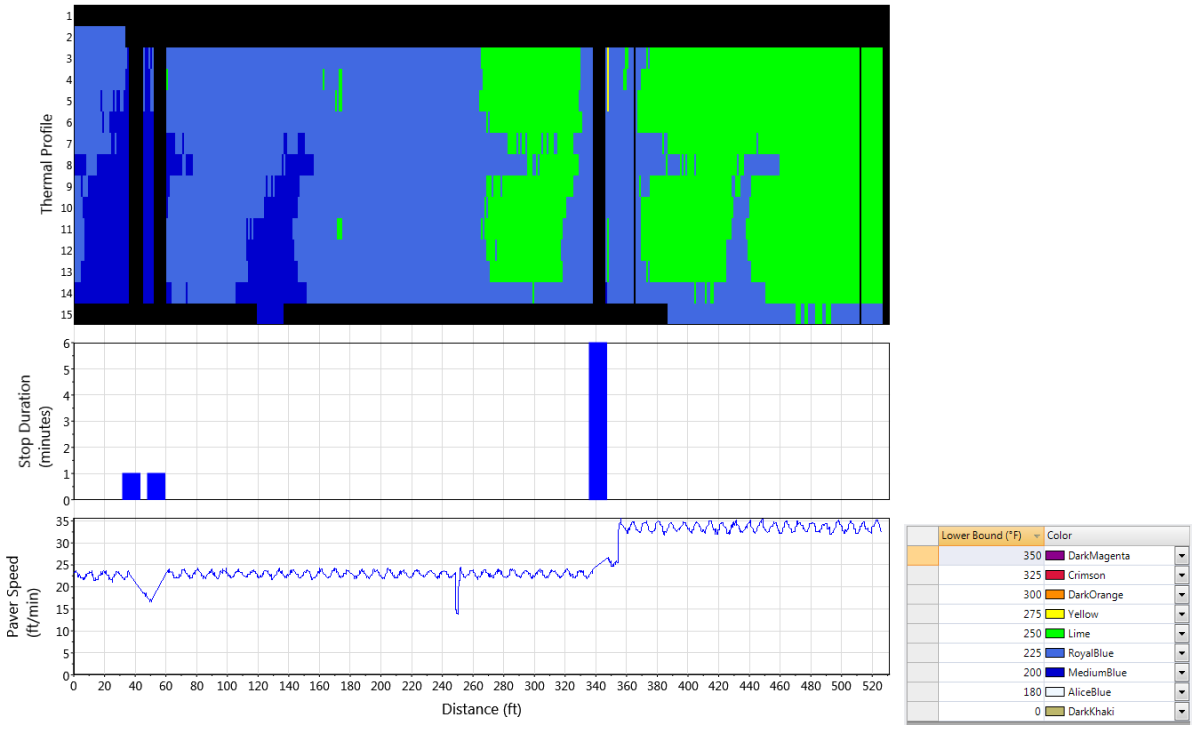

Cell 20 Lift 1 Passing Lane

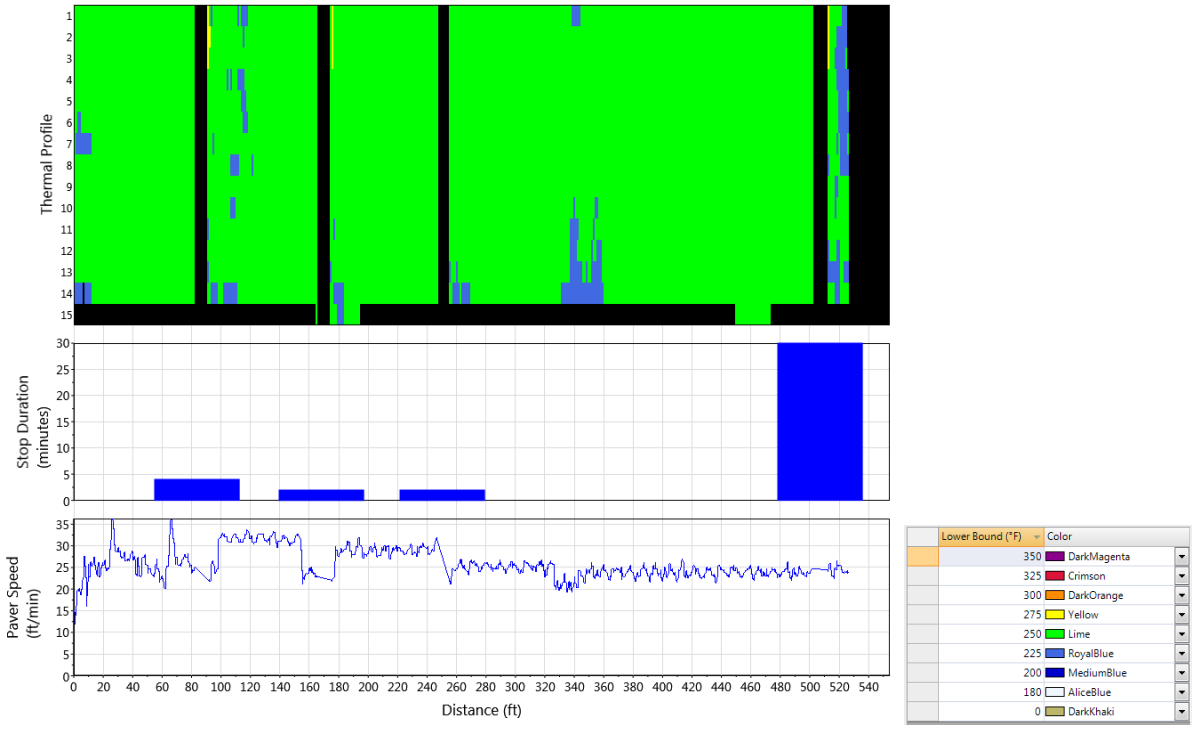

Cell 20 Lift 2 Driving Lane

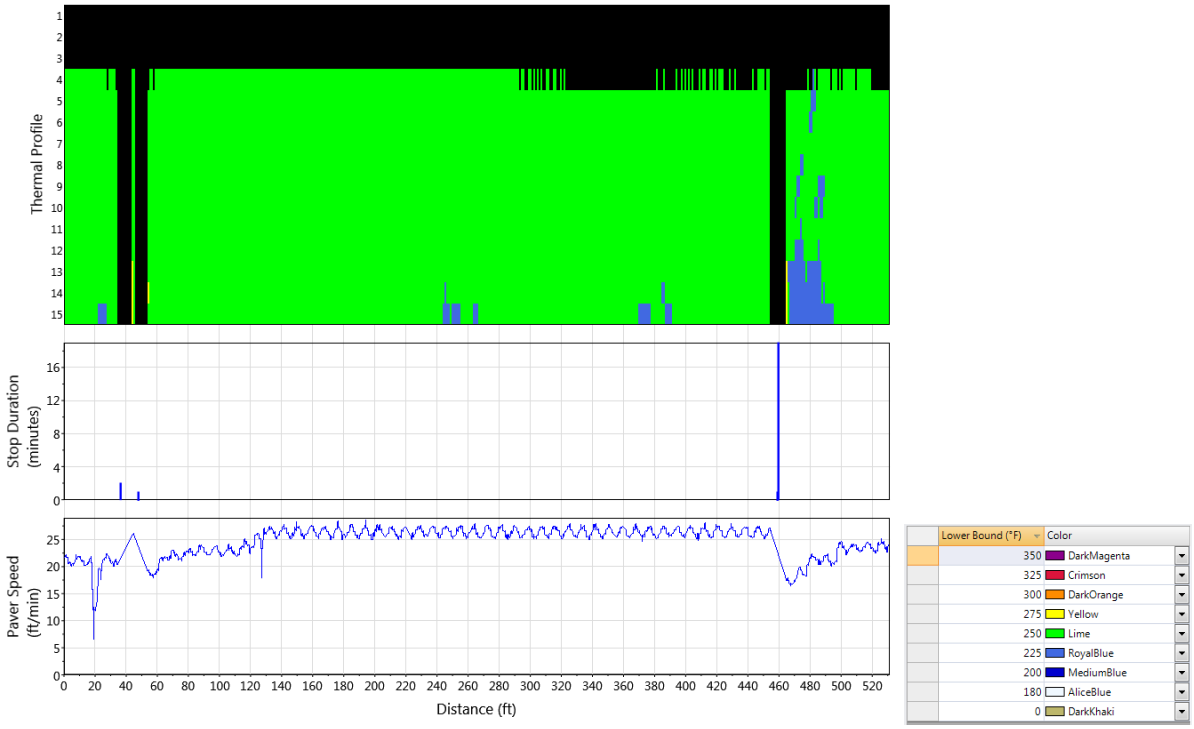

Cell 20 Lift 2 Passing Lane

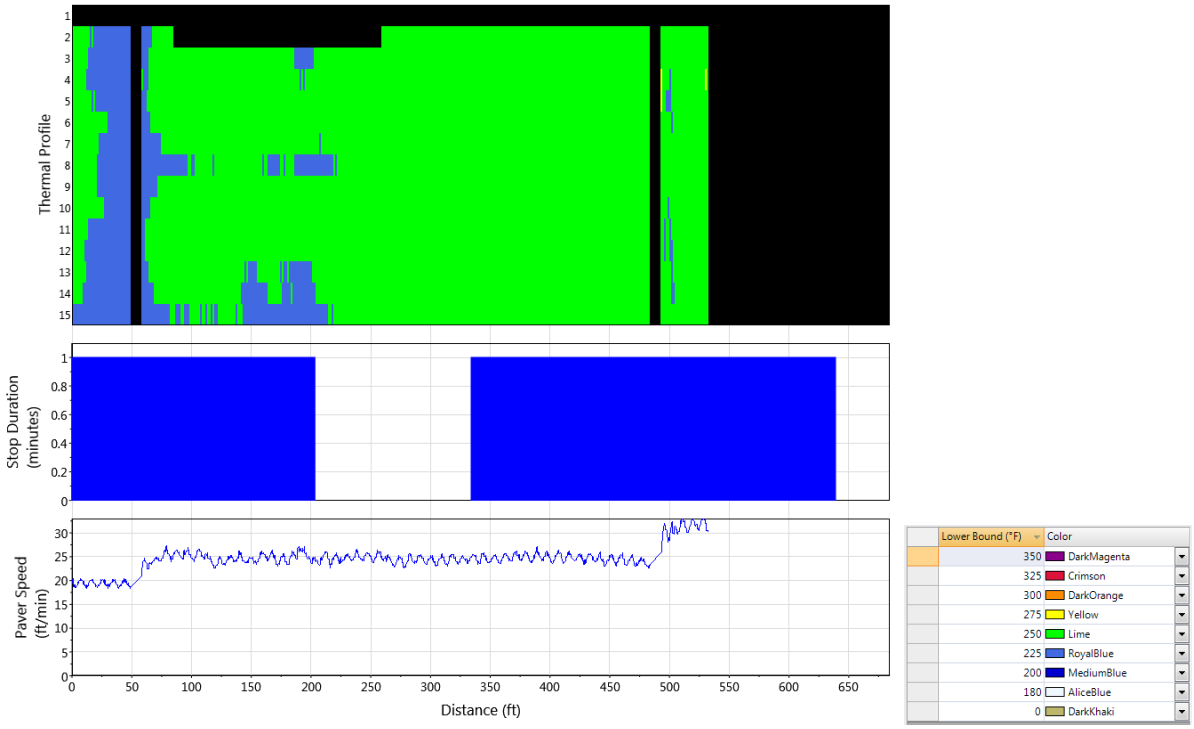

Cell 21 Lift 1 Driving Lane

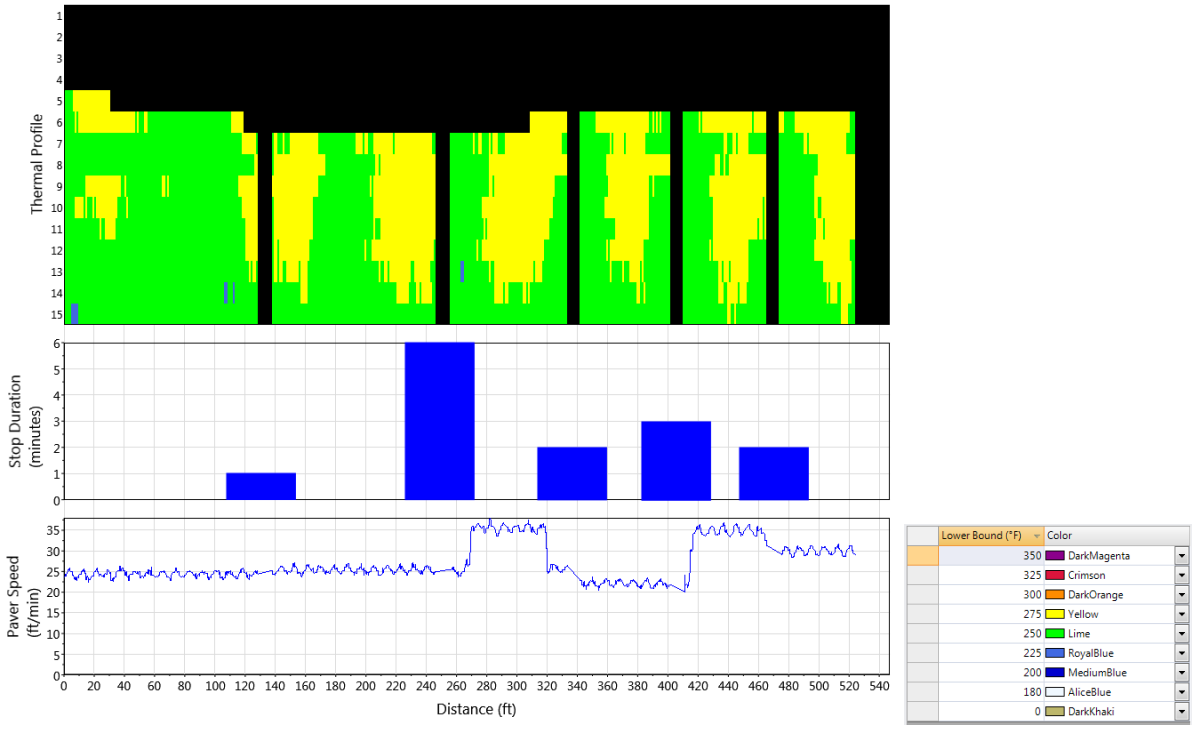

Cell 21 Lift 1 Passing Lane

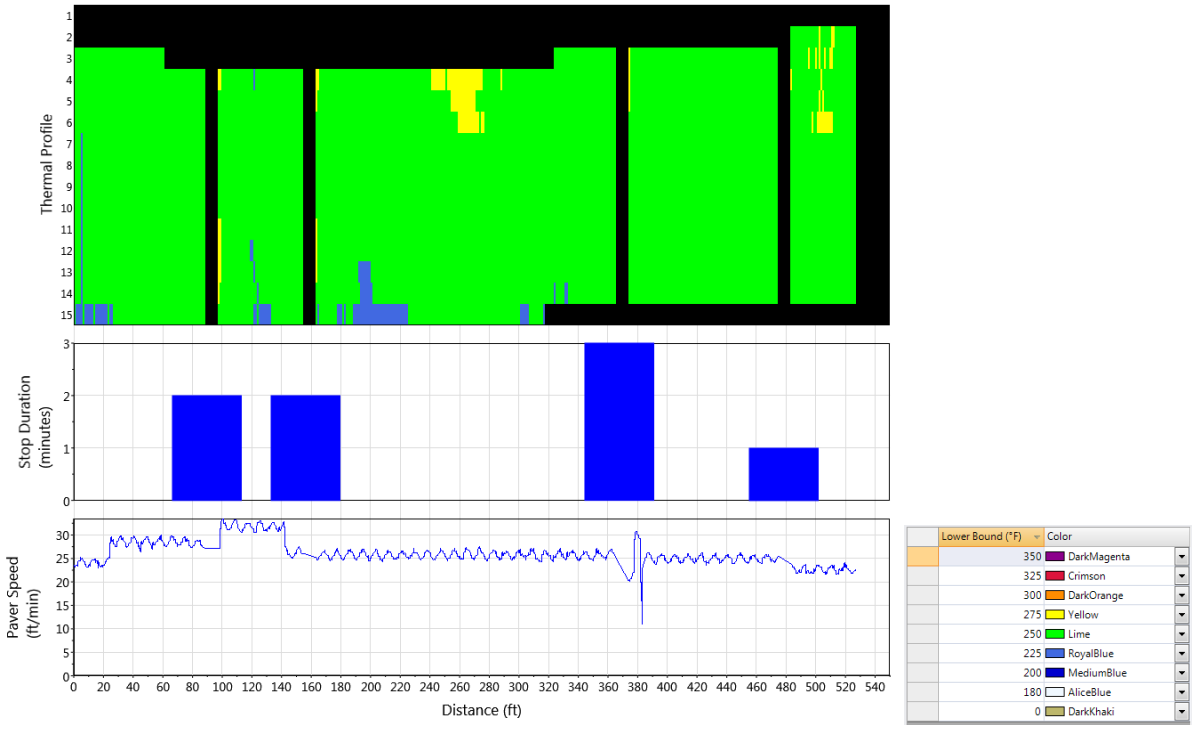

Cell 21 Lift 2 Driving Lane

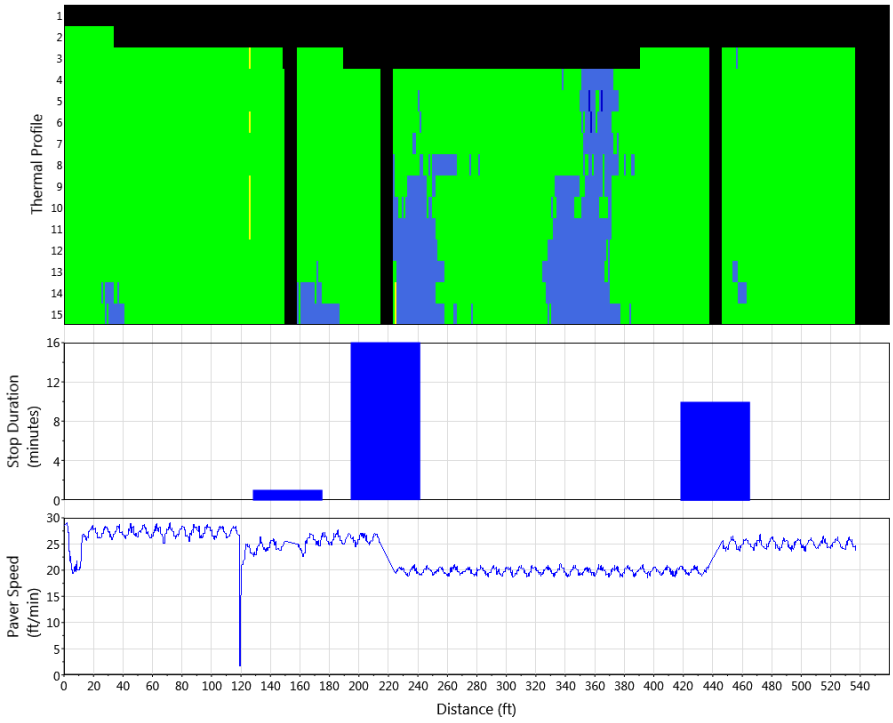

Lower Bound (°F)	Color
350	DarkMagenta
325	Crimson
300	DarkOrange
275	Yellow
250	Lime
225	RoyalBlue
200	MediumBlue
180	AliceBlue
0	DarkKhaki

Cell 21 Lift 2 Passing Lane

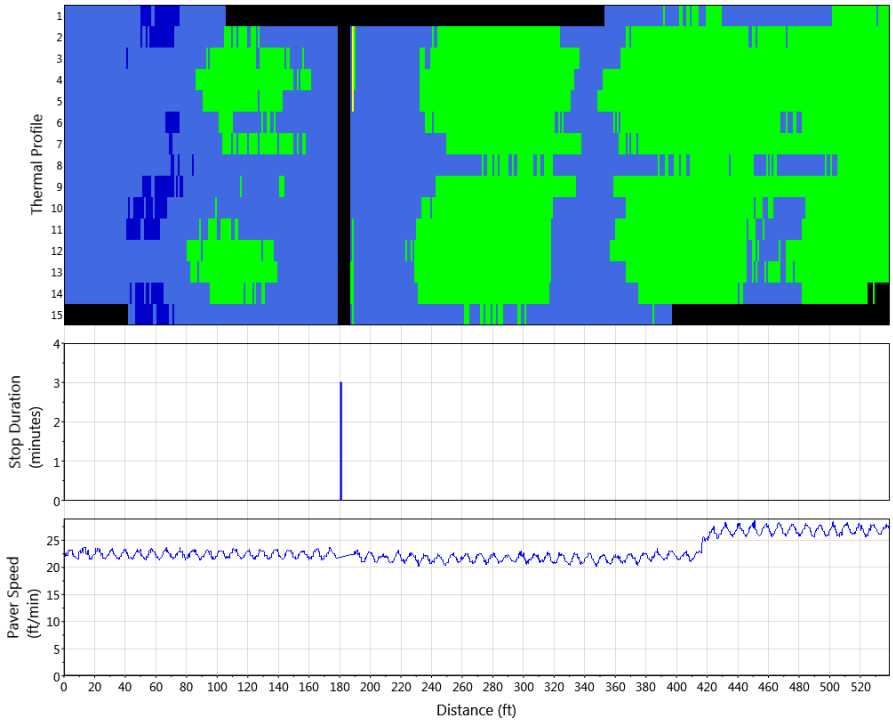

Lower Bound (°F)	Color
350	DarkMagenta
325	Crimson
300	DarkOrange
275	Yellow
250	Lime
225	RoyalBlue
200	MediumBlue
180	AliceBlue
0	DarkKhaki

Cell 22 Lift 1 Driving Lane

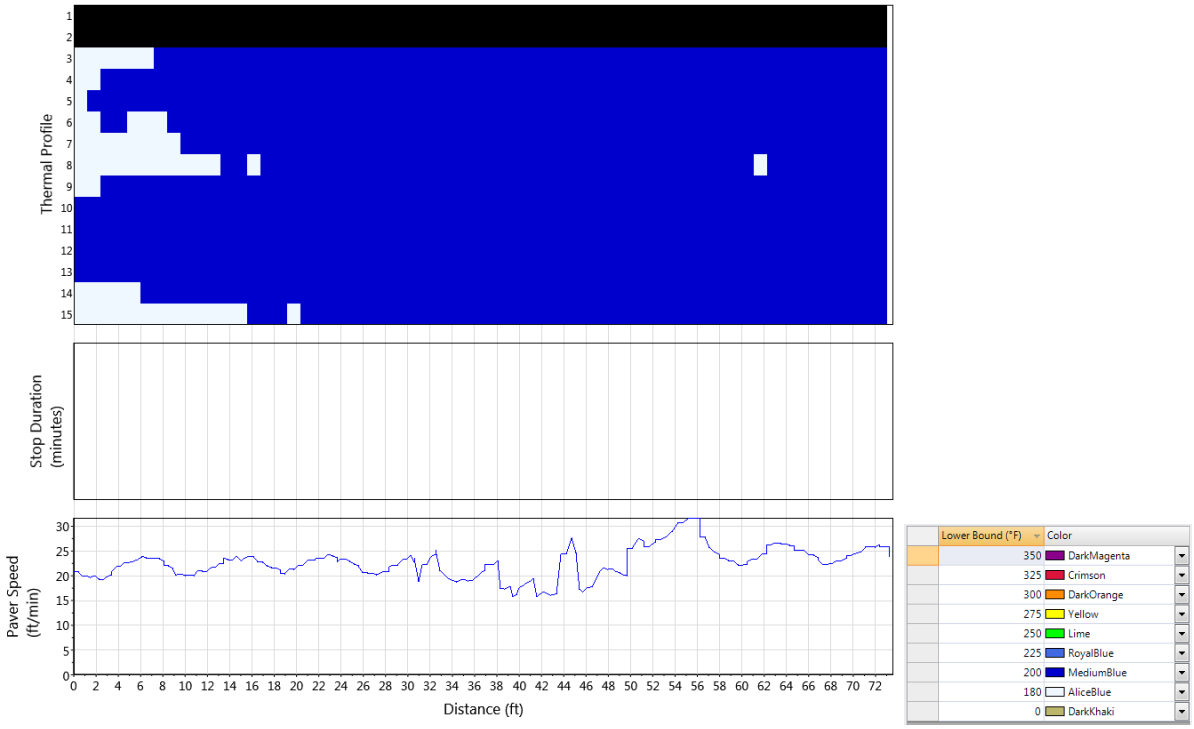

Cell 22 Lift 1 Passing Lane

NA due to data collection error.

Cell 22 Lift 2 Driving Lane

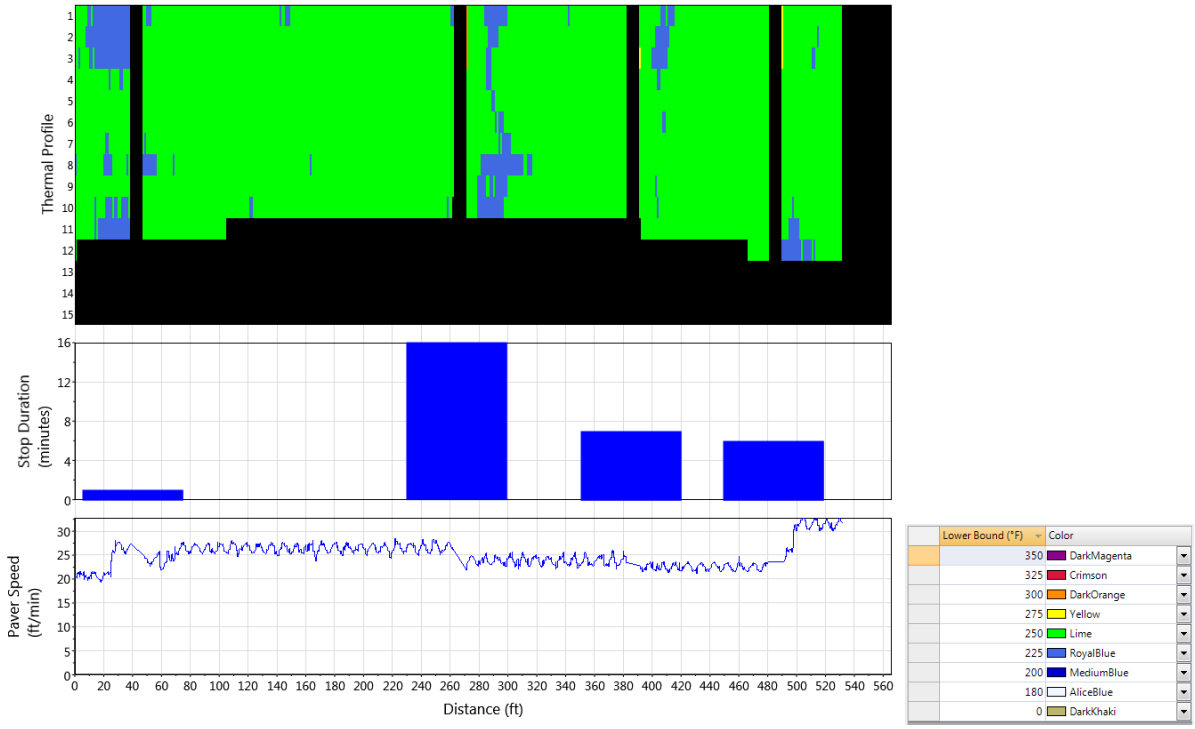

Cell 22 Lift 2 Passing Lane

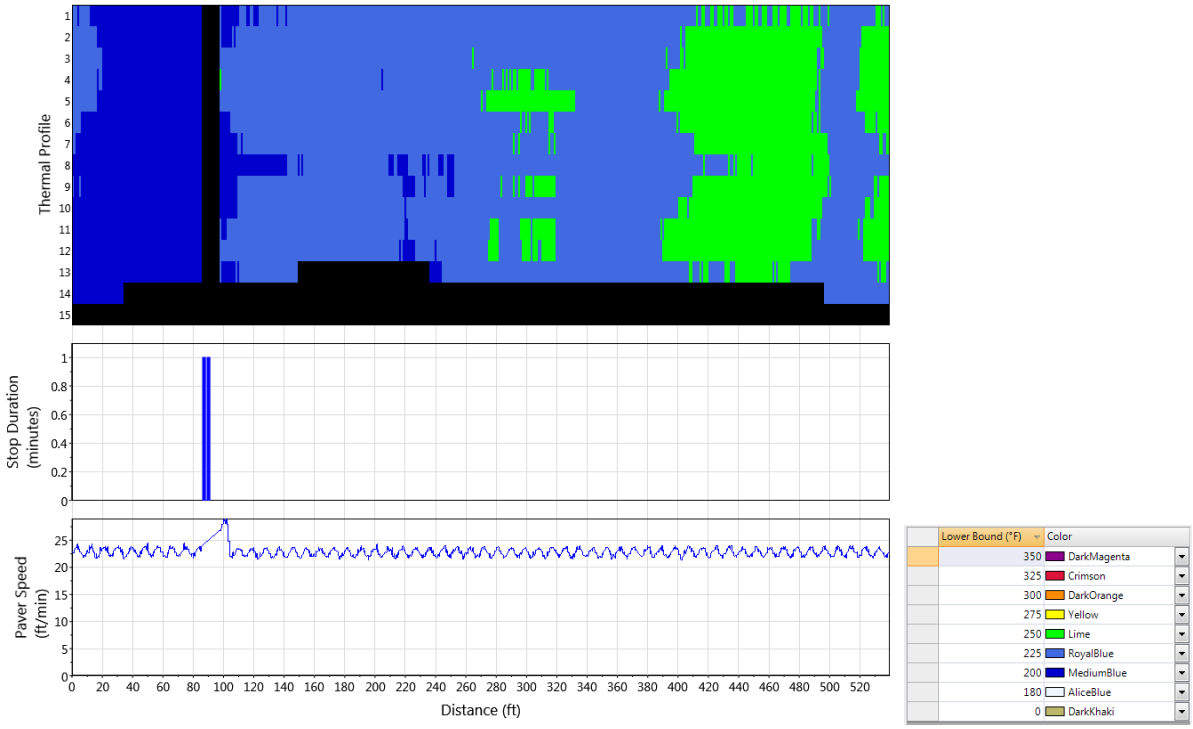

Cell 23 Lift 1 Driving Lane

NA due to data collection error.

Cell 23 Lift 1 Passing Lane

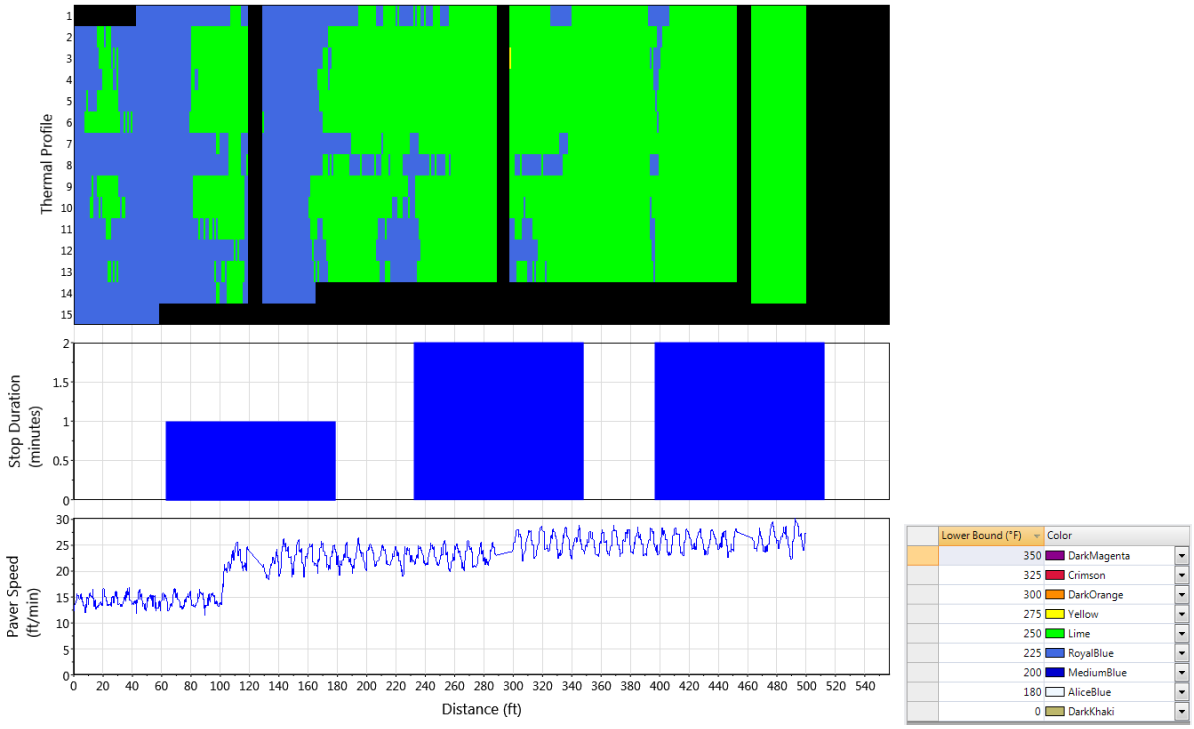

Cell 23 Lift 2 Driving Lane

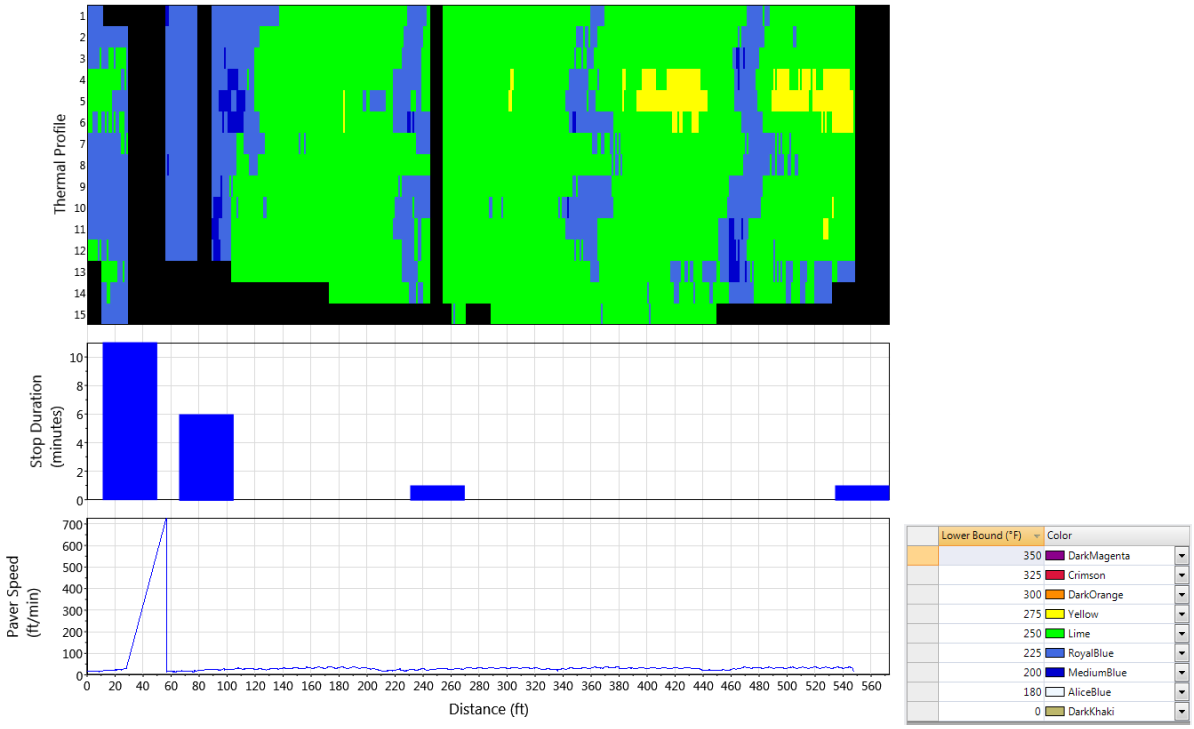

Cell 23 Lift 2 Passing Lane